5.1 Inversion algorithms

The *inversion* or *retrieval problem* is common for almost all satellite observations. This is how a parameter can be obtained from measured data. In the SMOS case the inversion algorithm consists of computing salinity from a set of radiometric measurements T_B, at given incidence angles and polarisations.

The so-called *forward problem* is the opposite one. This problem deals with the description of the physical laws that, given the geophysical parameter values, can predict the values that will be measured. In our case it is the law that describes the transition from SSS (among other variables) to T_B. This problem is already treated in chapter 3.

It is usually important to appreciate the degree of linearity of any given inverse problem, that is the degree to which the knowns and unknowns of the problem can be separated out into a linear equation. When dealing with linear equations, the variables to be retrieved can be calculated with some well established methods.

In our case, T_B models are not linear neither with SSS, nor SST, since dielectric constant models are clearly non-linear with those parameters. On the other hand, when using semi-empirical models, T_B is assumed linear with U_{10} and SWH.

For the SMOS case, three different inversion methods have been taken under consideration:

- Analytical inversion
- Iterative methods
- Neural network methods

A description of these methods and a comparison of the last two applied to retrieve real data can be found in the documents: 'Synergetic aspects and Auxiliary Data Concepts for Sea Surface Salinity Measurements from Space', ESTEC ITT 1-4505/03/NL/Cb Workpackage 1100 and also in the final report of the ESA 15165/01/NL/SF contract, both documents from the European Space Agency.

The iterative methods are very flexible, since the models and the auxiliary parameters can very easily be modified. This is not possible with the neural network approach because, for every modification a new database should be learnt, a procedure that could take a lot of time and effort. It is necessary, also, to know very well the properties and physical characteristics of the parameters before programming the neural networks (Hertz et al., 1991).

Furthermore, the iterative methods permits to have a clear comprehension of the physical processes and understand what is happening during the inversion

process. On the other hand, neural networks can be considered as 'black boxes', since once they are trained, their characteristics and behaviour is not known (Hertz et al., 1991).

Thence, considering the advantages described above, only *iterative methods* have been used in this work.

The iterative methods follow the procedure described bellow:

1. A first-guess for SSS is chosen (or any parameter to be retrieved).
2. A weighting function is calculated by giving different weights to different observations, depending on the quality of observations.
3. Using the chosen forward model, T_B is calculated.
4. The computed brightness temperatures are compared with the measured ones.
   - If they are similar $\|T_B^{model} - T_B^{measured}\|^2 < threshold$, then the current SSS is accepted as final result.
   - If convergence has not been achieved, then a δSSS is added to the current SSS value.
5. Steps 3 through 5 are repeated until a solution is found.

When solving an overdetermined system of equations, where there are more equations (M) than unknowns (N), it can be easily handled by obtaining a "least square error solution." It consists of finding a solution which for all possible vectors of dimension N minimise the norm of $\|T_B^{model} - T_B^{measured}\|$.

Thanks to its multi-angularity capability, SMOS retrieval will be an overdetermined problem. It means that a large number of different incidence angles (from 0° to 55°) will look at the same pixel (target), so there will be more equations than unknowns. Retrievals from WISE, EuroSTARRS and FROG measurements are also overdetermined systems.

The least square error methods have been used here. The definition of the cost function (what should be minimised) is an important issue, and it can be considered with constraints or without them.

In these calculations a normal distribution of the errors is assumed. May be this is not a strictly correct assumption, but for a preliminary analysis it is a good enough approximation. Further work can be oriented on the analysis when these errors do not follow a normal distribution, but this is out of the scope of this thesis.

5.1.1 Cost function

The cost function is the function that needs to be minimised by the least square method to solve for the unknowns.

It can be defined with restrictions or without restrictions. It means that when no restrictions are considered, all possible solutions are valid. On the other hand, when dealing with restrictions, the possible solutions are constrained to within a range of values, which are already specified in the cost function.

When no restrictions are considered, the cost function is defined as:

$$\chi^2(SSS, SST, U) = \sum_{i=0}^{N-1} \frac{[\, T_{B_i}^{meas} - T_{B_i}^{model}(\theta_i, SSS, SST, U)\,]^2}{\sigma_i^2}, \tag{5.1}$$

where i is the different incidence angle, $T_{B_i}^{meas}$ is the measured brightness temperature, and $T_{B_i}^{model}$ is the modelled brightness (obtained through the forward model).

On the other hand, when considering some restrictions, then the cost function is defined as follows:

$$\chi^2(SSS, SST, U) = \sum_{i=0}^{N-1} \frac{[\, T_{B_i}^{meas} - T_{B_i}^{model}(\theta_i, SSS, SST, U)\,]^2}{\sigma_i^2} + \sum_j \frac{[\, P_j - P_{j\,ref}]^2}{\sigma_{P_j}^2}, \tag{5.2}$$

where P is the parameter to be found, with j possible parameters (in this case they could be: SSS, SST, U_{10} or SWH), P_{ref} is a reference value for each of the parameters (obtained from satellite or model outputs) from which the final solution should not be far, and σ_P^2 is the variance of the expected error of the reference values. The value of P at the first iteration is the so-called "a priori" or "first guess" value[1]. Then the possible solutions of P can be between $P_{ref} - \sigma_P$ and $P_{ref} + \sigma_P$. Another way to understand the importance of this parameter is the following: when a reference value of the parameters is known with low precision, then σ_P is big, then the term of this parameter is small, and have less weight in the overall equation.

Thereafter, a different number of unknowns have been considered. Sometimes only SSS is treated as unknown, while in some occasions other parameters (U_{10}

[1] Attention should be put with the names. Here we use *a priori* value for the first guess value, and *reference value* for the value of each parameter independently known with an expected error. Other authors call *a priori* the *reference value*

or SWH, SST), as well as the SSS, are dealt as parameters to be retrieved[2]. The necessity of using one or more unknowns will be argued later on.

5.1.2 Methodology

For the retrieval process the IDL software (Iterative Data Language, from RSI systems) has been used. When dealing with cases where the cost function does not have restrictions then the Levenberg-Marquardt least square algorithm has been used (Marquardt (1963)). When cost functions with restrictions are necessary, then downhill simplex method of optimisation is utilised (Nelder and Mead (1965)). For more information on those methods see appendix **??**.

The datasets that have been used for the retrieval study are from WISE, EuroSTARRS and FROG campaign. For WISE data, the best suited measurements to study the retrieval problems are the data acquired with elevation scans, and in particular data acquired with scans at 9 angles (25°, 30°, 35°, 40°, 45°, 50°, 55°, 60° and 65°), unless when specified. Regrettably not a lot of scans were performed for 9 incidence angles. On the other hand a set of elevation scans measurements were performed in steps of 10° (5 different incidence angles), but they are not as much useful as the case before. During EuroSTARRS measurements where done in 6 fix incidence angles (the radiometer has 6 beams). For FROG campaign, measurements were done with 25 incidence angles, in 1° steps.

All atmospheric corrections has been done; Up-welling and down-welling corrections and cosmic and galactic noise correction. However Faraday rotation is not necessary to correct for, since at the height of measurement, this effect is not present (this is produced in the ionosphere).

5.2 Number of incidence angles

As explained before, the acquisition strategy of WISE campaign was to measure brightness temperature in both polarisations (H and V) with three different modes of measurements:

- Mode 1, fixed observations: Long observations (1h.) at fixed incidence and azimuth angles to study the stability time scale of the sea state and its consequences on L-band emissivity.

[2]Sometimes, when some parameters other than SSS are considered as unknowns they are also called free, since they are not set to a specified value.

- Mode 2, azimuthal scan: 6 angular positions in 140º at fixed incidence angle, to study the azimuthal modulation at L-band. Measurements were 20 minutes long.

- Mode 3, elevation scans between 25° to 65°. In WISE 2001 two types of elevation scans where performed. The first was with steps of 10° pointing towards the west. The second one acquired data in steps of 5° and the radiometer was pointing towards the North, this was done during sun-shine. Mode 3 was specially selected to study the emissivity forward model at L-band.

The measurements performed in elevation scan (mode 3) are the best suited to study retrieval problems, and in consequence, these are the ones used in this work.

Figure 5.1 shows the error in the retrieved salinity (using the semi-empirical emissivity model dependent on U_{10}) as a function of the number of incidence angles. The number of incidence angles acquired (x axis) comes from five or nine different acquisitions angles per two polarisations minus the discarded measurements. Measurements were discarded when the level of radio frequency interferences (RFI), present during the whole measurement or part of it, led to too large variance in T_B values. The plot shows that the SSS retrieval quality increases with the number of acquisition angles used in the retrieval. This conclusion could be expected, since with more independent views of the same target, better will be the retrieved parameter, because the noise in each measurement has less weight.

5.3 Models comparison with salinity retrieval

In chapter 3, three groups of models have been presented: dielectric permittivity models, wave spectrum models, and scattering models. In this section the retrieved salinity results by using different combinations of them are compared and evaluated.

5.3.1 Dielectric permittivity models

The three constant dielectric models which are presented in section 3.1.1 have been used to retrieve salinity from 20 files acquired during the FROG experiment. These files were obtained for a completely flat surface, with elevation scans between 25° and 50° in steps of 1°.

In this retrieval process a cost function with restrictions is considered, and the parameters used are the following: $SSS_{ref} = SSS_{insitu} + 0.5$, $\sigma^2_{SSS} = 1.0$

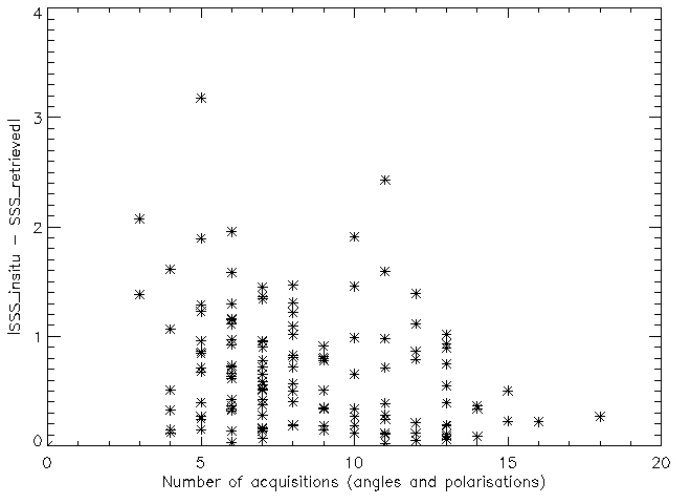

Figure 5.1: Retrieved salinity errors as function of the number of acquisition angles. The computations were performed with the semi-empirical model dependent on U_{10}.

psu and the initial guess for SSS was set to 37.5 psu. The model that has been used is the Fresnel reflection with the $\Delta T_{B\,rough}$ equal 0, since no roughness was present (flat surface).

Table 5.1 summarises the mean and the variance of the retrieved salinity results ($\Delta SSS = |SSS_{insitu} - SSS_{retrieved}|$) for the 20 files, for the three models. The retrieved salinities are compared with the salinity measured in situ by the MICROCAT instrument which has an absolute accuracy of 0.02 psu. The table shows that the model that makes a prediction of T_B closer to the measurements is the Klein & Swift model. Blanch & Aguasca shows relatively close behaviour, while Ellison model gives seriously biased results.

Dielectric const. model	$\overline{\Delta SSS}(psu)$	$\sigma^2_{\Delta SSS}$
Klein & Swift	0.261	0.025
Ellison	2.125	0.511
Blanch & Aguasca	0.596	0.061

Table 5.1: Comparison of retrieved salinity errors when using different dielectric constant models and FROG data set.

For the following calculations the Klein & Swift dielectric constant model has been used, except when explicitly stated.

Only the FROG data set has been used in this study, because only this one permits to isolate the problem of the dielectric constant from other issues which are not well known (for example the effect of roughness in emissivity). This is because during FROG the measurements were done with completely flat water surface.

5.3.2 Scattering and wave spectrum models

Results from WISE data set

Four different combinations of scattering and wave spectrum models have been used to retrieve salinities from the WISE 2001 data set. The four combinations used are dependent on the wind speed only and are the following:

- Two-scale Method with Durden and Vesecky spectrum × 2.
- SPM/SSA scattering model with Elfouhaily wave spectrum
- Semi-empirical model with Hollinger's linear regression model (equation 3.3)
- Semi-empirical model with WISE's derived linear regression model, which depends on wind speed (equation 3.4).

These models have been run over 25 different files obtained during WISE2001 with 9 different elevation angles. They were acquired on different days and therefore under different wind and temperature conditions. In order to run the algorithm to retrieve salinity, in addition to the measured T_B, it is necessary to introduce as input the wind speed and sea surface temperature. For that, data measured by oceanographic and meteorological buoys and have been used.

Figure 5.2 shows the difference between the in situ salinity (with an absolute accuracy of 0.02 psu) and the retrieved salinity for the models under study, when no restrictions were considered. It shows that the model that best fits in situ measurements is WISE-derived model, as was expected since a model function derived from the same data set is used. The mean and the variance of the errors in the retrieved salinities for the 25 files have been calculated and are presented in table 5.2.

The retrieved salinities have also been obtained using the individual points of the WISE-derived model, measured T_B for a specific U_{10} instead of the linear

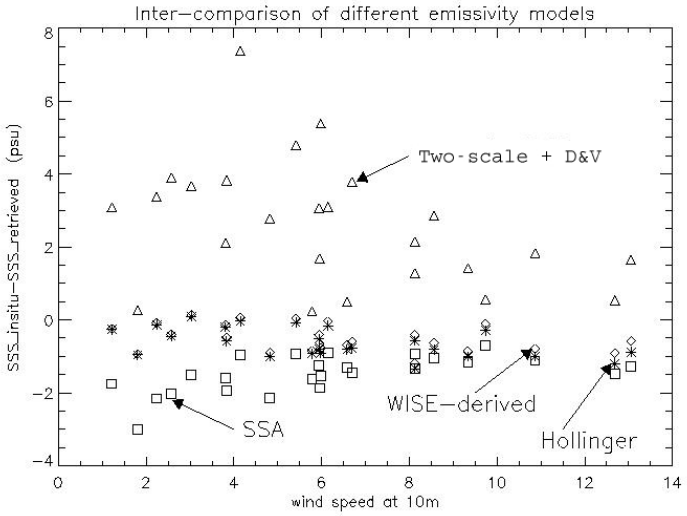

Figure 5.2: Error on the salinity retrieved using different emissivity models.

fit. The results demonstrate that the approximation made with the linear fit produces the errors in the retrieved salinity by less than 0.01 psu.

The Two-Scale model always highly underestimates the salinity. This problem could be due to a bias on the modelled T_B of about 1-1.5K that produces a negative bias of 2-3 psu in the salinity. It may also be due to a weak wind dependence that forces the algorithm to decrease salinity in order to increase T_B.

The SSA model overestimates salinity, i.e. the wind dependence is too high. In figure 5.3 it can be observed that the accuracy on the retrieved salinity is poorer for events with low wind speed and small waves than in other conditions. This is in agreement with Voronovich and Zavorotny (2001), because they conclude

Model	$\overline{\Delta SSS}$ (psu)	$\sigma^2_{\Delta SSS}$
Hollinger's model	0.63	0.15
WISE-derived model	0.52	0.12
Two-scale + Durden & Vesecky ×2	4.28	3.18
SSA + Elfouhaily	1.48	0.27

Table 5.2: Mean and variance of the retrieved salinity errors for different models, considering $\Delta SSS = |SSS_{insitu} - SSS_{retrieved}|$.

that the Elfouhaily spectrum overestimates the probability of having short waves by 2-4 dB in the cross-wind direction. The results show that this model is not recommended for low wind events.

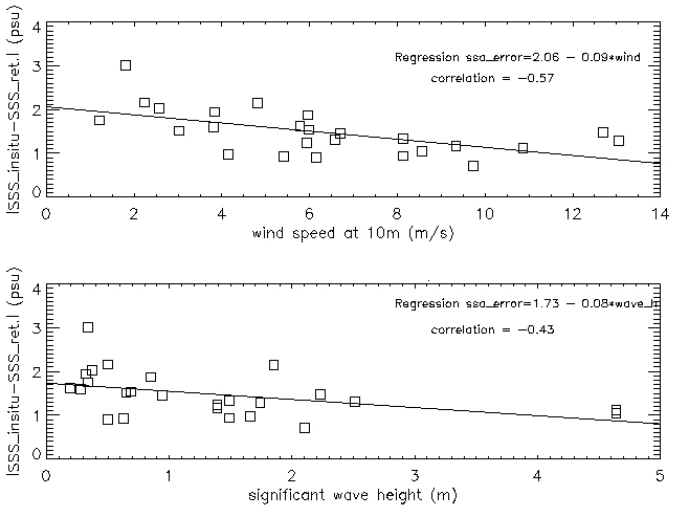

Figure 5.3: Error on the salinity retrieved when using the SSA + Elfouhaily model as function of the wind speed and significant wave height.

From these results it can be concluded that semi-empirical models seem to recover salinity better than the analytical ones, and that the best model to use in order to retrieve salinities from WISE data is the WISE-derived model.

Figure 5.4 shows that the error in the retrieved salinities using the WISE-derived model tends to increase linearly with increasing wind speed and wave height. This effect can be explained by the fact that the influence of foam has not been taken into account in the models. Normally, the foam coverage increases with wind speed (or wave height) and its effect can be considered negligible only with wind speeds below 10m/s. The foam increases the brightness temperature. If this $\Delta T_{B\,foam}$ is not expressed in the model equations, the inversion algorithm will decrease the salinity to compensate for this increase in T_B. On the other hand, as the model was derived from measurements, and more measurements for low wind speeds than strong wind speeds were acquired, higher uncertainties appear for the high wind speed region.

Vall-llossera et al. (2003) showed that models and WISE measurements have some disagreements with $\Delta T/\Delta U$, especially at low wind speeds. Figure 5.5 plots the sensitivity of T_B to U_{10} respect to U_{10} and θ_i for Durden and Vesecky×2, Elfouhaily×2 and Kudryavtsev. It can be seen that their behaviour mainly differ

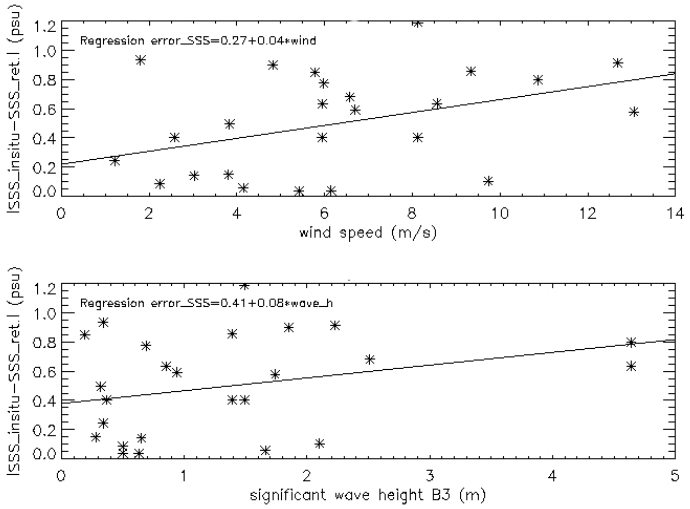

Figure 5.4: Error on the salinity retrieved when using the WISE-derived model as function of the wind speed and significant wave height.

for low wind speeds, since for that range the sensitivity is high non-monotonic. Therefore, since 45% of measurements in WISE 2001 campaign were performed in the range of 0-5m/s, 34% in the range 5-10m/s and only 21% for higher winds than 10m/s, it is clear that an error in the computed sensitivities at low wind speeds has a large impact in the mean salinity error values.

This different behaviour of the sensitivity of T_B for low wind speed with respect to higher values has also been observed with WISE 2001 measurements by Etcheto et al. (2004). They observed that $\Delta T_{B\,rough}$ abruptly decreases for wind speed lower 3 m/s, as shown in figure 5.6. This behaviour was observed at 2.65 GHz by Blume et al. (1977) during a flight above Chesapeake Bay. It is known that the scatterometer measurements are very inaccurate below 3 ms^{-1}. The reason for this decrease is probably the threshold effect in the generation of capillary waves: the wind speed needs to be above a threshold for the friction to overcome the viscosity effects of the water.

For these calculations the WISE-derived model used to retrieve salinity, is the one which is computed when all that points are used.

Another way to retrieve salinity is to use a model that considers the sea surface roughness term as a function of the significant wave height instead of the wind

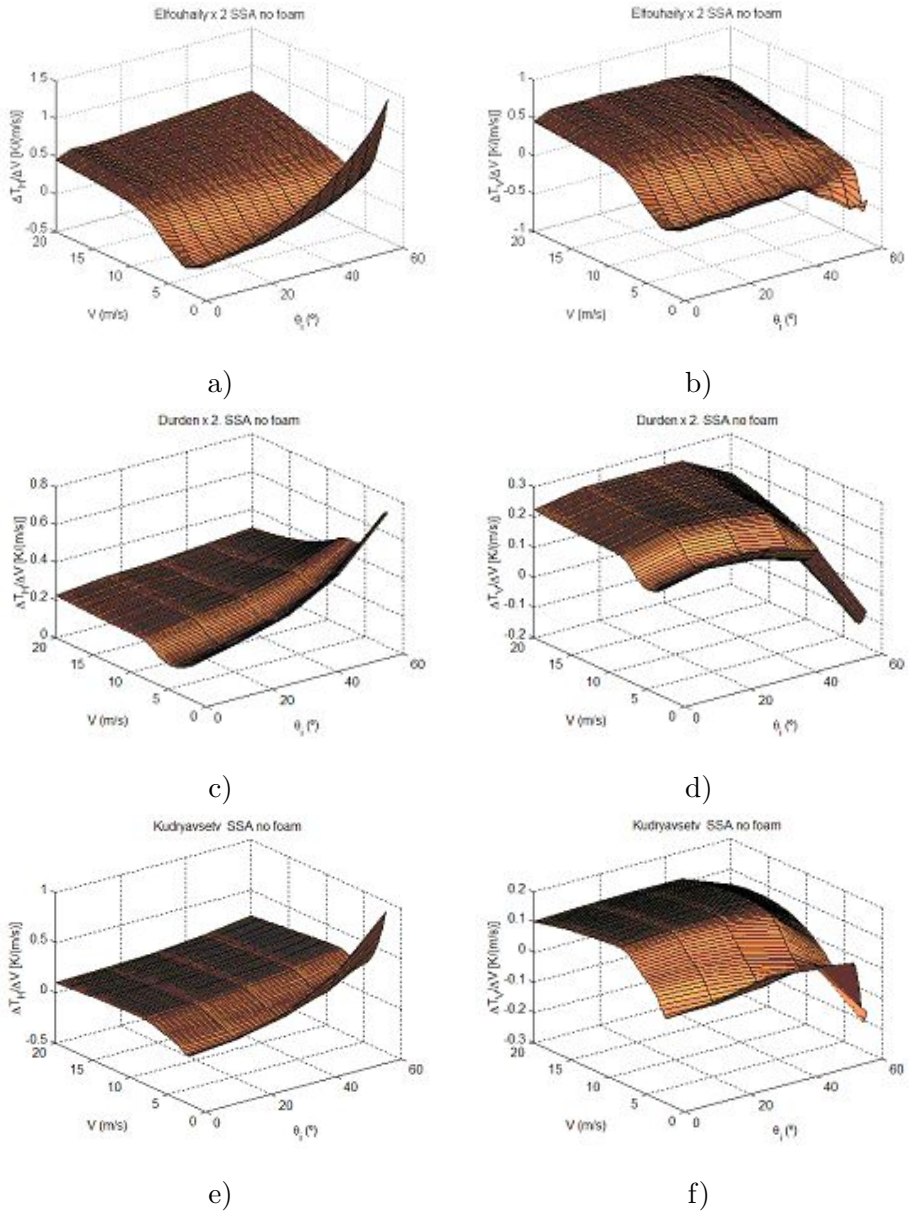

Figure 5.5: $\Delta T_h/\Delta U_{10}$ respect to U_{10} and θ_i predicts by SSA for a) Elfouhaily×2 c) Durden and Vesecky×2 e) Kudryavtsev. $\Delta T_v/\Delta U_{10}$ respect to U_{10} and θ_i predicted by SSA for b) Elfouhaily×2 e) Durden and Vesecky×2 f)Kudryavtsev (from Vall-llossera et al. (2003)).

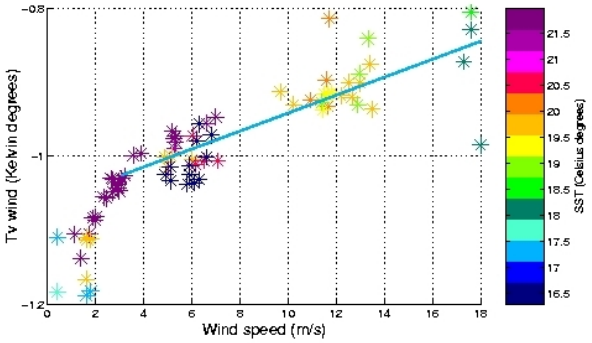

a)

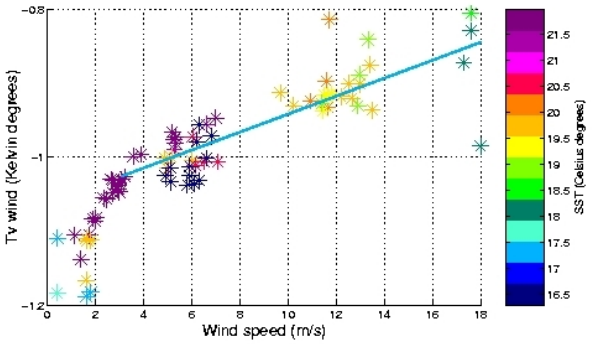

b)

Figure 5.6: $T_{B\,rough}$ in vertical (a) and horizontal (b) polarisations measured at 44° incidence angle from WISE 2001 measurements. (from Etcheto et al. (2004)).

speed. The advantage of this dependence should be that the wave height is not as variable as the wind. In addition, surface roughness may be due to the swell and not only to wind waves. The theoretical spectrum models usually consider fully developed seas dependent only on the actual local wind (they usually neglect the swell effect).

Salinity retrieved errors have also been calculated when using the WISE-derived semi-empirical model, presented in section 3.2.2, which is dependent on significant wave height.

In addition, model-2P, which depends on both wind speed and significant wave height presented in section 3.2.3, has been used to compute the retrieved salinities as well.

Table 5.3 compares the errors on retrieved salinities when using the three WISE-derived models: the U_{10} dependence model, the SWH dependence model and model-2p that depends on both. The data used here are the measurements acquired at 9 different incidence angles that where pointing towards north. The buoys measurements of U_{10} and SWH have been used. The model of SWH dependence does not give satisfactory results, probably due to the fact that the dominant wind during WISE 2001 was from the North. Then some reflection waves produced by the platform legs were observed when using observations from this direction. Of course, the most sensitive model to these roughness deformations is the SWH dependence model. The table shows that the model dependent on the two parameters is the one that better retrieves salinity from radiometric measurements.

Model	$\overline{\Delta SSS}$ (psu)	$\sigma^2_{\Delta SSS}$
U_{10} dependence	0.52	0.12
SWH dependence	0.80	0.34
U_{10} & SWH dependence	0.33	0.05

Table 5.3: Mean and variance of the retrieved salinity errors using three WISE-derived models, considering $\Delta SSS = |SSS_{insitu} - SSS_{retrieved}|$. Measurements were done with scans of 9 incidence angles, pointing towards north.

Also a comparison of the three WISE-derived model has been performed, using not only the 25 mentioned data files but a total of 132 measurements from WISE with incidence angles varying from 2 to 9 values. The results of comparing the three models are shown in table 5.4. These values are worse than in the case above, since all the recorded data have been now considered, even though corresponding to cases were few incidence angles were acquired, and so

this produces a reduction on the quality of retrieved salinities.

Model	$\overline{\Delta SSS}$ (psu)	$\sigma^2_{\Delta SSS}$
U_{10} dependence	0.68	0.30
SWH dependence	0.69	0.39
U_{10} & SWH dependence	0.56	0.26

Table 5.4: Mean and variance of the retrieved salinity error using three WISE-derived models considering $\Delta SSS = |SSS_{insitu} - SSS_{retrieved}|$. 132 files measurements, with incidence angles from 2 to 9 have been used.

The average error on the retrieved salinity obtained with this derived model-2P is considerably smaller than using other models that considers only local wind speed or wave height. The standard deviation has also been reduced. A reduction in the error budget is expected in any regression when the degree of freedom is increased. However, in this case it has a physical meaning since SWH data contain information from processes that modify the sea surface spectrum other than contemporaneous local winds. Considering only SWH is not enough (as shown in the results), since it does not provide information on the wind-induced capillary waves. The substantial reduction on the SSS error (about 35%) when using this model confirms that swell and varying winds play an important role in the final balance of sea emissivity.

Results from EuroSTARRS dataset

These models have also been applied to retrieve salinity from the EuroSTARRS data set, although the radiometric data happened to be very noisy and some beams were affected by calibration problems.

If only one measurement, of six beams, is used to retrieve salinity, the error on the SSS retrieved is large (~ 3 psu), since noise and other errors are present on the measured value. On the other hand, if several T_B measurements are averaged, before doing the retrieval process, better salinity values are retrieved. This is because the averaging performs a reduction of the uncorrelated noise by a factor of $\sqrt{N}$ (being N the number of averaged data). This technique can only be used when very similar conditions are present. For example, a change on SSS would produce a change on T_B, and by averaging it could be masked.

A sequence of 762 T_B measurements along a straight line over relatively homogeneous fields has been averaged to retrieve salinity. The flight height for this line was 2700 m. Table 5.5 shows the errors on the retrieved salinities from this

averaged value. These confirm that the new model-2P retrieves salinity better than the models only dependent on U_{10}. Results underline, again, that semi-empirical models give better results than theoretical ones. The table shows up, also, the tendency of the two scale model to underestimate the retrieved salinity and the tendency of the SSA model to overestimate it, since during this campaign the wind speed was low, and then the error important, as also observed for the WISE data sets.

These EuroSTARRS results are highly improved with respect to WISE results due to the large number of radiometer snapshot measurements averaged before retrieval.

Model	ΔSSS (psu)
Hollinger's model U_{10} dependence	0.24
WISE-derived U_{10} dependence	0.35
Two-scale + Durden & Vesecky × 2	-3.07
SSA + Elfouhaily	5.17
WISE-derived U_{10} & SWH dependence	0.13

Table 5.5: Retrieved salinity error using WISE-derived U_{10} dependence and U_{10} + SWH dependence, considering $\Delta SSS = SSS_{retrieved} - SSS_{insitu}$ from EuroSTARRS data.

Part of this work has been published in Gabarró et al. (2003) and Gabarró et al. (2004b).

5.4 Impact on retrieved salinity of auxiliary parameters errors

To retrieve salinity from SMOS good quality auxiliary variables (wind speed, wave height and SST) are needed as simultaneous both in time and space as possible to the spaceborne radiometer measurements.

A theoretical study of the impact on the retrieved SSS of errors on the auxiliary variables is shown in figure 5.7. The semi-empirical model-2P has been used. The results are calculated by averaging 25 retrieved salinities from different measurements, and the standard deviations are expressed in the vertical bars of the plots. X-axis expresses the error on the auxiliary parameters, and Y-axis

plots the salinity retried error, when using the corresponding U_{10} error. When U_{10} error equals zero, salinity errors are not zero, since other sources of error are present in the brightness measurements.

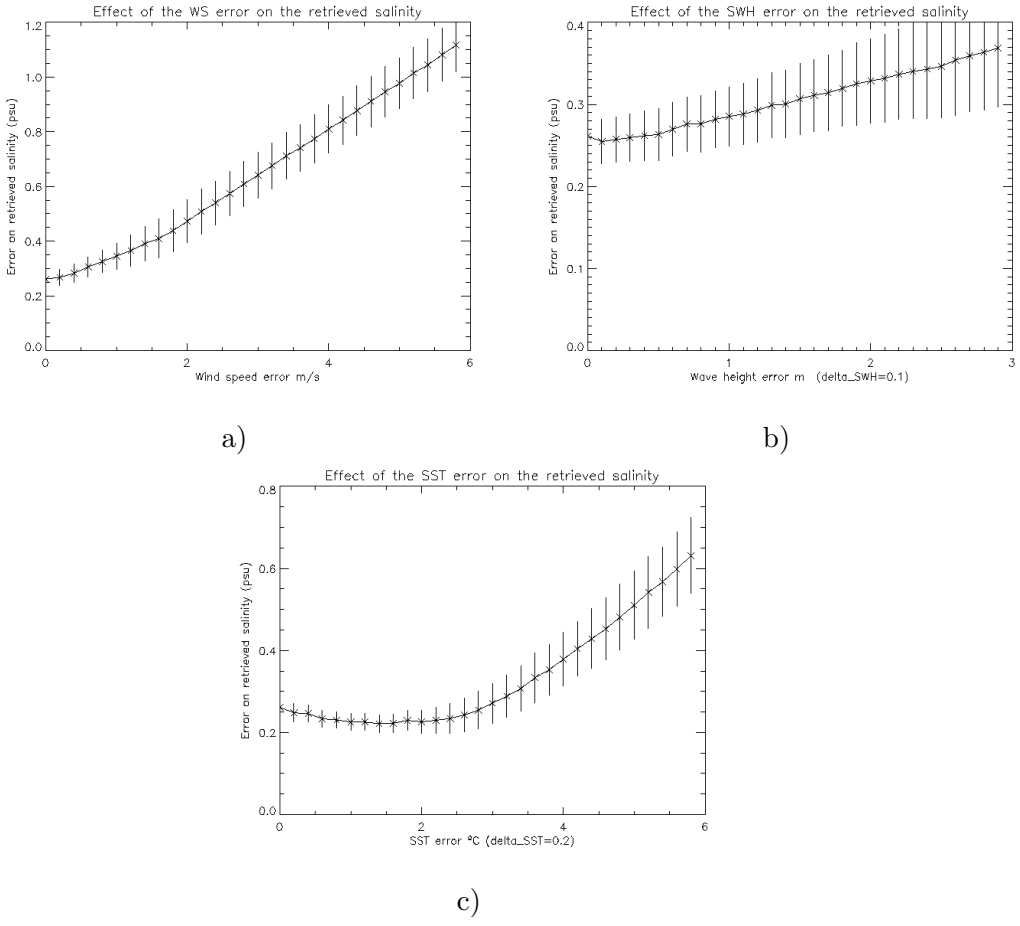

Figure 5.7: Errors on the retrieved salinity as function of errors on the auxiliary parameters, by using the model dependent on U_{10} and SWH. a) error on U_{10}, b) error on SWH and c) error on SST.

These plots show again that the auxiliary parameter that requires higher accuracy is the wind speed. For example, 2 m/s error on U_{10} produces an extra error (additional uncertainty over the case with zero U_{10} error) on the retrieved salinity of about 0.2 psu, and an error on SWH of 1 m brings to an extra error on salinity of less than 0.025 psu. On the other hand figure 5.7c shows almost no influence of the SST errors below 2.5 ^{o}C, and even an improvement on retrieved SSS for

SST 1.5 ºC above in situ values. This apparently anomalous behaviour (results in fact are indistinguishable within error bars) requires additional investigation.

This section also studies the salinity retrieved errors when using different existing sources of auxiliary parameters, in particular wind speed and significant wave height. In chapter 4 some sources have been presented, the theoretical accuracies have been discussed, as well as the time and space resolutions for each source.

The errors on the retrieved salinities, from WISE 2001 dataset, when setting the parameters to different combinations of U_{10} and SWH sources are presented in table 5.6. These values have been computed using the semi-empirical model-2P, since in the above sections it has been shown to be the best model to retrieve salinity from WISE and EuroSTARRS dataset. Cost functions without constrains is considered.

Source U_{10}	Source SWH	ΔSSS	ΔU_{10}	ΔSWH
In situ	in situ	0.33	–	–
HIRLAM	WAM	0.59	1.98	0.22
ARPÈGE	WAM	0.49	1.94	0.22
QuikSCAT	ERS	0.61	1.59	0.46

Table 5.6: Retrieved salinity error using WISE-derived model-2P, considering $\Delta P = |P_{insitu} - P_{retrieved}|$, being P each parameter, from WISE 2001 data set.

The table shows that that an important deterioration is suffered by the retrieved salinity when fixing the auxiliary parameters to data obtained from external source.This is because these data have some accuracy errors as well as a spatial and temporal lack of simultaneity between its acquisitions and radiometric measurements. It also manifest that the usage of meteorological (HIRLAM, ARPEGE) and oceanographic (WAM) model data (with assimilation of spaceborne observations) is better than to use satellite data directly, since the latter have much worse temporal resolution.

5.4.1 Auxiliary parameters obtained from the T_B

With the above situation in mind other possible ways for obtaining the parameters information have been studied in this thesis.

As explained before, SMOS, as well as WISE and EuroSTARRS measurements form overestimated systems, since there are more measurements than un-

knowns. Then the possibility of retrieving the auxiliary parameters from brightness temperature measurements themselves as well as the salinity has been investigated.

The model-2P is used in the retrieval algorithm. Firstly the cost function without restrictions has been employed to retrieve salinity, wind speed and wave height. The sea surface temperature has been fixed by in situ measurements. The inversion algorithm has been modified now to consider U_{10} and SWH as parameters to retrieve as well as salinity. The first guess values given to the inversion algorithm are: for salinity 37.5 psu, for U_{10} the HIRLAM output data and for SWH the WAM output data. After some iterations the algorithm converges.

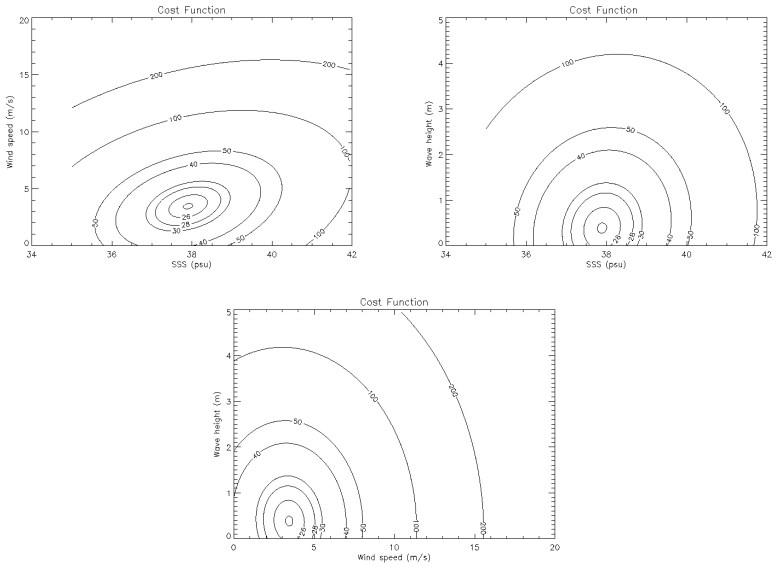

Figure 5.8: Cost function contour plot when varying SSS, U_{10} and SWH parameters.

Figure 5.8 plots the cost function behaviour when varying SSS, U_{10} and SWH. It shows that it is a convex function and consequently only one minimum is present, i.e. there is not the possibility that the solution falls down into a local minimum. This situation persists for both cases: when restrictions and no restrictions are considered in the cost function.

When performing the inversion algorithm with the cost function without constrains from the WISE 2001 data, the retrieved parameter errors are $\overline{\Delta SSS} = 0.40$, $\overline{\Delta WS} = 1.22$ and $\overline{\Delta SWH} = 2.44$.

The comparison of these results with the ones presented in table 5.6 (lines 2 to 4), reveals that better results are obtained when considering the auxiliary

parameters as variables to be optimised, than fixing them with excessively erroneous values (those provided by models). Furthermore, the error on the wind speed retrieved with the optimisation process is smaller than model outputs and satellite errors. Figure 5.9 compares the results of retrieved U_{10} with in situ measurements and HIRLAM output model for several measurements. It shows that the retrieved U_{10} is closer to in situ measurements than the HIRLAM output, even though these values were used as first guess values. So it seems that by leaving U_{10} as parameter to be retrieved, the algorithm can improve its initial values. On the other hand, the significant wave height has not been retrieved with good quality.

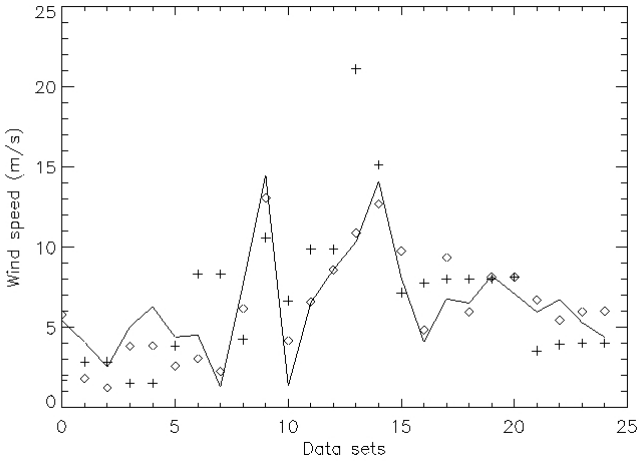

Figure 5.9: Comparison of the wind speed measurement determinations: measured in situ (diamonds), output from HIRLAM (crosses) and retrieved by the algorithm when it is set to retrieve wind speed (line).

In a second step, a cost function with constrains has been used to retrieve all these parameters, and has been shown to obtain better results than when no constrains are considered, as it is explained below.

The cost function with restrictions requires to have a reference value for each parameter to calculate and its expected error (σ_p^2). For the case study, the cost function results as follows:

$$\chi^2(SSS, SST, U_{10}, SWH) = \sum_{i=0}^{N-1} \frac{[\, T_{B_i}^{meas} - T_{B_i}^{model}(\theta_i, SSS, SST, U_{10}, SWH)\,]^2}{\sigma_i^2} + \frac{[\, SSS - SSS_{ref}]^2}{\sigma_{SSS}^2} + \frac{[\, U_{10} - U_{10\,ref}]^2}{\sigma_{U_{10}}^2} + \frac{[\, SWH - SWH_{ref}]^2}{\sigma_{SWH}^2} \tag{5.3}$$

A comparison of retrieved salinities with insitu measurements when using several auxiliary parameters combinations has been performed. Calculations have been done considering the following parameters: $\sigma_{T_B} = 1.0$ K, $\sigma_{SSS} = 0.5$ psu, $\sigma_{U_{10}} = 2.0$ m/s, $\sigma_{SWH} = 0.5$ m, $SSS_{ref} = 37.7$ psu, $U_{10\,ref} = HIRLAM$, $SWH_{ref} = WAM$. The emissivity model-2P has been used for the calculations.

The new method of permitting the auxiliary parameters to be retrieved from radiometric measurements has been used, also. Table 5.7 summarise all these results, and it reveals the same conclusions as before: It is much better to retrieve all these parameters from radiometric measurements themselves than fixing them to an erroneous value.

Source U_{10}	Source SWH	$\overline{\Delta SSS}$ (psu)	$\sigma^2_{\Delta SSS}$
In situ	in situ	0.13	0.01
HIRLAM	WAM	0.33	0.06
ARPÈGE	WAM	0.26	0.06
QuikSCAT	ERS	0.30	0.08
Free	free	0.16	0.02

Table 5.7: Retrieved salinity errors using model-2P, and cost function with restrictions, from WISE 2001 data-set.

The comparison between tables 5.7 and 5.6 shows that better results are obtained when considering constrains in the cost function, since in the latter more information is given to the algorithm.

Quality of the reference parameters

Since by enhancing the quality of the reference values the quality of the retrieved salinity is improved. To try to understand a little bit better this problem, an analysis of three different conditions on the reference value qualities has been done. The considered conditions are the following:

1. Good conditions: The reference values of the parameters are known with good quality, then their variance are low. The values are: $\sigma_{T_B} = 1.0$ K, $\sigma_{SSS} = 0.5$ psu, $\sigma_{U_{10}} = 2.0$ m/s, $\sigma_{SWH} = 0.5$ m, $SSS_{ref} = 37.7$ psu, $U_{10\,ref} = HIRLAM$, $SWH_{ref} = WAM$.

2. Relaxed conditions: The reference values of the parameters are considered to be a little bit worse than in the case before. The values are: $\sigma_{T_B} = 1.0$ K, $\sigma_{SSS} = 1.0$ psu, $\sigma_{U_{10}} = 2.5$ m/s, $\sigma_{SWH} = 1$ m, $SSS_{ref} = 37.7$ psu, $U_{10\,ref} = HIRLAM$, $SWH_{ref} = WAM$.

3. Bad conditions: The reference values of the parameters are not known with good accuracies. This is a similar situation to the SMOS situation, since it will be impossible to have these reference values coincident in time and space to the SMOS track. The values chosen here are: $\sigma_{T_B} = 1.0$ K, $\sigma_{SSS} = 2.0$ psu, $\sigma_{U_{10}} = 3.5$ m/s, $\sigma_{SWH} = 2.0$ m, $SSS_{ref} = 37.7$ psu, $U_{10\,ref} = HIRLAM$, $SWH_{ref} = WAM$.

For the above conditions, the reference values are the same for the three cases but the expected quality σ_P of them are different. Following these conditions the three parameters have been retrieved from WISE 2001 dataset, by using only the files with 9 incidence angles.

Table 5.8 summarises the retrieved values of the parameters (SSS, U_{10}, SWH) and shows that, as expected, better knowledge of the reference values leads to better retrieved parameters. For each condition, the table shows two results. The first one represents the case of knowing exactly the SST value, by using in situ measurements, while the second one is the case of having a bias on the SST of 1°C. Results also indicate that an error on the SST measurement of 1°C does not introduce significant additional errors on the retrieved parameters, and in particular to the retrieved salinity, that is the most important parameter to retrieve.

Figure 5.10 plots the SSS, U_{10} and SWH retrieved for the case of good conditions. The plot shows that the retrieved values are closer to the in situ measurements than the model output, which have been used as references values. It means that this method can improve the given reference values.

Conditions	$\overline{\Delta SSS}$ (psu)	$\overline{\Delta U_{10}}$ (m/s)	$\overline{\Delta SWH}$ (m)
Good conditions with in situ SST	0.16	1.05	0.37
Good conditions with in situ SST+1°C	0.17	1.09	0.37
More relaxed conditions with in situ SST	0.28	1.11	0.48
More relaxed conditions with in situ SST+1°C	0.32	1.08	0.48
Bad conditions with in situ SST	0.35	1.15	1.14
Bad conditions with in situ SST+1°C	0.41	1.13	1.13

Table 5.8: Retrieved salinity error using model-2P, for the three conditions and using restrictions on the cost function.

Also, a study to understand the dependences of the retrieved salinity on the quality of the reference values, when fixing the σ_p of the parameters, has been developed.

Plots in 5.11 show the retrieved salinity errors as function of errors on reference salinity value (x axis), for the same σ_{SSS}, and errors on reference wind speed values (c). The errors of the reference salinity values are calculated by the differences between the SSS_{ref} and the in situ measurements. Errors on two different conditions have been calculated, plot (a) is for good conditions, and plot (b) is for relaxed conditions. The plots show that by deteriorating the SSS reference value (always obeying the σ_{SSS} condition) the retrieved salinity is worse, and the standard deviation increases. The plots also compare the results when restrictions and no restrictions are considered, and in general better results are obtained with the former case. When worsen the U_{10} and SWH references values (figures c) and d)), the impact on the SSS retrieved is ≈ 0.02 psu, which is negligible.

Further work should be done to study the required quality of the SSS_{ref} for SMOS, and to find the way of obtaining this best reference value for SSS.

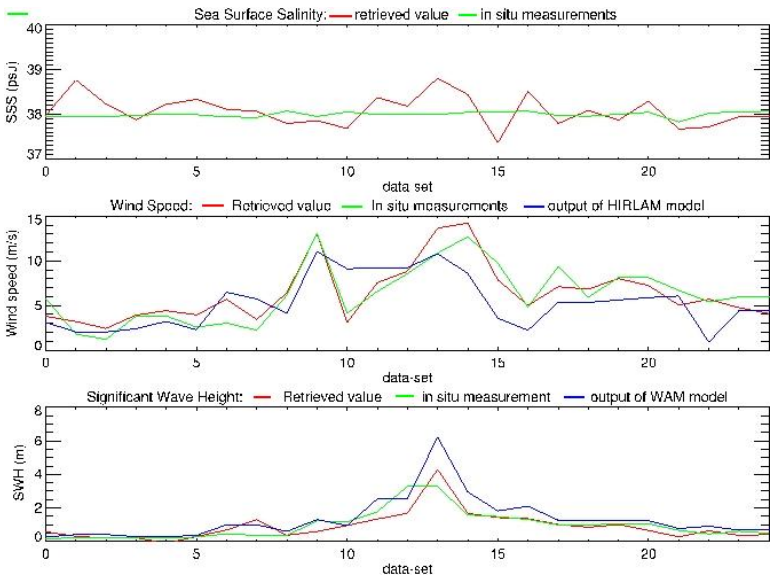

Figure 5.10: Comparison of the SSS, U_{10} and SWH calculated from different methods: measured in situ (green), output models (blue) and retrieved from radiometric measurements with restrictions (red).

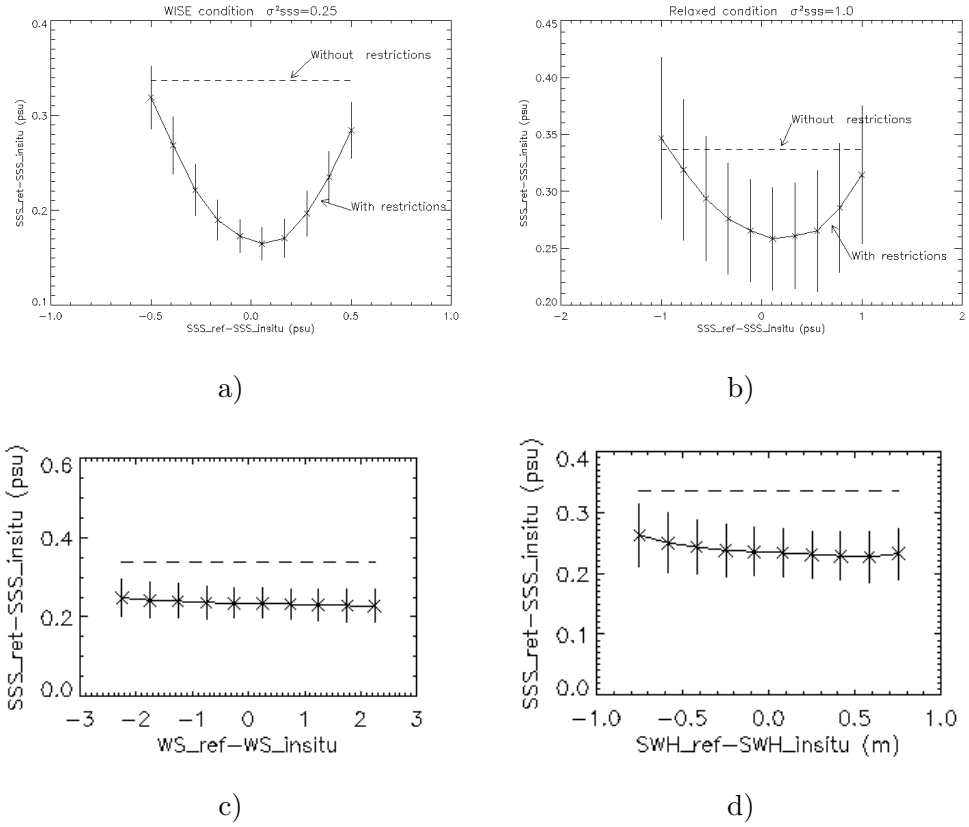

Figure 5.11: Plots of the retrieved SSS error (y axis) as function on the reference error (x axis). a) Calculations done with good conditions, b) calculations done with relaxed conditions. Vertical lines are the standard deviations. c) Retrieved SSS errors when the reference value of wind speed varies, for the case of relaxed conditions. d) Retrieved SSS errors when the reference value of SWH varies. This is done for two cases, when cost function with constrains are considered and when no constrains are considered.

SST parameter

The possibility of allowing the SST to be retrieved also with the inverse algorithm instead of setting it to a fixed value has been analysed as well.

Figure 5.12 shows the aspect of the cost function when varying SSS and SST values. Firstly it has been computed using no restrictions, and it shows that the function does not have a clear minimum (left plot). This is because T_B is highly non-linear with SSS and SST. On the other hand, when using restrictions, i.e. allowing only some possible solutions, the cost function presents only one minimum (right plot).

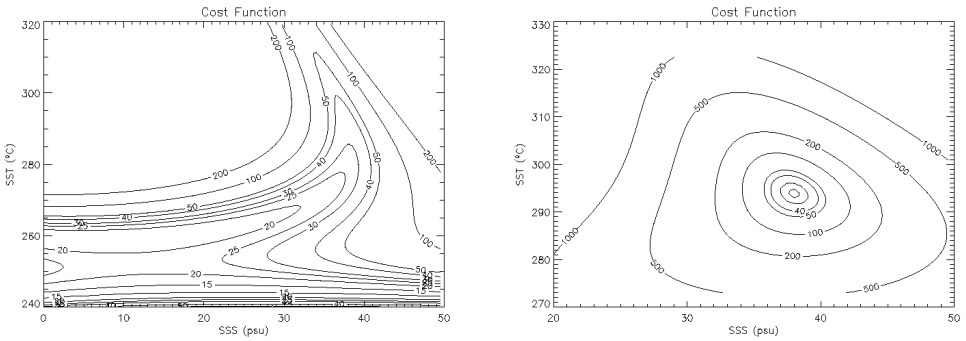

a) b)

Figure 5.12: Cost function contour plot when varying SSS and SST parameters. a) when no restrictions are considered in the cost function, b) when restrictions are considered.

The results of the 4 retrieved parameters are summarised in table 5.9, when restrictions are considered.

Conditions	$\overline{\Delta SSS}$ (psu)	$\overline{\Delta U_{10}}$ (m/s)	$\overline{\Delta SWH}$ (m)	$\overline{\Delta SST}$
Good conditions	0.16	1.08	0.28	0.66
More relaxed conditions	0.25	1.13	1.48	0.64

Table 5.9: Retrieved salinity error using WISE-derived model-2P, when SST is a parameter to retrieve.

Comparisons of the above table with table 5.8 shows that a small improvement (0.01-0.06 psu) occurs when considering SST as a parameter to retrieve with

respect to fixing SST to a value with 1°C of error. Since SST measurements are obtained from satellites and models with an accuracy better than 0.5°C and high temporal resolution, this parameters does not represent a problem for the SMOS retrieval process.

5.5 Retrieved salinity from the Plata survey

For the Plata campaign the STARRS instrument calibration was clearly improved with respect to EuroSTARRS campaign, and several tests shown that radiometric measurements suffered fewer noise than during EuroSTARRS measurements. Another advantage that presents this survey with respect EuroSTARRS is that the sea in La Plata delta area presents important variations on salinity, which ranges from 28 psu to 36 psu, since La Plata river brings an important amount of fresh water to the ocean. This will allow to investigate if salinity changes are detectable with the STARRS instrument.

A draw back of this data-set is that in situ measurements performed by the oceanographic ship were, most of the time, not simultaneous with the plane track. The lack of precise auxiliary parameters makes more difficult the validation of the retrieved salinity.

Figure 2.14 shows the ship and the plane tracks over the area of LaPlata Delta. For the retrieval process analysis, only data of LEG2 transect called 'Rio Grande' has been used. This transect starts near the coast and finishes at 185 km (100 nautical miles) offshore, and is located in the North of the delta of the river. Since the currents in the area follow a South-North direction near the coast, the transect traverses an important gradient of surface salinity, being fresher water near the coast and saltier offshore (see figure 2.14c). Three areas of this track have been selected to perform the retrieval process, as they present different salinities and few variation on pitch and roll of the plane.

Figure 5.13 shows the salinity measured by the thermosalinograph and the interpolated wind speed measured in the CTD stations as function of time, for the whole LEG2 transect. It has to be remarked that the ship survey wan in the area 4 days before the STARRS plane measurements. Therefore the wind speed data is not reliable any more after 4 days, but in the other hand, SSS is not suppose to suffer large changes in that period of time. The three areas used for the analysis are marked as A, B and C. Each part has been chosen to be 300 radiometric measurements long, to be comparable with WISE measurements, in which each angle measurement was averaged during 5 minutes, and one measurement was done every second (i.e. 5*60=300).

Bias on the pitch and roll of the plane produce an increment/decrement on T_B measured, depending on the incidence angle. For example 1° of roll produce

an increment on T_B of 1.23 K at the 38.5° incidence angle beam. Corrections for that misalignment of the plane have been performed. On the other hand, the galactic noise has not been corrected for, since that data are not available at the time of writing this document, so a fixed value of 3.8 K has been considered. The up-welling, and down-welling atmospheric corrections have been done as well as the correction for the cosmic noise.

The cost function with constrains has been used to retrieve salinity from STARRS data over the Plata area. Three semi-empirical models have been compared; Hollinger and WISE 2001 models, which only depend on U_{10}, and the WISE derived model-2P, which depends also on the SWH. Since this last variable was not recorded in the campaign, the regression obtained from WISE2001 dataset ($SWH = -0.29 + 0.155U_{10}$) has been used to compute SWH as a very rough approximation.

The reference values used for the inversion algorithm with constrains were: $SSS_{ref} = SSS_{insitu} + 4.5$ psu, $U_{10\,ref} = U_{10\,insitu} + 3.5$, $SWH_{ref} = SWH_{calc} + 1$. The variance of those reference parameters have been fixed to: $\sigma_{T_B} = 1.0$ K, $\sigma_{SSS} = 5.0$ psu, $\sigma_{U_{10}} = 4.0$ m/s, $\sigma_{SWH} = 2.0$ m, therefore they are considered to be very poorly known, since salinity suffer big variations in a small area.

For this study three different methods of retrieval have been used. The first one considers only the SSS parameter to be retrieved, while U_{10} and SWH are fixed to the measured (or computed for SWH) values (this is called M1). The second method allows the algorithm to retrieve SSS and U_{10} while SWH is fixed to the computed value (M2). The last case is when all three parameters are considered to be retrieved from brightness temperature (M3). When using the models only dependent on WS then of course M3 is not used, and the comments on SWH do not apply.

Firstly the retrieved salinity has been calculated directly for individual T_B measurements, without performing any averaging. Figure 5.14 shows the retrieved SSS for each of the areas (300 points each) when using the model-2P for M1 and M2 methods. The variable line is the retrieved salinity while the stable line is the measured one. The plots show that the retrieved salinity follow the increments on SSS, except on area C, where retrieved salinity is highly underestimated. An explanation for that behaviour can not be found, since local wind speed or SWH at the time of radiometric measurements were not available.

However, by performing the average of several T_B measurements, the white noise of the measured value can be reduced. Therefore the average of 300 T_B measurements of each area has been done and a slight improvement on the retrieved values has been observed. The in situ measurements for each area are presented bellow, but it should be retained that the wind speed was measured 4 days before the radiometric measurements:

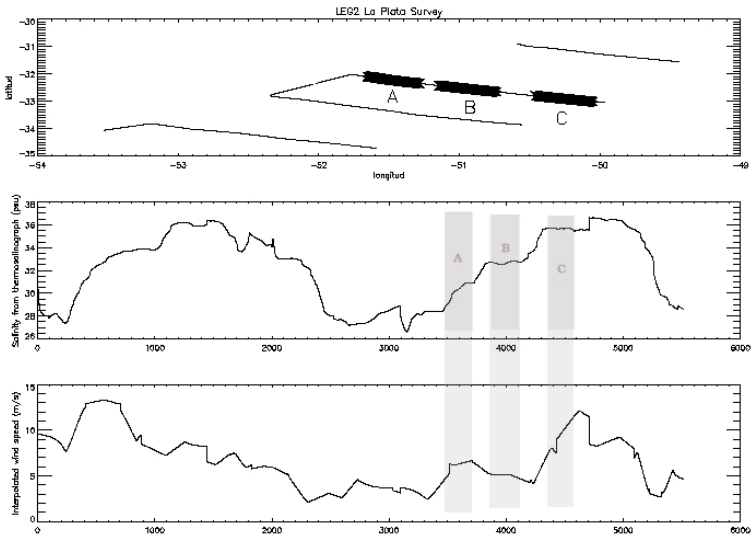

Figure 5.13: Top, LEG2 track map, middle, salinity measured by the thermosalinograph and bottom, interpolated U_{10} measured in the stations. The three study areas are marked by A, B and C.

- Area A : The in situ mean values are: $\overline{SSS_{insitu}} = 30.183$, $\overline{U_{10\,insitu}} = 6.022$ and $\overline{SWH_{calc}} = 0.645$
- Area B : the in situ mean values are: $\overline{SSS_{insitu}} = 32.692$, $\overline{U_{10\,insitu}} = 5.028$ and $\overline{SWH_{calc}} = 0.489$
- Area C : the in situ mean values are: $\overline{SSS_{insitu}} = 35.642$, $\overline{U_{10\,insitu}} = 9.987$ and $\overline{SWH_{calc}} = 1.258$

Retrieved results are summarised in tables 5.10, 5.11 and 5.12, for area A, B and C respectively. The inversion analysis has been performed for the three semi-empirical models and for the three methods explained above. Tables show the retrieved SSS, U_{10} and SWH.

Quite good salinity retrievals have been obtained from STARRS measurements from the Plata campaign. They show that the instrument is capable to distinguish between different waters with different salt concentration. Retrieved salinity errors better than 0.5 psu have been obtained for A and B areas.

A comparison of tables 5.10, 5.11 and 5.12 shows up that in general, better results are achieved when using the emissivity model-2P which is dependent on WS and SWH even though not significant differences are observed.

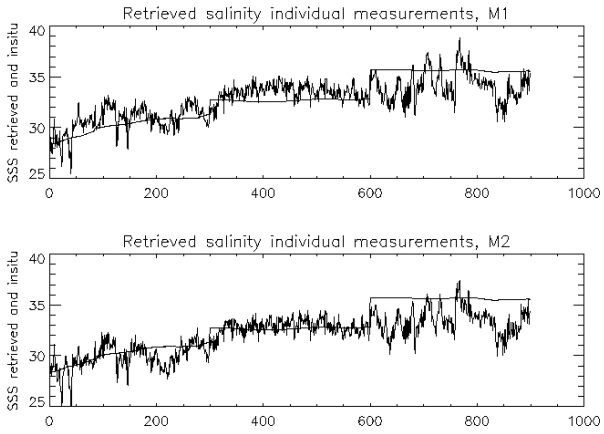

Figure 5.14: Retrieved salinity (variable line) for the three areas (each area is 300 measurements), when using the model-2P comparing with measured salinity (stable line). Top when fixing U_{10} to the measured values (M1), bottom when allowing U_{10} to be retrieved (M3)

Another important conclusion that can be derived is that much better results are obtained when allowing the inverse algorithm to retrieve WS as well as salinity than fixing it to an erroneous value. On the other hand, when allowing the algorithm to retrieve also SWH (M3) results get degraded. A possible explanation for that could be that few independent observations are obtained for each measurements, they are only 3 different incidence angles, since the instrument was mounted without tilt. Then the case of having 3 unknowns can not properly be resolved.

Bad retrieval results are obtained from area C, salinity is always underestimated. This area is the most offshore region from the transect analysed. May be the U_{10} was very high and important roughness was present for that period of time, but since this information is not available, a clear conclusion on why this SSS is poorly retrieved can not be given by the author.

A study of the errors on the retrieved salinity due to inaccuracies on the auxiliary parameters can not be done with this data set, since in situ data simultaneous with radiometric measurements have not been measured.

This analysis of the Plata campaign indicates again, that the model-2P, which depends on U_{10} and on SWH is the one that better retrieve salinity from radiometric measurements. Furthermore this analysis confirms the robustness of this model, even it was obtained under very different conditions from La Plata Delta area.

Area A	SSS_{ret}	ΔSSS	$U_{10\,ret}$	SWH_{ret}
Method	Model-2P			
M1	30.656	-0.473	-	-
M2	29.781	0.402	2.368	-
M3	27.804	2.379	5.924	-1.723
	Hollinger model			
M1	30.851	-0.668	-	-
M2	29.438	0.745	2.495	-
	WISE 2001 model			
M1	31.340	-1.157	-	-
M2	28.934	1.249	1.018	-

Table 5.10: Retrieved parameters for three different emissivity models and three different methods for area A. $\Delta SSS = SSS_{insitu} - SSS_{ret}$

5.6 Conclusions

Results show up that better predictions of brightness temperature can be achieved by semi-empirical models than using theoretical ones. This behaviour is observed for two campaigns with independent radiometers, but both located on the same area.

An important conclusion that can be also extrapolated from this chapter is that to retrieve salinity from WISE and EuroSTARRS data sets, the model dependent on wind speed as well as on significant wave height is better than other models only dependent on wind speed, or only SWH.

From the auxiliary parameters work, one can conclude that using data from meteorological models to retrieve salinity is better than using direct satellite data, since the former have smaller temporal resolution. Even though, the necessary accuracy of U_{10} is high (of the order of 1 m/s to obtain an extra salinity error lower than 0.1 psu), and this is impossible to achieve nowadays by using satellite data (the temporal resolution is low), and probably neither using atmospheric models.

From the analysis of WISE data set it appears that, in absence of accurate in situ measurements, the best method to retrieve salinity is to leave U_{10} and SWH

Area B	SSS_{ret}	ΔSSS	$U_{10\,ret}$	SWH_{ret}
Method	Model-2P			
M1	33.468	-0.776	-	- 3
M2	32.800	-0.108	2.136	-
M3	31.172	1.520	5.279	-1.540
	Hollinger model			
M1	33.674	-0.982	-	-
M2	32.586	0.106	2.240	-
	WISE 2001 model			
M1	34.084	-1.392	-	-
M2	32.154	0.538	0.930	-

Table 5.11: Retrieved parameters for three different emissivity models and three different methods for area B. $\Delta SSS = SSS_{insitu} - SSS_{ret}$.

as free parameters, and let the inverse algorithm to retrieve them as well as SSS from the radiometric measurements, taking advantage of the multi-angular view capability of SMOS imaging configuration. Using this method, the U_{10} is retrieved with a mean error of the order of 1 m/s, and SWH of 0.3 m.

However, in this case, it is necessary to find the best reference values and to characterise very well their errors. Then, it is needed to tune very well these values in the cost function. When SMOS will be flying, the reference values for WS and SWH could be obtained from analysed models, and the reference value of SSS could be the SMOS measurement of that area obtained during the previous pass of the satellite.

Errors on SST of 1° C produce minimum errors on the retrieved SSS (less than 0.06 psu). Since the actual knowledge of SST parameter measured by satellites or models is better that that value, SSS errors due to SST inaccuracies can be neglected in the future SMOS operational procedures.

Results with the Plata experiment dataset show that the L-band radiometer, STARRS, is capable to detect variations on SSS in an area with strong surface salinity gradient. The study demonstrates that better results are obtained when allowing the algorithm to retrieve wind speed, as well as SSS, than fixing it to possibly erroneous values. Another conclusion is that when the model-2P,

Area C	SSS_{ret}	ΔSSS	$U_{10\,ret}$	SWH_{ret}
Method	Model-2P			
M1	34.113	1.529	-	-
M2	33.425	2.217	6.927	-
M3	31.762	3.880	10.175	-0.890
	Hollinger model			
M1	34.191	1.451	-	-
M2	33.323	2.319	7.639	-
	WISE 2001 model			
M1	34.973	0.669	-	-
M2	32.946	2.696	5.506	-

Table 5.12: Retrieved parameters for three different emissivity models and three different methods for area C. $\Delta SSS = SSS_{insitu} - SSS_{ret}$.

which is dependent on U_{10} and SWH, is used in the retrieval process, slightly better results are obtained than using other semi-empirical models. However, as the model-2P was derived from western Mediterranean conditions, better results should be expected by deriving one model for each ocean conditions. It would be interesting for further work to derive a model from the Plata data-set (if enough in situ data are available) and compare it with the WISE derived models.

The accuracy and resolution of meteorological models can also vary in other regions, as well as the accuracy of satellite data. This work is a regional study, but could be a first step for a global scheme applicable to SMOS observations.

Chapter 6

Salinity retrieved from images generated by the SMOS End-to-End performance simulator

In this chapter some aspects of the salinity retrieval are analysed using the SMOS End-to-end Performance Simulator (SEPS), which simulates the performance of MIRAS instrument very accurately.

This tool has been used to create three different brightness temperature scenes, as would be measured by MIRAS, after 78 consecutive SMOS snap-shots. These permit to have views from up to 78 different incidence angles in some pixels of the FOV. The three scenarios are representative of different ocean conditions.

Salinity has been retrieved from the pixels of the FOV using a Level2 processor prototype, created by UPC. First, a theoretical study of the effect of noise and bias in the retrieved salinity has been performed. Secondly salinity has been retrieved from the scenarios created by SEPS, with some limitations.

The approach of allowing the inversion algorithm to obtain the auxiliary parameters is also analysed.

6.1 Introduction to SEPS

The SMOS End-to-end Performance Simulator (SEPS) is a tool that allows the design engineers and scientists to simulate the full operation of the MIRAS instrument in a reliable and highly representative way (Corbella et al., 2003, Camps et al., 2003a). SEPS is based on the existing MIRAS End-to-end Performance Simulator created at the Polythecnical University of Catalonia (UPC) by Camps (1996), and has been implemented for ESA by a consortium led by EADS-CASA, with GMV, DLR and UPC.

It is a flexible software tool, modular and open to the integration of new routines and processing steps. It performs the simulation of all the aspects that are present in the process of imaging brightness temperature maps.

SEPS calculates the brightness temperatures of the FOV of SMOS for each snap-shot while orbiting, for land and ocean areas. It includes the following blocks:

- A detailed hardware modelling. It is based on MIRAS breadboard parameters and on the design experience obtained during the development of a X-band interferometric radiometer prototype, performed in the UPC.
- The implementation of the calibration and image reconstruction procedures.
- The implementation of an orbit propagator to generate the sequence of satellite positions at different times.
- The implementation of an L-band brightness temperature generator. Vertical and horizontal brightness temperatures are computed from emissivity models and the following physical parameters: soil and snow albedos, snow depth, soil roughness, vegetation albedos, soil moisture, soil surface temperature, ocean salinity, zonal and meridional winds over the oceans, vegetation height, ocean surface temperature and ocean ice cover.

Since the "vertical polarisation" antennas are oriented in the along-track direction, the brightness temperature that would be measured along the vertical line (ξ=0) would be the vertical one, and, since the array is tilted 31.2° with respect to nadir, the brightness temperature that would be measured along the horizontal line (η=0), would be a linear combination of the vertical and the horizontal ones.

The direct models used in SEPS to compute the emissivity of the sea surface is the Fresnel equation for the emissivity of a flat surface, and a linear approximation of Hollinger (1971) measurements for the roughness of the surface due to wind speed. The dielectric permittivity of sea water is computed using the Klein and

Swift (1977) model, however the tool allows to change this model to the Ellison et al. (1998) one.

Tables of geophysical parameters (SSS, U_{10} and SST) have been used to generate the brightness temperature maps over the sea. These tables have a spatial resolution of $1^\circ \times 1^\circ$ and are linearly interpolated.

Each pixel in the alias free field of view is seen under different incidence angle, radiometric sensitivity and spatial resolution. As the satellite moves, the projection of the FOV in cross-track/along-track Earth coordinates is displaced from snap-shot to snap-shot, and pixels are then seen in different positions in the FOV, so under different incidence angles, as shown in figure 6.1. This characteristic will allow us to do the retrieval process from T_B for each pixel when it is seen from different incidence angles (different snap-shots).

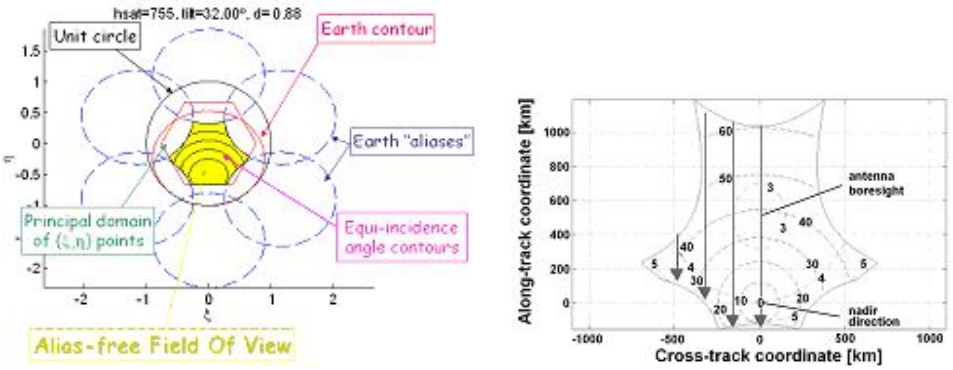

a) b)

Figure 6.1: a) SMOS observation geometry, mapped into the unit circle in (ξ, η). b) Imaging of a pixel through the alias free FOV under incidence angles (0°-60°, dashed contour centred at nadir), with different spatial resolution and radiometric sensitivities (from 3 K - 7 K, dashed-dot line centred at boresight). Parameters: 21 antennas per arm, d=0.875 λ antenna spacing, $\beta = 32^\circ$ tilt angle, and h=755 Km platform hight (from Camps et al. (2003b)).

SEPS is the tool that the SMOS community has to perform the analyses and studies necessary to solve the open issues of the project that are related to the instrument functioning under the specific configuration selected for SMOS.

6.2 Retrieval process

A complementary tool called Level 2 processor has been used to retrieve salinity from SEPS generated images. This tool has also been developed at the Polythecnical University of Catalonia, under the grant "MIDAS-2: Definición del proceso de datos de la misión espacial SMOS en la estación de Villafranca del Castillo (SMOS-GS-B) PARTE UPC", sponsored by Plan Nacional del Espacio ESP2002-11648-E.

The formulation of the retrieval problem has been done in terms of the first Stokes parameter (I) :

$$I = T_{xx} + T_{yy} = T_{hh} + T_{vv} \tag{6.1}$$

By this method the Faraday and the geometric rotations are avoided, while the radiometric sensitivity is not degraded since T_{xx} and T_{yy} can be computed in the dual-pol mode and not in the full-pol one. This alternative approach was first proposed in Camps et al. (2001).

The process to retrieve SSS from images generated by SEPS using the UPC tool is sketched below:

- Determine if a pixel is a land, sea or mixed pixel.
- Track the pixel as it moves in the alias-free FOV in a series of consecutive snap-shots. Tracking can be performed in the along-track/cross-track coordinates (figure 6.1b), or in the (ξ, η) director cosines coordinates (figure 6.1a).
- For each snap-shot, interpolate T_{xx} and T_{yy} from the (ξ, η) grid where the image reconstruction is performed to the geographical position of the pixel being tracked at that particular snap-shot. This process can be performed with the same window for all pixels, providing the same angular resolution in all directions, but different spatial resolution on ground, or with a "strip adaptative" processing window (Ribó, 2003) tailored to provide the same spatial resolution at all directions.
- Correct for sky (cosmic and galactic noise) and atmospheric/ionospheric effects: signal attenuation, upwelling brightness temperature, downwelling brightness temperature scattered in the direction of observation.
- For each snap-shot, the error (variance) between the model and the measured data at all incidence angles must be minimised, obtaining a set of estimated parameters (Camps et al., 2002a).

The inversion method selected is the Levenberg-Marquardt method with a cubic polynomial line search and Gill-Murray Hessian update methods.

First a theoretical analysis has been done. A scene with homogeneous salinity, wind speed and SST has been used to retrieve salinity with the level2 processor. This scene is an ideal scene, without any noise, bias nor perturbation, and follows the SMOS configuration with 78 snap shots. The original values are set to: SSS= 35 psu, wind speed=10 m/s and SST=15°. Afterwords, controlled noises and biases have been added to the computed brightness temperature , and the retrieved salinities have been calculated.

Figure 6.2 shows the number of incidence angles for each pixel of the image, the maximum is 78 since the image has been created with 78 snap-shots.

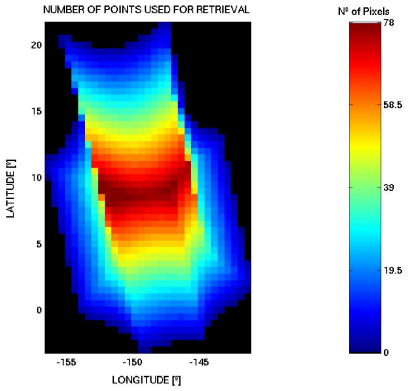

Figure 6.2: Number of incidence angles for each pixel.

Table 6.1 shows the mean and the variance of the retrieved salinity of the image for several combinations of noise and bias on T_B, as well as the case when a different emissivity model is used in the retrieval process (remember that the T_B images have been created using Hollinger's model).

Table shows up that when random added noise is present, the mean retrieved salinity does not suffer important errors, but the standard deviation (dispersion) increases. However, when bias is added to the brightness temperature, the retrieved salinity presents an important bias as well, but the dispersion is very low. Small deterioration of the retrieved salinity is observed when different emissivity models for the direct and the retrieval process are used. It should be pointed out that both models are very similar.

With an error on the auxiliary parameters of 2.5m/s on the wind speed and of 0.5° on the SST, and a random noise of 10K on T_B, the salinity is retrieved with an error of ≈ 0.15 psu. However, better results are obtained when the three

parameters (SSS, U_{10} and SST) are left to be retrieved by the inversion algorithm (error of ≈ 0.08 psu).

Case of study	$\overline{SSS}$ (psu)	σ_{SSS}
Ideal	34.997	0.009
T_B+5*rand	34.953	1.126
T_B+10*rand	34.930	2.343
T_B+5 (bias)	29.405	0.050
T_B+10*rand+5	29.314	2.429
WISE-derived model	35.048	0.194
T_B+10*rand / error on aux. param.	34.852	2.554
T_B+10*rand three param. free	34.922	2.575

Table 6.1: Mean and standard deviation of the retrieved salinity errors using different combinations of added noise and bias, and different models. The original salinity is 35 psu.

Figure 6.3 shows the results of retrieving salinity for the combinations of noise and biases added to the brightness temperature shown in the table. They show that the best retrieved values are found in the middle of the FOV, where more independent measurements are acquired (more incidence angles).

The second part of the study consisted of retrieving salinity from scenes created by SEPS, which are SMOS-like images. In this part all the effects involved in the creation of a brightness temperature image, as in the SMOS satellite, are considered. They considered errors on the receivers, on the antennas, and image reconstruction limitations. They also considered the atmosphere and ionosphere effects, as well as the extraterrestrial noises, and the Sun and the Moon direct and reflected contributions.

This is in opposition to what has been done in part one, that was an ideal case, without any of these effects.

Of course, when all these effects are considered, the brightness temperature measured differs from the ideal one. The bias and noise effecting to the T_B makes less effective the retrieval process, and will bring to a poorer retrieved salinity.

Camps et al. (2004b) identify three sources of bias. The first is the instrumental inaccuracies in the Noise Injection Radiometers used to measure the antenna temperature (thermal noise, offset, linearity). The second source is the inherent

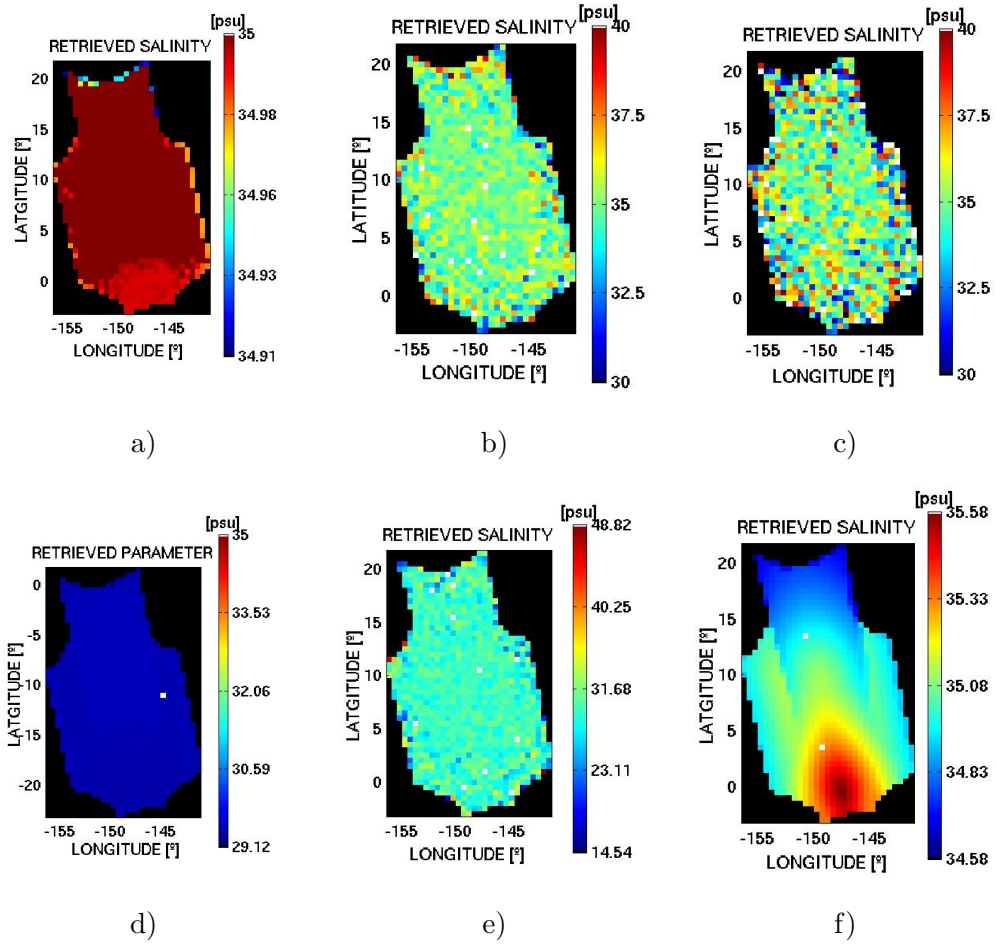

Figure 6.3: Retrieved SSS when the scene is homogeneous to SSS=35 psu. a) Ideal case (no noise neither bias) b) when a random noise of 5K is added to T_B c) when a random noise of 10K is added to T_B d) when a bias of 5K is added to T_B e) when a random noise of 10K and a bias of 5K is added to T_B f) when using WISE-derived model in the retrieval process (and no noise neither bias).

difference between the antenna temperature (measured in the whole unit circle) and the average brightness temperature in the alias free FOV, since in the last one, smaller area is considered (see figure 6.1a). Inhomogeneous scenes (near the coastline) produce more important bias of this kind. The third source is the Sun contribution which is not perfectly cancelled.

(Camps et al., 2004b) propose to correction for the bias with an external calibration. This calibration consists of, having an in situ measurement of SSS, U_{10} and SST for each scene, to calculate the brightness temperature at nadir for each snap shot. Later the first Stokes parameter is calculated by adding both polarisations of T_B. Therefore the bias can be calculated by performing the mean of the subtraction of the predicted first Stokes from the measured image. Finally this bias is deduced from the measured first Stokes parameter of each pixel. This would flap the level of brightness temperature to the correct one.

Three scenes have been generated with SEPS, on different ocean scenarios, to study the effects of meteorological and oceanographic conditions on the retrieved parameters. For the analysis 78 snap-shots are used. The different scenes are called A, B and C.

Scene A is located in the North Atlantic ocean, just south of Greenland, as shown in figure 6.4a. It is a region with very cold waters; sea surface temperatures in the FOV range from 7.5° (North area) to almost 20°. Salinity is 34.8 psu in the colder area, and increases until 36 psu. Figure 6.4e, shows the number of times each pixel is seen by the SMOS FOV, while satellite moves. This image was generated in an area with coordinates: latitude=[45,50], longitude =[-35,-30].

Scene B is located in the equatorial Pacific. This is a region with hot waters, as shown in figure 6.5. Sea surface temperatures range from 24° to more than 28°, in the FOV. Salinity ranges from 34.4 psu to near 35.6 psu. This image was generated in the area with coordinates: latitude=[0,5], longitude =[-150,-145].

Scene C is located over the Gulf Stream area, and present a big range of temperature and salinity, as shown in figure 6.6. Sea surface temperatures range from 3° to 26° and salinity ranges from 32.0 to 37.5 psu, in the field of view. This image was generated in the area with coordinates: latitude=[25,30], longitude =[-55,-50].

Figure 6.7 shows the retrieved salinity for each scene in two different scales. The results show a clear underestimation of the retrieved sea surface salinity from SEPS images. These results could be due to biases on T_B, therefore the inversion algorithm to compensate for this bias needs to decrease the salinity. If the bias is the same for the whole image, an increment on SSS should be added on the retrieved salinity images. Thereafter, the worse retrieval values would be located in the edge areas, as expected. The large variability of the retrieved salinity should be due to random noise, which increases the variability.

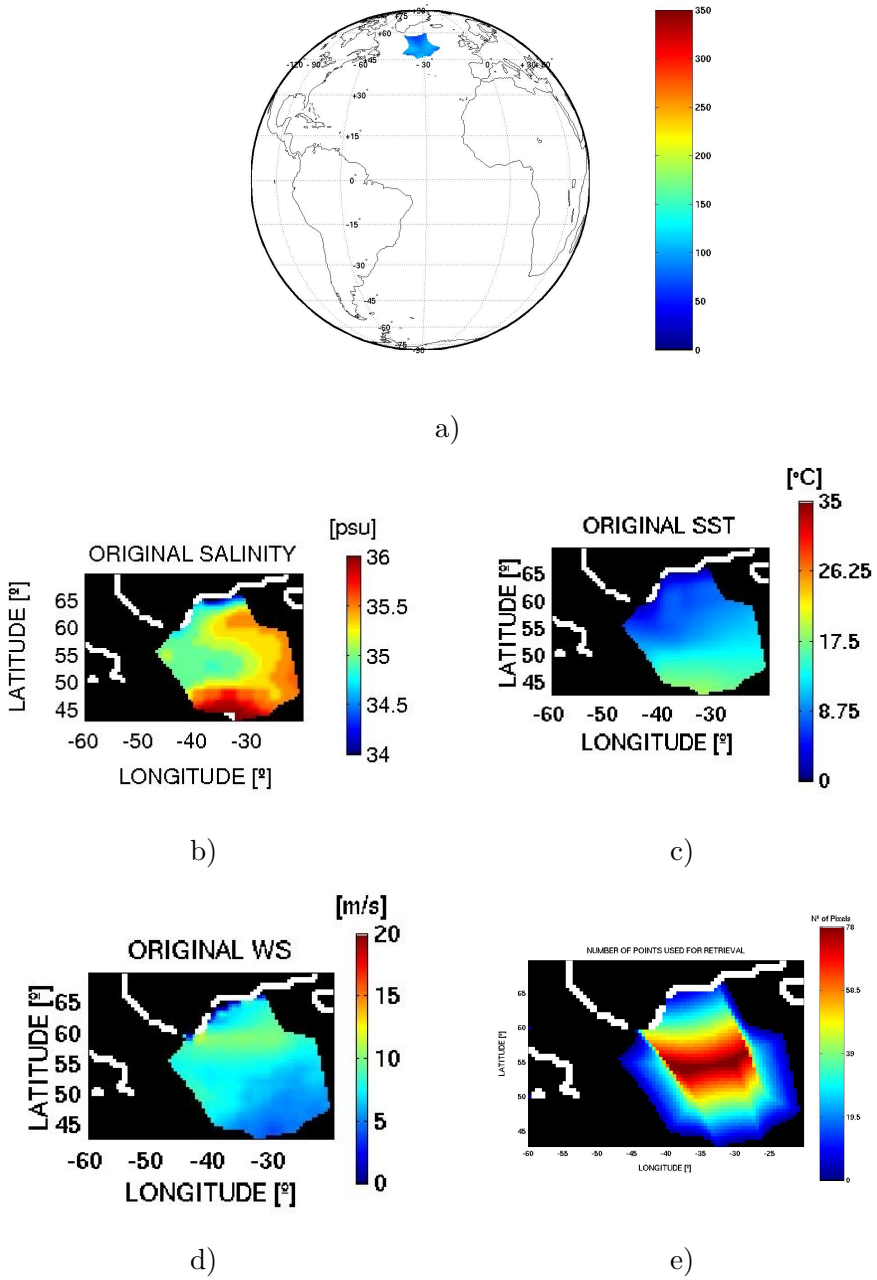

Figure 6.4: Scene A. a) Location of the scene. SSS insitu (b), SST insitu (c), and wind speed in situ (d) data used by the direct model to create T_B. e) Number of independent views of each pixel.

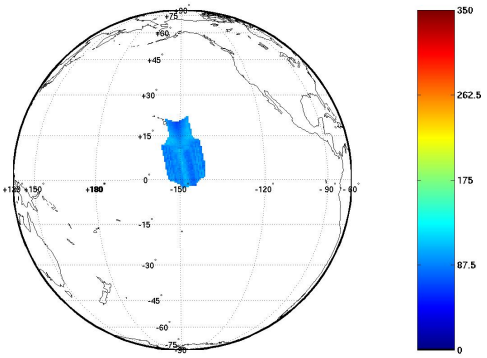

a)

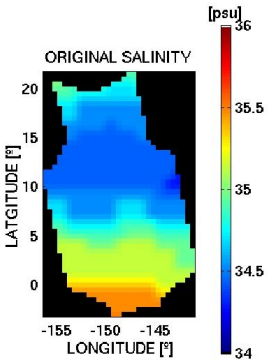

b)

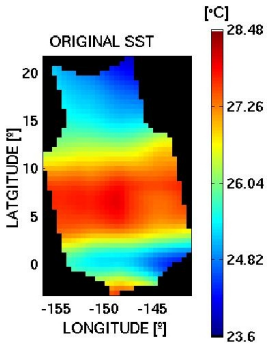

c)

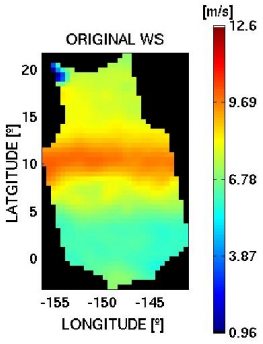

d)

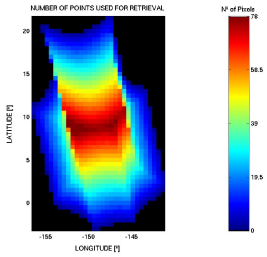

e)

Figure 6.5: Scene B. a) Location of the scene. SSS in situ (b), SST in situ (c), and wind speed in situ (d) data used by the direct model to create T_B. e) number of independent views of each pixel.

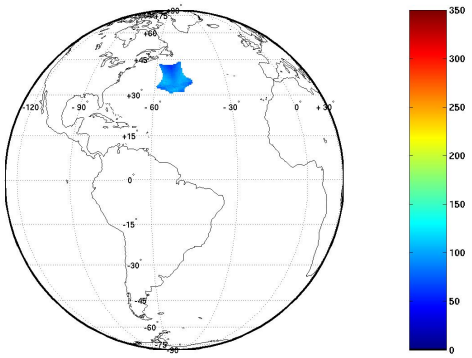

a)

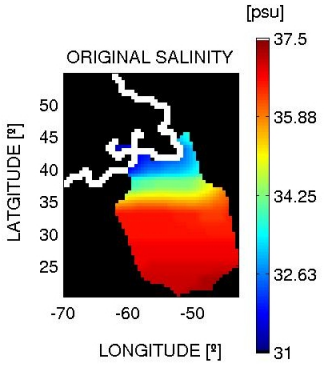

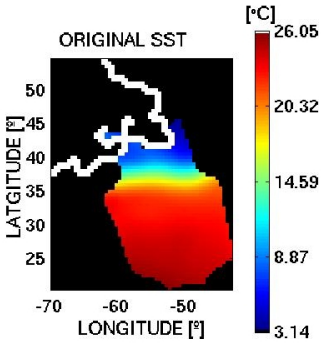

a) b)

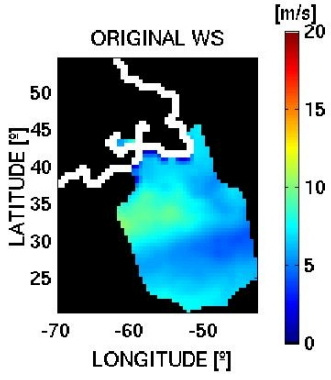

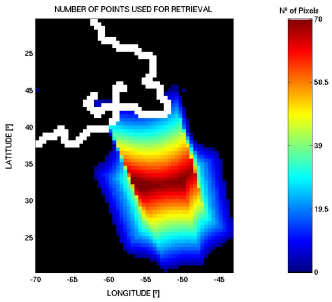

c) d)

Figure 6.6: Scene C. a) Location of the scene. SSS in situ (b), SST in situ (c), and wind speed in situ (d) data used by the direct model to create T_B. e) Number of snap shots for each pixel.

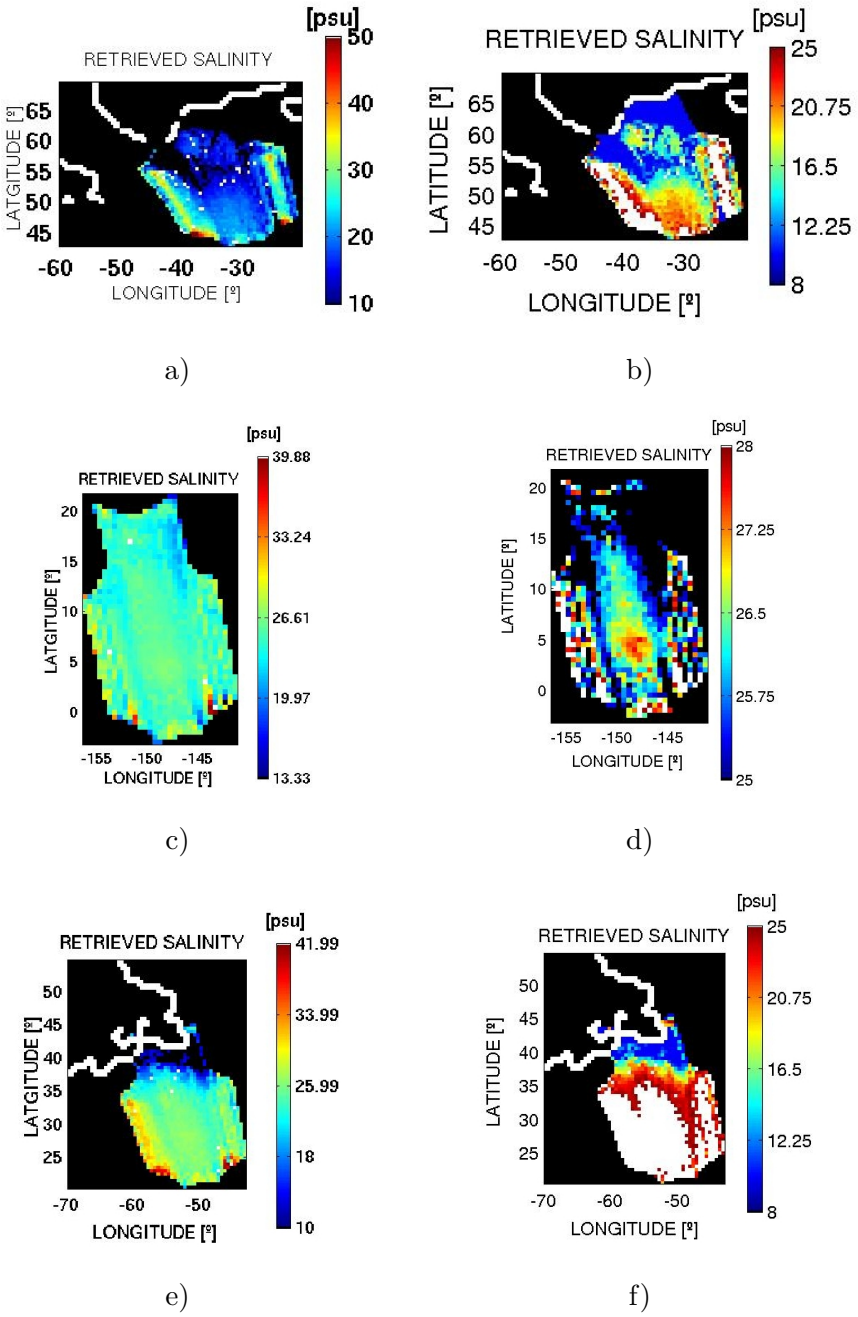

Figure 6.7: a) Retrieved SSS for scene A (b) and the error as $error = SSS_{original} - SSS_{retrieved}$ *for scene A (c) Retrieved SSS for scene B (d) and its error (e) Retrieved SSS for scene C (f) and its error.*

From figure 6.7 one can observe that scenes A and C present higher biases than scene B. These could be due to the second source of bias above explained, since scenes A and C are nearer to the coast, while B is in the middle of the Pacific.

However the figures also show a large dispersion of the retrieved values. This important dispersion can be due to random noise errors which effect the brightness temperature measurements. These random noises could be reduced by applying some statistical treatment. Scene B (figure 6.7d) is the one which presents less dispersion of the images. This is probably because the measurements have been done far away from coast.

Scene C is the one that presents more variability of SSS and SST. In the North area of this scene there is a front that shows a rapid decrease on SSS from $\approx$ 37 psu to near 34 psu. This variation of salinity in the area is also visible in the retrieved salinity image (figures 6.7e,f). Therefore it seems that the system is capable to detect variances on SSS, even though the absolute values are not correct.

These results are obtained with data of only one pass of the satellite and therefore pixel averaging has not yet been performed. Better results should be expected for the SMOS case, since temporal and spatial averaging will be performed, and thereby noise will be reduced.

Other works performed using these tools can be found in Camps et al. (2002a) and Camps et al. (2004c).

6.3 Conclusions

From the above work, it can be concluded that small errors on the retrieved salinity can be expected due to random noise on the brightness temperature. However, biases on the brightness temperature (for example 5K) produce important errors on the retrieved salinity (5.5 psu).

Errors on the auxiliary parameters, produce errors on the retrieved salinity which are not negligible. An important conclusion is that better salinity retrievals are obtained when the auxiliary parameters are left to be retrieved from the inversion algorithm, instead of fixing them to erroneous values . This is in accordance with what was concluded when experimental data set has been used (chapter 5).

From the SMOS images analysis, one can conclude that a lot of work is needed to investigate how to reduce the noise and biases that effects the measured T_B. May be, a statistical treatment should be used to decrease as much as possible the errors. Results, also, underline that probably an external calibration will

be necessary to correct the brightness temperatures from biases which are not controlled.

Results show that the system is capable to detect steps on SSS in one satellite overpass, when they are high ($\approx$ 3 psu), and therefore to detect fronts.

Chapter 7

Conclusions and recommendations

This thesis has been performed in the framework of the SMOS mission. The ICM has actively participated in two experiments sponsored by ESA, and has also participated in some ESA study contracts related with the SMOS mission.

In this thesis, errors on the sea surface salinity retrieved from L-band radiometric measurements have been investigated. This work has been done based in measurements acquired during campaigns organised by ESA as preparatory activities for the SMOS mission.

The study is a first step to understand which issues are more critical on the inversion process. Of course campaign measurements were not acquired exactly as SMOS will do, but the results can bring some insight on how the SMOS level 2 (geophysical products) processing chain should be developed.

The work has analysed two important issues that are still open for SMOS: the emissivity models and the auxiliary parameters.

7.1 Conclusions on emissivity models

The analysis of three dielectric constant models performed using the FROG campaign data-set, has shown that Klein and Swift (1977) model is the one that best retrieves salinity, while Blanch and Aguasca (2004) has a quite similar behaviour. Ellison et al. (1998) model gives biased results.

Salinity is properly retrieved from radiometric measurements obtained in dif-

ferent campaigns with an accuracy of 0.13-0.5 psu, depending on the emissivity models and the auxiliary parameters used. Therefore, it is possible to detect important gradients of salinity (the Plata campaign).

Retrieval salinity analysis from WISE and EuroSTARRS campaigns has shown that better results are obtained when using semi-empirical models to describe the emissivity of the sea than using the two tested theoretical models.

A new sea roughness semi-empirical model derived by the author from WISE 2001 data set has shown to retrieve salinity better than the other models, which depend only on wind speed. This conclusion is valid for the three campaigns tested in the study: WISE, EuroSTARRS and Plata. The new approach of this semi-empirical model is that the roughness of the sea is expressed as function of wind speed and also of the significant wave height, and therefore the swell events are considered. This model, derived from Mediterranean data (WISE), has been validated for completely different sea conditions (South Atlantic, Plata).

7.2 Conclusions on auxiliary parameters

An analysis of the auxiliary parameters used in the retrieval process has shown that important errors are introduced in the retrieved salinity due to imprecisions in these auxiliary parameters.

Comparisons of retrieved salinity have shown that better results are obtained when atmospheric and oceanographic models are used to obtain U_{10} and SWH parameters than using directly satellite observations. This is probably because this models have higher temporal resolution. However, this conclusion can not be directly extrapolated to other ocean conditions since this analysis has been performed in a determined area only.

A new method to obtain the auxiliary parameters has been proposed in this thesis. It consists of obtaining them (or some of them) from the radiometric measurements themselves. This is possible thanks to the multi-angular capability of SMOS, that allows each pixel to be repeatedly observed from several incidence angles. Therefore, having several measurements of the same pixel permits to retrieve several unknown parameters, since the system is overdetermined.

The introduction of constrains in the cost function (reference values for the parameters and their expected uncertainties) improves the quality of the salinity retrieval.

A better retrieval of the parameters is obtained when better quality reference values are used. However, the reference value for SSS is the one that has more impact on the retrieved salinity.

Following this new insight, wind speed can be retrieved with an error of 1 m/s, an accuracy that, until the present, no satellite measurement or model output can

achieve simultaneous to SMOS measurements. When using this method, since the parameters are not fixed to any specific value, the inversion algorithm can properly converge to good results.

The same analysis has been done using SMOS-like images generated by SEPS, and the best results are obtained when leaving the auxiliary parameters to be retrieved from the inversion algorithm also.

The usage of this method to retrieve sea surface temperature does not show big improvements on the quality of the retrieved salinity. This is because this parameter can be measured by other sources with enough good accuracy.

7.3 Recommendations

In many satellite missions, when the knowledge of the physical mechanisms responsible for the signal measured by a sensor in function of a geophysical variable is not sufficiently detailed, empirical approaches are often developed to obtain a practical algorithm to retrieve the geophysical variable. This is the case for example of the CMOD algorithm (Stoffelen and Anderson, 1993) to derive wind velocity from the ERS scatterometer.

For the case of SMOS, as nowadays few experimental data exist at L-band, it is difficult to validate the models. Thereby, maybe the emissivity model should be decided during the first period of SMOS live (commissioning phase), in which data validation will be performed. During this period, SMOS measurements will be compared with in situ salinity measurements obtained from thousands of floats that will be diving over the oceans (ARGO floats), as well as other in situ measurements. The large amount of data acquired will also permit to derive several semi-empirical models for different sea conditions, which might improve the retrieved salinity from SMOS measurements, since the model will be optimised for each area conditions.

A good approach for study this issue is to derive a new semi-empirical model of emissivity from the Plata data set, and to analyse if significant differences appear between models from different sea conditions.

Another interesting study would be to analyse if other auxiliary parameters could add important information to the emissivity model, as for example wave age or fetch.

An analysis similar to what has been done in this thesis, should be done considering the first Stokes parameter. As explained at the beginning of this document, when this parameter is used (I=$T_{BH} + T_{BV}$), besides using them separately, the Faraday and geometrical rotations are cancelled out. Nevertheless the number of independent measurements is reduced to the half, which produces a

small degradation on the quality of the retrieved salinity. During this thesis, preliminary analysis have been done using experimental data, and results show that the deterioration of the retrieve salinity is not large. However more exhaustive analysis should be performed.

A strong recommendation is done to SMOS community to use the method that permits the auxiliary parameters to be retrieved from SMOS measurements themselves. For SMOS, the last orbital pass of the satellite over the same pixel could be used as reference for SSS value to be used in the retrieval, since salinity does not present fast variations.

More work should be done to investigate how to reduce the noises and biases that effect the images measured by SMOS. The work done with the SMOS simulator images show that good quality salinity maps are not possible to obtain due to the important artifacts (specially bias) that affect the brightness images.

We are still far from closing all the open issues on the salinity retrieval from SMOS measurements, but several theoretical studies and experimental work performed during the last years have permitted to improve our understanding of the physical laws and the retrieval concepts. The work presented in this thesis gives some new insights to the SMOS level 2 data processing chain.

Appendix A

Compilation of articles

A.1 List of articles in which the author has participated

A list of published articles related with the work presented in this thesis is attached. The two articles in which the author of this thesis is the first author are also attached.

Articles published in peer review journals

A. Camps, J. Font, J. Etcheto V. Caselles, A. Weill, I. Corbella, M. Vall-llossera, N. Duffo, F. Torres, R. Villarino, L. Enrique, A. Julià, **C. Gabarró**, J. Boutin, E. Rubio, S. C. Reising, P. Wursteisen, M. Berger, M. Martín-Neira. "Sea Surface Emissivity Observations at L-band: First Results of the Wind and Salinity Experiment WISE-2000". *IEEE Trans. Geosciences and Remote Sensing*, Vol. 40, Nº 10, pp. 2117–2130, 2002.

A. Camps, I. Corbella, M. Vall-llossera, N. Duffo, F. Torres, R.Villarino, L. Enrique, F. Julbe, J. Font, A. Julià, **C. Gabarró**, J. Etcheto, J. Boutin, A. Weill, E. Rubio, V. Caselles, P. Wursteisen, M. Martín-Neira." L-band sea surface emissivity: Preliminary results of the WISE-2000 campaign and its application to salinity retrieval in the SMOS mission". *Radio Science*, Vol. 93, Nº 4, pp. 8071, doi:10.1029/2002RS002629, 2003.

C. Gabarró, J. Font, A. Camps, M. Vall-llossera. " Determination of Sea Surface Salinity and Wind speed by L-band Radiometry from a fixed platform.". *Internation Journal of Remote Sensing*, Vol. 25, Nº 1, pp. 111-128, 2004.

C. Gabarró, J. Font, A. Camps, M. Vall-llosera. "A New Empirical Model of Sea Surface Microwave Emissivity for Salinity Remote Sensing". *Geophysical Research Letters*, Vol. 31, Nº L01309, pp. 1-5, 2004.

A. Camps, J. Font, M. Vall-llossera, **C. Gabarró**, I. Corbella, N. Duffo, F. Torres, S. Blanch, A. Aguasca, R. Villarino, L. Enrique, J. Miranda, J. Arenas, A. Julià, J. Etcheto, V. Caselles, A. Weill, J. Boutin, S. Contardo, R. Niclós, R. Rivas, S.C. Reising, P. Wursteisen, M. Berger, M. Martín-Neira. "The WISE 2000 and 2001 field experiments in support of the SMOS mission: sea surface L-Band brightness temperature observations and their application to Multi-Angular salinity retrieval". *IEEE Trans. Geosciences and Remote Sensing*, Vol. 42, Nº 4, pp. 804-823, 2004.

Proceedings and communications to congresses

A. Camps, I. Corbella, M. Vall-llossera, R. Villarino, L. Enrique, J. Font, A. Julià, **C. Gabarró**, J. Etcheto, J. Boutin, A. Weil, F. Torres, N. Duffo, J. Barà, R. Niclòs, V.C aselles, P. Wursteisen, M.Martín-Neira. "Sea surface emissivity observations at L-band: First preliminary results of the Wind and Salinity Experiment WISE-2000", *Proceedings IEEE International Geosciences and Remote Sensing Symposium IGARSS 2001*, pp. 1371-1373, 2001.

J. Font, A. Camps, J. Etcheto, P.Wursteisen, M. Martin-Neira, J. Barà, I. Corbella, N. Duffo, L. Enrique, F. Torres, M. Vall-llossera, R.V illarino, M. Emilianov, **C. Gabarró**, A. Julià, J. Boutin, A. Weil, V. Caselles, L. Martínez, R. Niclòs, E.M. Rubio, M. Moll. "WISE 2000 : Can we measure salinity from satellite?".*Rapp. Int. Mer. Comm.* Int Mer Medit. Septiembre 2001.

C. Gabarró, J. Font, A. Camps, M. Vall-llossera. "Sea Surface Salinity and Wind speed retrieved from a Tower-based L-band Radiometer in the NW Mediterranean.". Congress: *Recent Advances in Quantitative Remote Sensing Symposium*, September 2002. Valencia, Spain 2002.

A. Camps, I. Corbella, M. Vall-llossera, F. Torres, N. Duffo, R. Villarino, L. Enrique, J. Miranda, J. Arenas, J. Font, A. Julià, **C. Gabarró**, J. Etcheto, J. Boutin, S. Contardo, A. Weill, R. Niclòs, V. Caselles, P. Wursteisen, M. Berger,

M. Martín-Neira. "Wind Effects on the Sea Surface Emissivity at L-band: Preliminary Results of WISE 2000 and 2001". *Proceedings URSI Commission-F Open Symposium*, 2002.

A. Camps, J. Font, J. Etchetto, A. Weill, V. Caselles, I. Corbella, M. Vall-llossera, F. Torres, N. Duffo, R. Villarino, L. Enrique, J. Miranda, A. Julià, **C. Gabarró**, J. Boutin, R. Niclòs, P. Wursteisen, M. Martín-Neira. "L-band Sea Surface Emissivity Radiometric Observations under High Winds: Preliminary Results of the Wind and Salinity Experiment WISE-2001". *Proceedings IEEE International Geosciences and Remote Sensing Symposium IGARSS 2002, Toronto*, 2002.

A. Camps, J. Font, J. Etcheto, V. Caselles, A. Weill, I. Corbella, M. Vall-llossera, F. Torres, N. Duffo, R. Villarino, L. Enrique, J. Miranda, J. Arenas, A. Julià, **C. Gabarró**, J. Boutin, S. Contardo, R. Niclòs, R. Rivas, S. C. Reising, P. Wursteisen, M. Berger, M. Martín-Neira. "Sea Surface Radiometric Observations At L-Band: Wind Speed Sensitivity Derived from WISE 2000 and 2001". *Proceedings International Union of Radio Science 27th General Assembly*, 2002

C. Gabarró, J. Font, A. Camps, M. Vall-llossera. "Errors on the Retrieved Sea Surface Salinity from Microwave Radiometry due to Inaccuracies in the Ancillary Data". Congress: *IEEE International Geoscience and Remote Sensing Symposium IGARSS 2003.* Toulouse, France 2003.

C. Gabarró, J. Font, A. Camps, M. Vall-llossera. "Retrieved sea surface salinity and wind speed from L-Band measurements for WISE and EuroSTARRS campaign.". *Proceedings of the WISE/LOSAC/EuroSTARRS Campaigns Workshop, ESA PUBLICATIONS*, Vol. SP-525, pp. 163-172, 2003.

J. Font, **C. Gabarró** , A. Julià, M. Emilianov, M. Lloret, M. Moll. " Oceanographic conditions during Wind and Salinity Experiment 2000 and 2001, NW Mediterranean Sea.". *Proceedings of the WISE/LOSAC/EuroSTARRS Campaigns Workshop, ESA PUBLICATIONS*, Vol. SP-525, pp. 163-172, 2003.

M. Emelianov, J. Font, A. Julià, **C. Gabarró** , M. Lloret, J. Solé, L. Enrique. "Sea Surface fields at Casablanca site during the EuroSTARRS Campaign". *Proceedings of the WISE/LOSAC/EuroSTARRS Campaigns Workshop, ESA PUBLICATIONS*, Vol. SP-525, pp. 163-172, 2003.

C. Gabarró, J. Font, A. Camps, M. Vall-llossera, M. Portabella. "A new

empirical model of sea surface microwave emissivity for salinity remote sensing". Congress:*MICRORAD 04*. Rome, Italy, 2004

C. Gabarró, J. Font, J. L. Miller. "Sea surface measured by an airborne microwave radiometer in the NW Mediterranean". Congress: *CIESM*. Barcelona, Spain, 2004.

A.2 International Journal of Remote Sensing

This manuscript was submitted in September 2002 and published in January 2004.

INT. J. REMOTE SENSING, 10 JANUARY, 2004,
VOL. 25, NO. 1, 111–128

Determination of sea surface salinity and wind speed by L-band microwave radiometry from a fixed platform

C. GABARRÓ*†, M. VALL-LLOSSERA‡, J. FONT† and A. CAMPS‡

†Institut de Ciències del Mar CMIMA – CSIC, Passeig Maritim de la Barceloneta 37–49, 08003 Barcelona, Spain
‡Departament de Teoria del Senyal i Comunicacions, UPC, Campus Nord, D4 08034 Barcelona, Spain

Abstract. In May 1999, the European Space Agency (ESA) selected SMOS (Soil Moisture and Ocean Salinity) as an Earth Explorer Opportunity mission. One of its goals is the generation of global sea surface salinity (SSS) maps. The satellite sensor is an L-band interferometric radiometer with full-polarimetric capability called MIRAS. The retrieval of SSS from microwave measurements is based on the fact that the brightness temperature (T_B) of seawater is a function of the dielectric constant, temperature and sea surface state (roughness, foam…). The sensitivity of T_B to SSS is maximum at L-band, but it is necessary to quantify the other effects to have reliable SSS retrieval. In order to improve the present understanding of these effects on T_B, ESA sponsored the Wind and Salinity Experiment (WISE) 2000 and 2001 field campaigns. These experimental results are of great importance for the development of sea surface emissivity models that will be used in the future SMOS SSS retrieval algorithms. This paper presents the influence of the emissivity models on the derived SSS from the data obtained in both campaigns. It also presents the impact on the retrieved SSS of using *in situ* measured or satellite derived wind information, or even simultaneously estimating the wind speed from the measured multi-angular T_B.

1. Introduction

The distribution and variability of salinity in the world oceans is a key parameter both for the marine ecosystems and for the role of the oceans in the climate system (Reynolds *et al.* 1998, Hopkins 2001). Systematic global surface sampling by satellite is now a usual tool for monitoring many ocean variables such as temperature, colour, topography and even surface winds. However, until now remote sensing of the sea surface salinity (SSS) has not been possible due to major technical difficulties. Using the interferometric microwave radiometry concept, in early 2007 the European Space Agency (ESA) will launch the Soil Moisture and Ocean Salinity (SMOS) mission to fill this gap and provide global SSS maps for climatic and large-scale ocean circulation studies (Kerr *et al.* 2000).

The brightness temperature (T_B) of the sea at L-band is dependent on the SSS, in particular through the dielectric constant (Klein and Swift 1977), as well as on other factors like the sea roughness (mainly produced by wind stress), the sea

*Corresponding author; e-mail: cgabarro@icm.csic.es

International Journal of Remote Sensing
ISSN 0143-1161 print/ISSN 1366-5901 online © 2004 Taylor & Francis Ltd
http://www.tandf.co.uk/journals
DOI: 10.1080/0143116031000115175

surface temperature (SST), the presence of foam, the incidence angle, etc. Even though the sensitivity of the brightness temperature on the SSS is maximum at L-band, it is quite low: $\sim 0.5\,\mathrm{K\ psu^{-1}}$ at SST = 20° C, decreasing to $\sim 0.25\,\mathrm{K\ psu^{-1}}$ at SST = 0° C (Skou 1995, Lagerloef *et al.* 1995, Lagerloef 1998). The sensitivity of T_B to SST is about the same order, $0.2\text{–}0.4\,\mathrm{K\ ^\circ C^{-1}}$ (Swift and McIntosh 1983) (see figure 1), and the sensitivity to wind speed (WS) is in the range $0\text{–}0.4\,\mathrm{K/m\,s^{-1}}$, depending on the incidence angle (Hollinger 1971, Webster and Wilheit 1976, Lerner and Hollinger 1977). These numbers indicate that it is important to have a good knowledge of all the variables affecting T_B to retrieve the salinity from radiometric measurements with good accuracy.

To improve the present understanding of these effects on T_B, the ESA has sponsored the WISE (Wind and Salinity Experiment) 2000 and 2001 field campaigns. This paper describes the results of salinity retrieval from WISE data using wind and SST data measured *in situ*, and also from satellite measurements. Furthermore, it considers the possibility of retrieving both the wind speed and the SSS simultaneously from the multi-angular T_B measurements. Previous efforts on measuring surface salinity with an L-band radiometer airborne can be found in Swift (1993), Miller *et al.* (1998) and Wilson *et al.* (2001).

2. Campaign description

The WISE experiments were held at the Casablanca oil platform 40 km from the coast of Tarragona (Catalonia, Spain), in the north-west Mediterranean Sea (40.72° N, 1.36° E). Both experiments took place in autumn, when there are usually high winds in the region. The WISE 2000 campaign was held from 16 November to 18 December 2000 and continued from 9–15 January 2001, while the WISE 2001 campaign was held from 23 October to 22 November 2001.

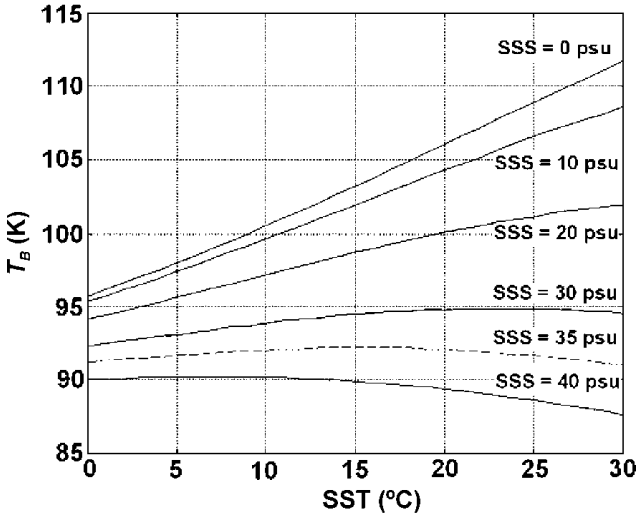

Figure 1. Brightness temperature (T_B) as a function of sea surface temperature (SST) and salinity.

The WISE participants were the Universitat Politècnica de Catalunya (UPC, Barcelona, Spain; the prime contractor with ESA), the Institut de Ciències del Mar (ICM–CSIC, Barcelona, Spain), the Laboratoire d'Océanographie Dynamique et Climatologie (LODYC, Paris, France), the Universitat of Valencia (UV, Valencia, Spain), the Centre d'Études Terrestres et Planétaires (CETP, Paris, France), and the University of Massachusetts (UMass, Amherst, USA) as a guest institution. The deployed instruments were:

- an L-band polarimetric radiometer—LAURA (L-band AUtomatic RAdiometer)
- a K_a-band polarimetric radiometer
- a stereo-camera to determine surface topography and rms slopes of the sea surface
- four oceanographic and meteorological moored buoys
- a sub-surface conductivity and temperature sensor
- a portable meteorological station
- a video camera to determine sea surface foam coverage
- an infrared radiometer to determine SST estimates

Additionally, ocean colour, wind vector and sea surface temperature were acquired simultaneously by several satellites.

A full description of the measurements performed can be found in Camps *et al.* (2002, 2003a). As can be appreciated in figure 2, during the WISE 2001 campaign the SST ranged between 16.0° C and 22.5° C, due to the seasonal variation. Measured sea surface salinity remained very stable around 38 psu, except on 18 November due to an intense rain event. The 10 m wind speed varied greatly, reaching up to 25.5 m s^{-1} during a strong storm on 15 November, when significant wave heights of almost 12 m were measured.

In the WISE campaigns the brightness temperatures in both (horizontal and vertical) polarizations were acquired by the radiometer LAURA. One of the modes of acquisition consisted of measuring in five or nine different elevation positions from $\theta_i = 25$–65°, in 5° or 10° steps respectively, at a fixed azimuth angle (Camps *et al.* 2002, 2003a). Data acquired in these conditions are used for the work presented below.

3. Applied methods

WISE campaign data are very useful for validating different empirical and theoretical sea surface emissivity models that exist in the literature for L-band. A new semi-empirical model based on these data has already been derived (Camps *et al.* 2003a). However, it should be noted that the data were obtained for west Mediterranean conditions (limited fetch), and the results may not be directly extrapolated to other ocean environments.

Different emissivity models and wave spectra were used in this study. The algorithm used to retrieve the salinity from T_B data is based on the minimization of a cost function (equation (1)) using a recurrent least-squares fit called Levenberg–Marquardt (Press *et al.* 1992).

$$\min \sum_{i=1}^{N} w_i \left(T_{B,i} - T_{B,i}^{\mathrm{mod}}(a) \right)^2 \tag{1}$$

where i indicates the acquisitions, a is the vector for the parameters to estimate and w is the weight assigned to each acquisition. Here the vector of parameters to

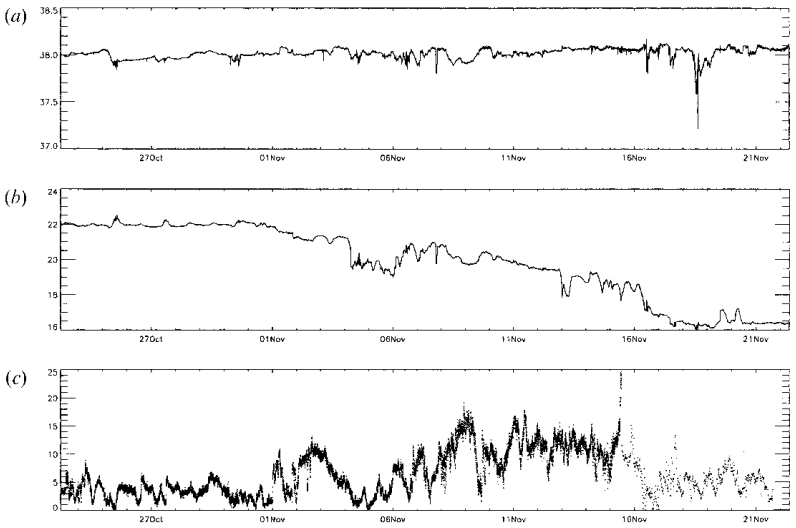

Figure 2. (*a*) Sea surface salinity (psu), (*b*) sea surface temperature (°C) and (*c*) wind speed (m s^{-1}) during WISE 2001.

estimate, a, is the salinity and in some cases also wind speed and the weights are set to 1.

This algorithm was chosen for its easy implementation and computational efficiency. T_B is computed setting an initial guess for SSS into the chosen direct emissivity model. This value is compared with the measured T_B by the radiometer and then an increment (ΔSSS) is added to the initial salinity. This recursive process is stopped when the difference between the measured and the computed T_B is smaller than a specified threshold (it might not be the smallest value).

Several aspects are studied in this work. We first consider the relationship between the retrieved salinity error and the number of incidence angles. The retrieval of SSS with different emissivity models is studied and compared with the *in situ* SSS measurements from the WISE campaigns, which were obtained by the oceanographic buoys close to the radiometer field of view. We also compare the results using a wave height dependent model versus a wind speed dependent model. Finally we study the impact of errors in the ancillary data (wind speed, wave height and SST) on the salinity retrievals.

3.1. *Emissivity models*

In the past few years, improved methods have been developed to model the polarimetric emission of the sea surface (Gasiewski and Kunkee 1994, Yueh *et al.* 1997, Camps and Reising 2001, Laursen and Skou 2001). However, these models have been developed or tuned at frequencies higher than L-band (1.4 GHz), typically 19 and 37 GHz. Additionally, sea foam effects at L-band are difficult to model since they have never been measured. According to recent modelling results

(Reuil and Chapron 2001), only sea foam thicker than 2 cm may produce an increase in the L-band brightness temperatures, but experimental validation has not yet been performed.

For the different emissivity models, the brightness temperature collected by the radiometer antenna follows equation (2) (Ulaby *et al.* 1981),

$$T_B = \left(T'_B + T_{SC}\right)/L_A + T_{UP} \tag{2}$$

where T'_B is the terrain emission, and T_{SC} is the radiometric temperature of energy scattered by the terrain. The primary source of T_{SC} is the downward-emitted atmospheric radiation (T_{DN}), although it may also have a component due to extraterrestrial radiation incident upon the terrain (T_{EBT}). The atmospheric attenuation L_A and the atmospheric upwelling self-emission T_{UP} can be neglected for the WISE conditions (radiometer located at 33 m above sea level). The term T_{SC} is estimated from numerical models and the knowledge of the antenna radiation pattern (Camps *et al.* 2003b).

Four different emissivity models have been studied in this work, two of them are semi-empirical and two analytical.

3.1.1. *Semi-empirical models*

The effect of wind on the T_B at L-band is quite small, even though it is great compared to the salinity effect. For this small effect an approximation considering a first order Taylor series can be applied. Thus, equation (2) can be reduced to equation (3),

$$T_B = e_p(\mathrm{SSS}, \mathrm{SST}, \theta_i)\ \mathrm{SST} + \Delta T_{w,p}(\theta_i, U_{10}) \tag{3}$$

where the first term is the contribution of a flat surface and the second one is the brightness temperature variation produced by the surface roughness. The ocean emissivity at angle θ_i, $e(\mathrm{SSS}, \mathrm{SST}, \theta_i)$, can be calculated from the Fresnel power reflection coefficients at horizontal and vertical polarization, as shown in equation (4).

$$\begin{aligned} e_H &= 1 - \left| \frac{\cos(\theta_i) - \sqrt{\varepsilon - \sin^2(\theta_i)}}{\cos(\theta_i) + \sqrt{\varepsilon - \sin^2(\theta_i)}} \right|^2 \\ e_v &= 1 - \left| \frac{\varepsilon \cdot \cos(\theta_i) - \sqrt{\varepsilon - \sin^2(\theta_i)}}{\varepsilon \cdot \cos(\theta_i) + \sqrt{\varepsilon - \sin^2(\theta_i)}} \right|^2 \end{aligned} \tag{4}$$

The dielectric constant ($\varepsilon = \varepsilon' + i\,\varepsilon''$) is calculated following Klein and Swift (1977), and θ_i is the incidence angle. $\Delta T_{w,p}$ is the brightness temperature due to the roughness of the surface (mainly due to wind speed) and U_{10} is the wind speed at 10 m height.

Considering the above approximation, two different wind speed dependencies are studied in this work,

A. *Hollinger's linear regression model*. This is a derived wind speed sensitivity from measurements made at Argus Island Tower by Hollinger (1971), and it is

shown in equation (5)

$$\begin{cases} \Delta T_h \approx 0.2\left(1+\theta_i/55^\circ\right) U_{10} \\ \Delta T_v \approx 0.2\left(1-\theta_i/55^\circ\right) U_{10} \end{cases} \quad (5)$$

for incidence angles, θ_i, smaller than 55°. This model was used by the National Oceanic and Atmospheric Administration (NOAA) for their experiments in 1997 with the SLFMR (Scanning Low-Frequency (L-Band) Microwave Radiometer) sensor (Goodberlet and Miller 1997).

B. *WISE-derived model*. The brightness temperature to wind dependence for each incidence angle is now derived from WISE 2001 data (Camps *et al*. 2003a), considering an unstable atmosphere. Figure 3 shows the points obtained after performing the regression of the measurements for each angle and the linear-fit to these points, which results in equation (6):

$$\begin{cases} \Delta T_h \approx 0.25\left(1+\theta_i/94^\circ\right) U_{10} \\ \Delta T_v \approx 0.24\left(1-\theta_i/48^\circ\right) U_{10} \end{cases} \quad (6)$$

3.1.2. *Analytical models*

Among the different analytical physically-based scattering models we have used, the Two-Scale Method and the Small Slope Approximation, as in a recent comparison (Vall-llossera *et al*. 2003), appear to best fit with the WISE data.

C. *Two-Scale Method—Durden and Vesecky* ×2. The Two-Scale Method (TSM) employed in this study is the one developed by Yueh *et al*. (1997). Two-scale sea surface models approximate the sea surface as a two-scale surface with small ripples

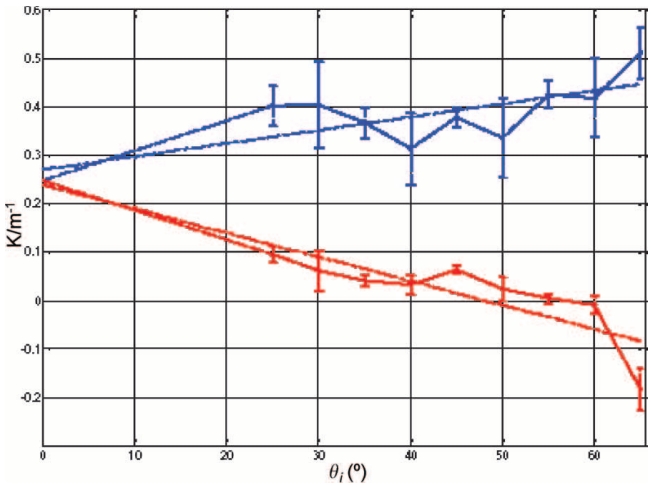

Figure 3. Brightness temperature dependence to wind speed with respect to incidence angle, derived from WISE 2001 measurements.

or capillary waves on the top of large-scale surfaces. With this approximation, the total thermal emission from the surface is the sum of emissions from individual, slightly perturbed surface patches tilted by the underlying large-scale surface. This model uses the Durden and Vesecky (1985) wave spectrum multiplied by a factor of two. It has been recently found to compare well with brightness temperature measurements made at higher frequencies (Lagerloef 2001). The input values to the model are SSS, SST, wind speed, azimuth and incidence angle.

D. *SPM/SSA model—Elfouhaily*. This model follows the Small Slope Approximation (SSA) theory for free-foam rough surfaces (Voronovich 1994) with the wave spectrum derived by Elfouhaily (Elfouhaily *et al*. 1997). We have used the theoretical development by Johnson and Zhang (1999) in which the physics of the emission process predicted by SPM/SSA was clarified. Use of the SPM/SSA up to the second order produces an expansion in surface slope, with zero order terms reproducing flat surface emission results, first order terms identically zero, and the second order terms providing the first prediction of changes from flat surface brightnesses. Second order terms take the form of an integral of a set of weighting functions over the surface directional spectrum. Properties of a directional spectrum result in no first harmonic variation being obtained; a third order SPM/SSA is required to obtain the first harmonics. Only the second order expansion is considered in this study. No artificial cut-off wavenumber is required to separate small- and large-scale waves in this method. The input values to the model are SSS, SST, wind speed, azimuth and incidence angle.

None of those models considers the foam effects. All of them have been implemented with the Klein and Swift dielectric constant model because, after some studies at the Jet Propulsion Laboratory (National Aeronautics and Space Administration (NASA)), it seems to be more accurate at L-band than the Ellison dielectric constant model (Ellison *et al*. 1996). This state is also confirmed when both dielectric models are tested with WISE data.

4. Results and discussion

The measurements performed in elevation scan are the best suited to study the retrieval problems. Figure 4 compares the results using different numbers of acquisition angles. It shows the error in the retrieved salinity (using the WISE-derived wind sensitivity model) as a function of the number of incidence angles. Only measurements acquired when the radiometer was pointing in a north direction (nine incidence angles) were considered. The number of incidence angles acquired (x axis) in the plot means nine different acquisition angles per two polarizations minus the discarded measurements. Measurements were discarded when the level of radio frequency interference (RFI), constant during the whole measurement or part of it, led to too large variance in T_B values. It is clear that the SSS retrieval quality increases with the number of acquisition angles used in the retrieval. For the following work only the datasets obtained with a number of incidence angles higher than 12 were considered, except when explicitly stated.

4.1. *Analysis of the results using different models*

The four models described above were run over 25 different datasets. They were acquired on different days and therefore under different wind and temperature conditions. In order to run the algorithm for retrieving the salinity, in addition to the measured T_B, it is necessary to introduce as input the wind speed and SST.

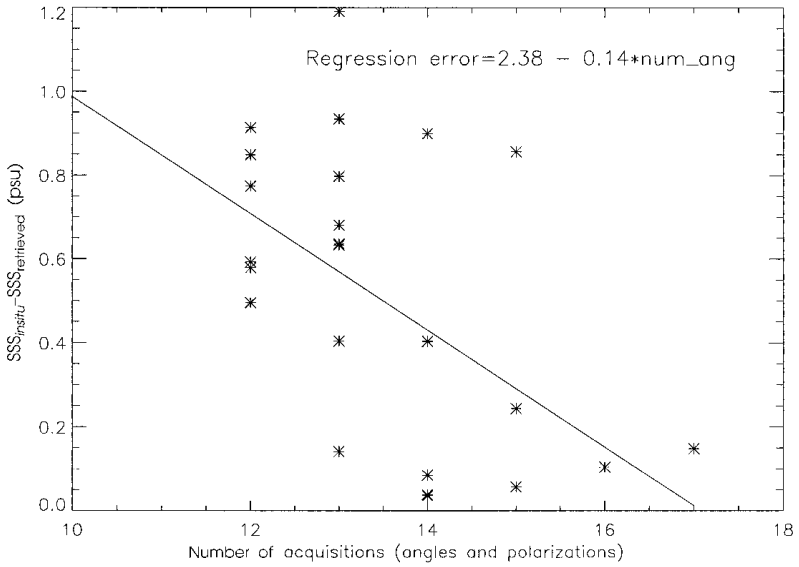

Figure 4. Retrieval errors as a function of the number of acquisition angles. The computations were performed with the UPC model.

Those variables were measured by the oceanographic buoys simultaneously to T_B measurements (Font *et al.* 2003).

Figure 5 shows the difference between the retrieved salinity and the salinity measured *in situ* (with an absolute accuracy of 0.02 psu) for all the studied models. It is clear that the one that best fits with the campaign measurements is the WISE-derived model, as was expected. The mean and the variance of the errors in the retrieved salinity for the 25 measurements were calculated and are presented in table 1.

The retrieved salinity was also obtained using the individual points of the WISE-derived model, and not the linear fit (figure 3). The results demonstrate that the approximation made with the linear fit produces errors in the retrieved salinity lower than 0.01 psu.

The TSM model always highly underestimates the salinity. This problem could be due to a bias on the modelled T_B of about 1–1.5 K that produces a negative bias of 2–3 psu in the salinity. It may also be due to a weak wind dependence that forces the algorithm to decrease the salinity in order to increase the T_B.

The SSA model overestimates the salinity, i.e. the wind dependence is too high. In figure 6 it can be observed that the retrieved salinity accuracy is poorer for events with low wind speed and small waves than in other conditions. This is in agreement with Voronovich and Zavorotny (2001), because they conclude that the Elfouhaily spectrum overestimates the probability of having short waves by 2–4 dB in the cross-wind direction. The results show that this model is not recommended for low-wind events.

From these results it can be concluded that the semi-empirical models seem to recover better than the analytical ones, and that the best model to use in order to

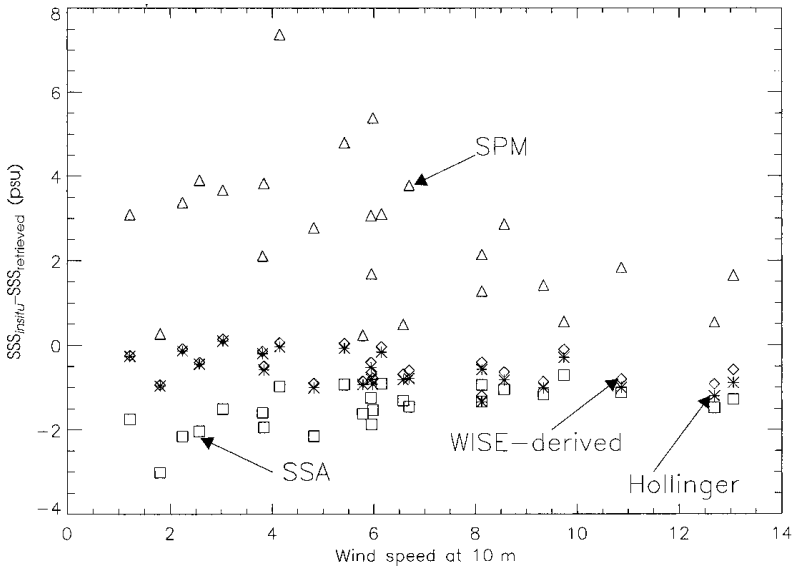

Figure 5. Error in the salinity retrieved using different emissivity models.

Table 1. Mean and variance of the retrieved salinity error for different models, considering $\Delta\mathrm{SSS} = |\mathrm{SSS}_{insitu} - \mathrm{SSS}_{\mathrm{retrieved}}|$.

	Mean (ΔSSS) (psu)	$\sigma_{\Delta\mathrm{SSS}}$ (psu)
Hollinger's model	0.63	0.15
WISE-derived model	0.52	0.12
Two-scale + Durden and Vesecky $\times 2$	4.28	3.18
SSA + Elfouhaily	1.48	0.27

retrieve salinities from WISE data is the WISE-derived model. Consequently, the work presented below was done using this model.

Figure 7 shows that the error in the retrieved salinity tends to increase linearly with increasing wind speed and wave height. This effect can be explained by the fact that the foam effect has not been taken into account in the models. Normally, the foam coverage increases with wind speed (or wave height) and its effect can be considered negligible only with wind speeds below $10\,\mathrm{m\,s^{-1}}$. The foam increases the brightness temperature. If this ΔT_{Bfoam} is not expressed in the model equations, the inversion algorithm will decrease the salinity to compensate for this increase in T_B. This is exactly what can be seen in the results.

Another way to retrieve salinity is to use a model that considers the sea surface roughness term as a function of the significant wave height (SWH) instead of the wind speed. The advantage of this dependence should be that the wave height is not as variable as the wind. In addition, surface roughness may be due to the swell and not only to wind waves. The spectrum models usually consider fully developed sea dependent on the local wind (they usually neglect the swell effect). The retrieval

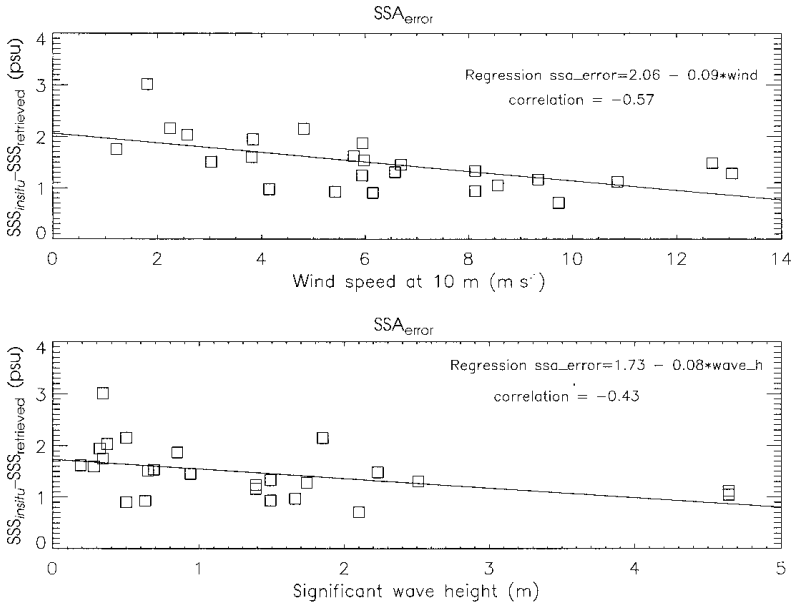

Figure 6. Error in the salinity retrieved for the SSA + Elfouhaily model as a function of wind speed and significant wave height (defined as the average of the highest third of the waves).

computation was performed using the wave height dependence derived from WISE 2000 and 2001 data (Camps *et al.* 2003a):

$$\begin{cases} \Delta T_h \approx 1.09 \left(1 + \theta/142^\circ\right) \mathrm{SWH}_{(m)} \\ \Delta T_v \approx 0.92 \left(1 - \theta/51^\circ\right) \mathrm{SWH}_{(m)} \end{cases} \quad (7)$$

SWH being the significant wave height, defined as the average of the highest third of the waves, measured by one of the moored buoys. Since the dominant wind during WISE 2001 was from the north, some reflection waves produced by the platform legs were observed. It is therefore recommended to use only data acquired when the radiometer was pointing west, so to compute the retrieved salinities here, only these data (with five incidence angles) were used. To obtain better results the T_B of different measurements made on the same day were averaged (minimum three measurements).

Figure 8 presents the comparison of the retrieved salinity errors using the wind speed dependence and the wave height dependence. The results considering the SWH appear to be slightly worse than those considering the wind dependence (see table 2).

4.2. *Impact on the retrieved SSS due to errors in ancillary data*

To retrieve salinity from SMOS, other variables (wind speed or wave height and SST) are needed as simultaneously as possible in time and space to the radiometer

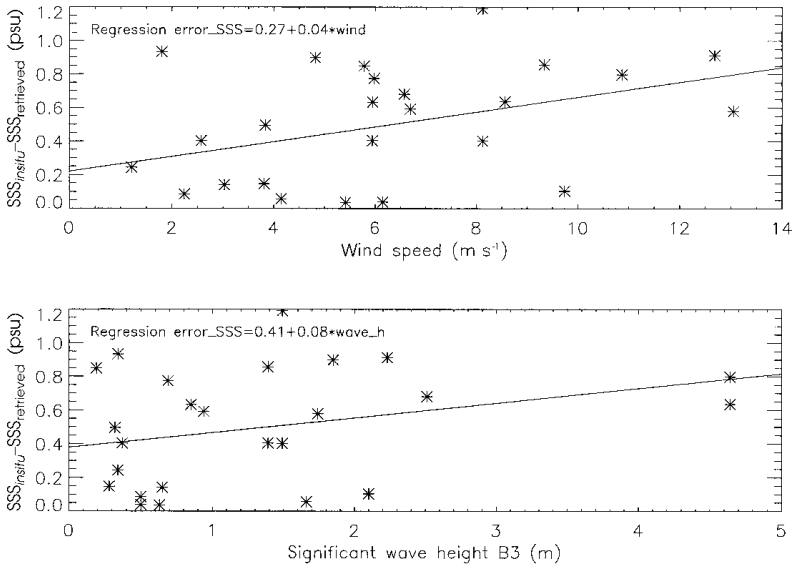

Figure 7. Relation between error in the retrieved salinity and wind speed and wave height with WISE-derived model.

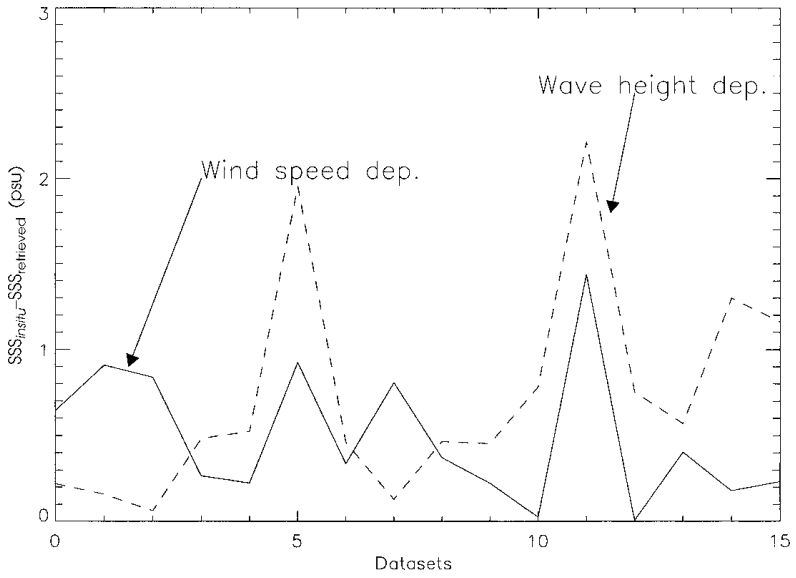

Figure 8. Comparison of the retrieval error using the wind and wave height dependence model for files acquired with five incidence angles (pointing to the west).

Table 2. Mean and variance of the retrieved salinity error using wind speed dependence and wave height dependence, considering $\Delta SSS = |SSS_{insitu} - SSS_{retrieved}|$ (five θ_i files + average). Only daily averages (with similar wind speed) of west pointing data are used.

	Mean (ΔSSS) (psu)	$\sigma_{\Delta SSS}$ (psu)
Wind speed dependence	0.30	0.07
Wave height dependence	0.34	0.07

measurement. In the first SMOS proposal, a second frequency radiometer to measure wind speed was foreseen. But this initial idea was cancelled due to budget constraints. There is the possibility of retrieving wind speed from the L-band measurements (third and fourth Stoke parameters), but this is under study at the moment. Another possibility is to obtain these data from other sensors embarked on a satellite with a similar orbit, but these measurements will have instrumental errors (accuracy) and non-simultaneously orbit errors. Data from meteorological models with satellite data assimilation could also be used.

In this section the errors in the retrieved salinity produced by errors in the wind speed (or SWH) and SST measurements from the satellite and from a model are quantified.

Wind speed measured by the QuikSCAT satellite during the WISE campaigns was collected. This scatterometer has an accuracy of $2\,m\,s^{-1}$ and a spatial resolution of $25 \times 25\,km^2$. Wind speed computed from the ARPEGE model (Météo France) in the Casablanca area was also obtained. This model gives data every 6 hours with a net of 0.250° in latitude and longitude, but does not assimilate satellite data. Figure 9 compares the wind speed measured by an *in situ* buoy, the QuikSCAT satellite and the ARPEGE model.

Figure 10 shows the errors in the retrieved salinity obtained using the three different sources of wind speed explained above plus leaving the wind speed as an unknown parameter, and allowing the inversion algorithm to converge simultaneously to a value for the wind speed and another for the salinity. Consequently, in this last situation the algorithm uses an initial guess for both wind speed and salinity values.

It is noticeable that when the wind measured by the satellite shows large errors (cases 10–14), the retrieved salinity increases excessively. The option of leaving the wind as a free parameter seems to retrieve with reasonably good accuracy both the salinity and the wind speed. The dependence of the initial wind and salinity guess values on the results was also studied. It was found that the results are almost independent of these initial values. The wind speed must be considered in a wide range of values, and the QuikSCAT wind speed measurement could be used as an initial guess.

Table 3 shows the mean and the variance of the errors of 25 retrieved salinities using the WISE-derived model with four different wind sources. It can be concluded that it is better to leave the wind variable as a free parameter to retrieve, than to use the satellite measurement of QuikSCAT. On the other hand, when the wind speed obtained from the ARPEGE model is used, quite good results are achieved (the time resolution of this model is 6 hours).

The use of the SWH from a satellite instead of the wind speed could be a good solution since SWH shows smoother changes in time and space. The SWH

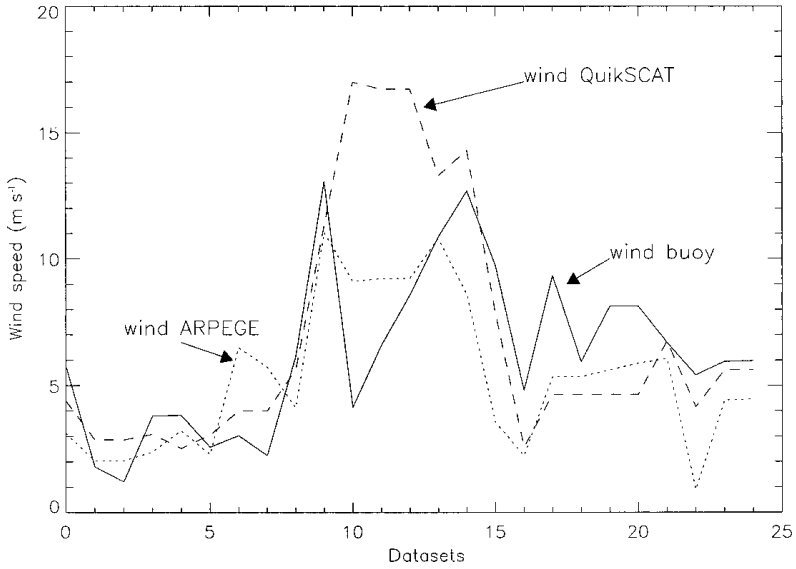

Figure 9. Comparison of wind speed measured by a buoy, QuikSCAT and the ARPEGE model.

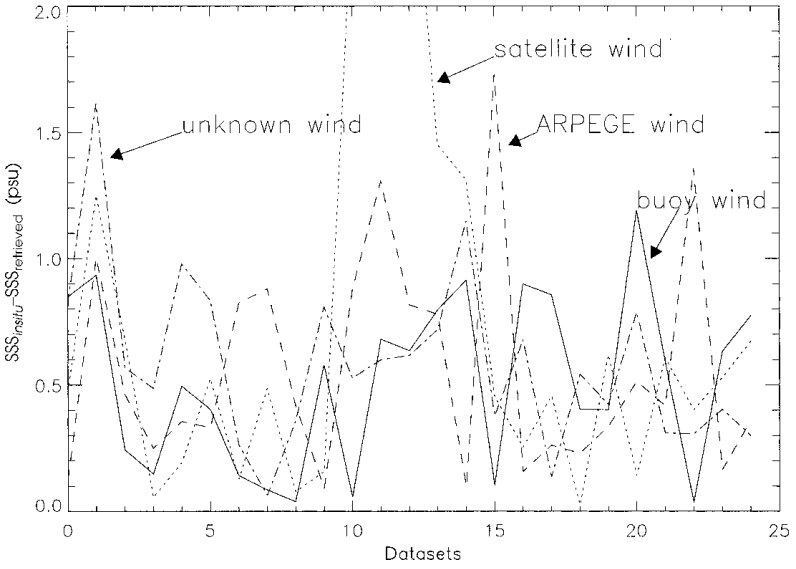

Figure 10. Retrieved salinity using four different methods for measuring wind speed.

Table 3. Mean and variance of the retrieved salinity error for different wind speed sources, considering $\Delta SSS = |SSS_{insitu} - SSS_{retrieved}|$ and $\Delta WS = |WS_{insitu} - WS_{retrieved}|$.

	Mean (ΔSSS) (psu)	$\sigma_{\Delta SSS}$ (psu)	Mean (ΔWS) m s^{-1}	$\sigma_{\Delta WS}$ m s^{-1}
In situ wind measurements	0.52	0.12	–	–
QuikSCAT wind measurements	0.77	0.72	2.63	10.12
Wind speed from ARPEGE model	0.57	0.19	2.23	2.78
Wind unknown parameter	0.59	0.12	1.15	0.54

measured by the radar altimeter (RA) onboard ERS-2 (ESA) for the Casablanca area during the WISE campaigns was obtained. This instrument has an accuracy of 0.5 m or 10%, whichever is smaller, and a spatial resolution of $20 \times 20\,km^2$. The measurement is defined as four times the standard deviation of the wave slope (as one of the WISE buoys, wave rider B3) which is a different definition from the one used above (average of the highest third of the waves, WISE buoy B2). To convert from one definition to the other, the first definition must be divided by $\sqrt{2}$. Figure 11 shows the comparison between the wave height obtained by buoy B2, that obtained by B3 and that obtained by the RA satellite (the latter two with the necessary correction).

Table 4 compares the errors in the retrieved salinities using wind speed or SWH both measured from satellite. The results show that it is better to use the wave height measurement from the European Remote Sensing Satellite (ERS)-2 RA than to use the QuikSCAT data to retrieve the salinity, even though the differences

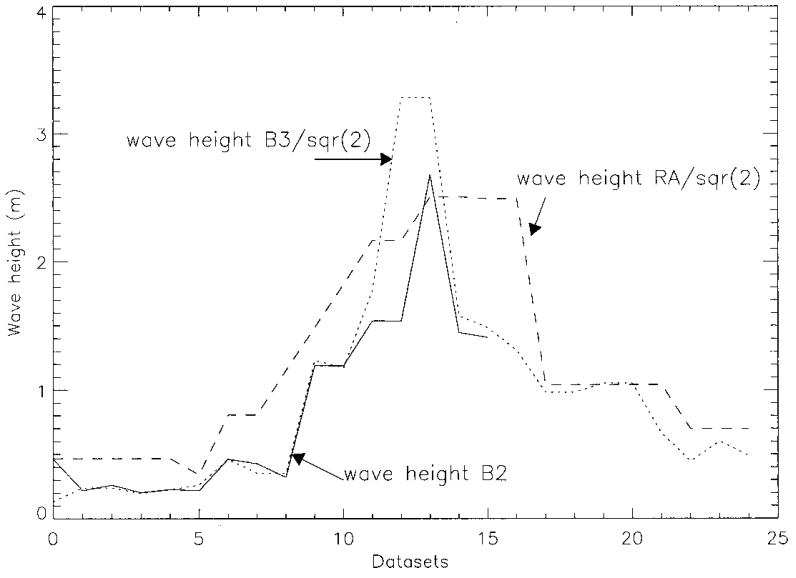

Figure 11. Comparison of wave height from two buoys and from the satellite.

Table 4. Error in the retrieved salinity using different dependence (dep.) and satellite data, considering $\Delta SSS = |SSS_{insitu} - SSS_{retrieved}|$.

	Mean (ΔSSS) (psu)	$\sigma_{\Delta SSS}$ (psu)
Wind speed dep. QuikSCAT	0.69	0.17
Wave height dep. RA-ERS	0.60	0.27

are not significant. The problem of RA from ERS-2 is its low temporal resolution (35 days repetition), so to have data with the required time resolution we averaged all the measurements in a $170 \times 440\,km^2$ area. This of course will introduce additional error due to the horizontal inhomogeneity of the wave field.

Figure 12 presents the errors in the retrieved salinity using SST measured by the *in situ* buoy plus a Gaussian noise with a standard deviation of 0.3 K (accuracy of the onflight satellites) (Au Li *et al.* 2001, Llewellyn-Jones *et al.* 2001). It can be observed that errors in SST do not produce high errors in the retrieved SSS: the maximum error is 0.1 psu. Then, SST measured by satellite is accurate enough for SSS retrieval.

5. Conclusions

The WISE campaigns provided new data to better understand the emissivity process of the sea at L-band. The results of this work confirm that it is feasible to retrieve salinity from these measurements with reasonably good accuracy. They show that the empirical emissivity models retrieve salinity with greater accuracy

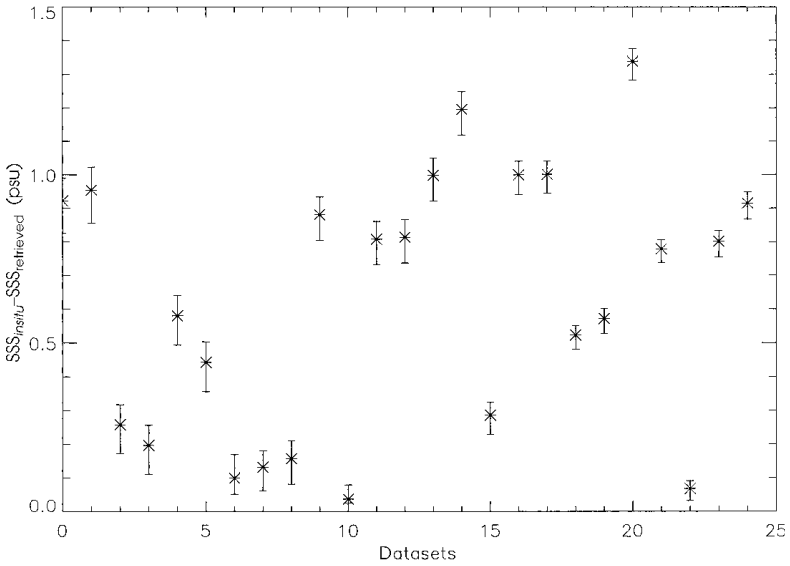

Figure 12. Uncertainty in the retrieved salinity errors due to adding random noise ($\sigma = 0.3^\circ$ C) to SST.

than the theoretical models. They also show that errors on the wind speed measurement produce large errors on the salinity retrievals. The main conclusions of this study can be summarized as follows.

• As was expected, the retrieved salinity accuracy increases with the number of incidence angles used in T_B measurements.

• An inverse algorithm applied to the brightness temperature measured by the LAURA radiometer and by different emissivity models indicates that the most realistic model is the one with the wind dependence derived from WISE. This result, expected here, must be verified by applying this model to measurements in other sea conditions. It is also shown that the Yueh model (Two-Scale Method with Durden and Vesecky $\times 2$ wave spectrum) gives poor results. The SSA model with Elfouhaily spectrum seems to work quite well for high wind speed (high wave) conditions, but for low wind conditions the retrieved salinity errors are large.

• It is necessary to study the effect of the foam at L-band, because it may be important for wind speeds higher than $10\,\mathrm{m\,s^{-1}}$. In these conditions the data retrieved with the WISE-derived model were underestimated. This can be explained because the increase in the emissivity due to the foam was not taken into account and the inverse algorithm thus compensates for its effect.

• From the study of the errors in the retrieved salinity due to errors in the ancillary data, the main conclusion is that unacceptable errors appeared when the wind speed measured by the QuikSCAT scatterometer was used for salinity retrieval. It was also demonstrated that better accuracy is achieved using the ARPEGE data. To allow the inverse algorithm to find a value of wind speed as well as salinity is a potential solution when there are a large number of different views (incidence angles).

• Errors in the SST of the order of 0.3°C (accuracy of onflight satellites) produce a small impact on the retrieved salinity.

• The attempt to retrieve salinity using a wave height dependence model (instead of wind speed dependence) gives quite good results, although they are worse than using wind speed dependence when ancillary data are obtained from the buoys for WISE data. Nevertheless, it has been demonstrated that when one is using satellite data it is better to use data of wave height measured by a radar altimeter (RA–ERS) than to use wind speed data obtained by a scatterometer (QuikSCAT), since wave height has a lower variability than wind speed.

Further research should focus on studying the effect of the spatial and temporal lags between ancillary data and SMOS T_B measurements, using different data analysis and models. It should also study the possibility of considering wind speed obtained from meteorological models to retrieve the salinity for SMOS, and determine which model would be the most appropriate. We have also initiated the retrieval of salinity from L-band data acquired during the ESA sponsored EuroSTARRS airborne campaign (Gabarró *et al.* 2003).

Acknowledgments

This study was funded by ESA–ESTEC under WISE contract 14188/00/NL/DC and by the Spanish National Program on Space Research under grant ESP2001-4523-PE. The authors very much appreciate all the cooperation and help provided by the personnel of Repsol Investigaciones Petrolíferas in the Casablanca platform and the crew of the different boats that were used. The authors also thank the

LODYC team for providing them with the Yueh model output tables, and J. Miranda for providing the analytical models.

References

AU LI, X., PICHEL, W., CLEMENTE-COLON, P., KRASNOPOLSKY, V., and SAPPER, J., 2001, Validation of coastal sea and lake surface temperature measurements derived from NOAA/AVHRR data. *International Journal of Remote Sensing*, **22**, 1285–1303.

CAMPS, A., and REISING, S. C., 2001, Wind direction azimuthal signature in the Stokes emission vector from the ocean surface at microwave frequencies. *Microwave and Optical Technology Letters*, **29**, 426–432.

CAMPS, A., FONT, J., ETCHETO, J., CASELLES, V., WEILL, A., CORBELLA, I., VALL-LLOSSERA, M., DUFFO, N., TORRES, F., VILLARINO, R., ENRIQUE, L., JULIÀ, A., GABARRÓ, C., BOUTIN, J., RUBIO, E., REISING, S. C., WURSTEISEN, P., BERGER, M., and MARTÍN-NEIRA, M., 2002, Sea surface emissivity observations at L-band: first results of the Wind and Salinity Experiment WISE-2000. *IEEE Transactions on Geoscience and Remote Sensing*, **40**, 2117–2130.

CAMPS, A., FONT, J., VALL-LLOSSERA, M., GABARRÓ, C., VILLARINO, R., ENRIQUE, L., MIRANDA, J., CORBELLA, I., DUFFO, N., TORRES, F., BLANCH, S., ARENAS, J., JULIÀ, A., ETCHETO, J., CASELLES, V., WEILL, A., BOUTIN, J., CONTARDO, S., NICLÒS, R., RIVAS, R., REISING, S. C., WURSTEISEN, P., BERGER, M., and MARTÍN-NEIRA, M., 2003a, The WISE 2000 and 2001 campaigns in support of the SMOS mission: sea surface L-band brightness temperature observations and their application to multi-angular salinity retrieval. *IEEE Transactions on Geoscience and Remote Sensing*, in press.

CAMPS, A., VILLARINO, R., ENRIQUE, L., VALL-LLOSSERA, M., MIRANDA, J., and CORBELLA, I., 2003b, Sea surface emissivity at L-band: derived dependence with incidence and azimuth angles. *Proceedings of the WISE/LOSAC/EuroSTARRS Campaigns Workshop*, ESA SP-525 (Noordwijk: ESTEC).

DURDEN, S. L., and VESECKY, J. F., 1985, A physical radar cross-section model for a wind-driven sea with swell. *IEEE Journal of Oceanic Engineering*, **10**, 445–451.

ELFOUHAILY, T., CHAPRON, B., KATSAROS, K., and VANDERMARK, D., 1997, A unified directional spectrum for long and short wind-driven waves. *Journal of Geophysical Research*, **102**, 15 781–15 796.

ELLISON, W. J., BALANA, A., DELBOS, G., LAMKAOUCHI, K., EYMARD, L., GUILLOU, C., and PRIGENT, C., 1996, Study and measurement of the dielectric properties of the sea Water. European Space Agency contract No. 11197/94/NL/CL.

FONT, J., GABARRÓ, C., JULIÀ, A., EMELIANOV, M., LLORET, M., ETCHETO, J., CONTARDO, S., LOURENÇO, A., BOUTIN, J., and MOLL, M., 2003, Oceanographic conditions during WISE 2000 and 2001. *Proceedings of the WISE/LOSAC/EuroSTARRS Campaigns Workshop*, ESA SP-525 (Noordwijk: ESTEC), pp. 51–59.

GABARRÓ, C., CAMPS, A., FONT, J., and VALL-LLOSSERA, M., 2003, Retrieved sea surface salinity and wind speed from L-band measurements for WISE and EuroSTARRS campaigns. *Proceedings of the WISE/LOSAC/EuroSTARRS Campaigns Workshop*, ESA SP-525 (Noordwijk: ESTEC), pp. 163–171.

GASIEWSKI, A. J., and KUNKEE, D. B., 1994, Polarized microwave emission from water waves. *Radio Science*, **29**, 1449–1466.

GOODBERLET, M., and MILLER, J., 1997, NPOESS sea surface salinity. NOAA Contract No. 43AANE704017, Final Report.

HOLLINGER, J. P., 1971, Passive microwave measurements of sea surface roughness. *IEEE Transactions on Geoscience Electronics*, **9**, 165–169.

HOPKINS, T. S., 2001, Thermohaline feedback loops and natural capital. *Scientia Marina*, **65** (suppl. 2), 231–256.

JOHNSON, J. T., and ZHANG, M., 1999, Theoretical study of the small slope approximation for ocean polarimetric thermal emission. *IEEE Transactions on Geoscience and Remote Sensing*, **37**, 2305–2316.

KERR, Y., FONT, J., WALDTEUFEL, P., and BERGER, M., 2000, The second of ESA's Opportunity Missions: The Soil Moisture and Ocean Salinity Mission—SMOS. *Earth Observation Quarterly*, **66**, 18–26.

KLEIN, L., and SWIFT, C. T., 1977, An improved model for the dielectric constant of sea

water at microwave frequencies. *IEEE Transactions on Antennas and Propagation*, **25**, 104–111.

LAGERLOEF, G., 2001, Oral communication at 3rd SMOS Workshop, Oberpfaffenhofen, Germany.

LAGERLOEF, G. S. E., 1998, Report of the First Workshop, Salinity Sea Ice Working Group, La Jolla, USA, 7–8 February.

LAGERLOEF, G. S. E., SWIFT, C. T., and LEVINE, D. M., 1995, Sea surface salinity: the next remote sensing challenge. *Oceanography*, **8**, 44–50.

LAURSEN, B., and SKOU, N., 2001, Wind direction over the ocean determined by an airborne, imaging, polarimetric radiometer system. *IEEE Transactions on Geoscience and Remote Sensing*, **39**, 1547–1555.

LERNER, R. M., and HOLLINGER, J. P., 1977, Analysis of 1.4 GHz radiometric measurements from Skylab. *Remote Sensing of Environment*, **6**, 251–269.

LLEWELLYN-JONES, D., EDWARDS, M. C., MUTLOW, C. T., BIRKS, A. R., BARTON, I. J., and TAIT, H., 2001, AATSR: global-change and surface-temperature measurements from Envisat. ESA Bulletin, European Space Agency.

MILLER, J. L., GOODBERLET, M. A., and ZAITZEFF, J. B., 1998, Airborne salinity mapper makes debut in coastal zone. *EOS Transactions of the American Geophysical Union*, **79**, 175–177.

PRESS, W., TEUKOLSKY, S., VETTERLING, W., and FLANNERY, B., 1992, *Numerical Recipes in C. The Art of Scientific Computing*, 2nd edn (New York: Cambridge University Press).

REUIL, N., and CHAPRON, B., 2001, Foam emissivity at L-band. ESA Salinity Requirement Study, WP1300 Report.

REYNOLDS, R., JI, M., and LEETMAA, A., 1998, Use of salinity to improve ocean modelling. *Physics and Chemistry of the Earth*, **23**, 545–555.

SKOU, N., 1955, An overview of requirements and passive microwave radiometer options. Consultative Meeting on Soil Moisture and Ocean Salinity measurement requirements and radiometer techniques (SMOS). Noordwijk, ESA, pp. 41–48.

SWIFT, C. T., 1993, ESTAR—The Electronically Scanned Thinned Array Radiometer for remote sensing measurement of soil moisture and ocean salinity. NASA Technical Memorandum 4523, 40 pp.

SWIFT, C. T., and MCINTOSH, R. E., 1983, Considerations for microwave remote sensing of ocean-surface salinity. *IEEE Transactions on Geoscience Electronics*, **21**, 480–491.

ULABY, F., MOORE, R., and FUNG, A., 1981, *Microwave Remote Sensing. Active and Passive*. vol. I, 1st edn (Reading, MA: Addison-Wesley).

VALL-LLOSSERA, M., CAMPS, A., and VILLARINO, R., 2003, Sea surface emissivity modeling at L-band: an intercomparison study. *Proceedings of the WISE/LOSAC/Euro-STARRS Campaigns Workshop*, ESA SP-525 (Noordwijk: ESTEC).

VORONOVICH, A. G., 1994, Small-slope approximation for electromagnetic wave scattering at rough interface of two dielectric half-spaces. *Waves in Random Media*, **4**, 337–367.

VORONOVICH, A. G., and ZAVOROTNY, V. U., 2001, Modelling of backscattering of radar signals from sea surface at Ka- and C-bands. Proceedings of the URSI General Assembly Maastricht, The Netherlands, (CD ROM).

WEBSTER, W. J., and WILHEIT, T. T., 1976, Spectral characteristics of the microwave emission from wind derived foam coverage sea. *Journal of Geophysical Research*, **81**, 3095–3099.

WILSON, W. J., YUEH, S. H., DINARDO, S. J., CHAZANOFF, S., LI, F. K., and RAHMAT-SAMII, Y., 2001, Passive Active L- and S-band (PALS) microwave sensor for ocean salinity and soil moisture measurements. *IEEE Transactions on Geoscience and Remote-Sensing*, **37**, pp. 1039–1048.

YUEH, S. H., WILSON, W. J., LI, F. K., NGHIEM, S. V., and RICKETTS, W. B., 1997, Polarimetric brightness temperatures of the sea surface measured with aircraft K- and Ka-band radiometers. *IEEE Transactions on Geoscience and Remote Sensing*, **35**, 1177–1187.

A.3 Geophysical Research Letters

This manuscript was submitted in October 2003 and published in January 2004.

GEOPHYSICAL RESEARCH LETTERS, VOL. 31, L01309, doi:10.1029/2003GL018964, 2004

A new empirical model of sea surface microwave emissivity for salinity remote sensing

C. Gabarró
Institut de Ciències del Mar, CMIMA-CSIC, Barcelona, Spain

J. Font
Institut de Ciències del Mar, CMIMA-CSIC, Barcelona, Spain

A. Camps
Departament de Teoria del Senyal i Comunicacions, UPC, Barcelona, Spain

M. Vall-llossera
Departament de Teoria del Senyal i Comunicacions, UPC, Barcelona, Spain

A. Julià
Institut de Ciències del Mar, CMIMA-CSIC, Barcelona, Spain

Received 31 October 2003; accepted 15 December 2003; published 14 January 2004.

[1] SMOS (Soil Moisture and Ocean Salinity) is a European Space Agency mission that aims at generating global ocean salinity maps with an accuracy of 0.1 psu, at spatial and temporal resolution suitable for climatic studies. The satellite sensor is an L-band (1400–1427 MHz) aperture synthesis interferometric radiometer. Sea surface salinity (SSS) can be retrieved since the brightness temperature of sea water is dependent on the frequency, angle of observation, dielectric constant of sea water, sea surface temperature and sea surface state. This paper presents a new empirical sea water emissivity model at L-band in which surface roughness effects are parameterized in terms of wind speed and significant wave height. For the SMOS mission these parameters can be obtained from external measurements and model diagnostics. An analysis has been done on the effect on SSS retrieval of different sources for this auxiliary information. *INDEX TERMS:* 4275 Oceanography: General: Remote sensing and electromagnetic processes (0689); 6969 Radio Science: Remote sensing; 0619 Electromagnetics: Electromagnetic theory; 6924 Radio Science: Interferometry. **Citation:** Gabarró, C., J. Font, A. Camps, M. Vall-llossera, and A. Julià (2004), A new empirical model of sea surface microwave emissivity for salinity remote sensing, *Geophys. Res. Lett.*, *31*, L01309, doi:10.1029/2003GL018964.

1. Introduction

[2] The distribution and variability of salinity in the world's oceans is a key parameter to understand the role of the oceans in the climate system. However, until now, remote sensing of the sea surface salinity (SSS) from space has not been attempted. Using the interferometric microwave radiometry concept (MIRAS instrument, Microwave Imaging Radiometer by Aperture Synthesis), SMOS will fill this gap and will provide global sea surface salinity maps for climate and large-scale ocean circulation studies [*Kerr et al.*, 2000]. The SSS maps are expected to have an accuracy of 0.1 psu at a spatial resolution of 100–200 km every 10–30 days.

[3] Salinity modifies the dielectric constant of sea water and it is one of the parameters that determine the sea surface emissivity [*Klein and Swift*, 1977]. At L-band (1400–1427 MHz), a restricted band for passive observations, the brightness temperature (T_B, measure of the sea surface emission) presents a maximum sensitivity to SSS. However, the sensitivity is quite low: 0.5 K/psu at sea surface temperature (SST) = 20°C, and decreases to 0.25 K/psu at SST = 0°C [*Lagerloef et al.*, 1995]. On the other hand, T_B at this frequency is also sensible to sea surface roughness, 0–0.4 K/(*m*/*s*), (when roughness is parameterised in terms of wind speed) depending on the incidence angle [*Hollinger*, 1971; *Webster and Wilheit*, 1976; *Lerner and Hollinger*, 1977], and to SST, 0.2–0.4 K/°C. This situation indicates that it is necessary to have an accurate knowledge of the surface roughness and SST to retrieve salinity with enough accuracy.

[4] To increase the present understanding of the L-band T_B sensitivity to wind speed and direction, the European Space Agency (ESA) sponsored the WInd and Salinity Experiments (WISE). These experiments aimed, among other activities, at improving and validating the actual sea surface emissivity models at L-band.

2. Campaigns Description

[5] WISE 2000 and 2001 [*Camps et al.*, 2004] took place at the Casablanca oil rig platform in the Mediterranean Catalan coast, at 40°43.02′N 1°21.50′E, 40 Km offshore. They were performed during one month in autumn, when maximum wind speed is expected in the region. An L-band full-polarimetric radiometer measured T_B from 33 m above sea level at different incidence and azimuth angles, while several oceanographic and meteorological buoys measured SSS, SST, wind speed and direction, significant wave height (SWH) and period, and wave spectrum.

[6] Radiometer measurements were performed at different elevation angles from 25° to 65° to emulate the

0094-8276/04/2003GL018964$05.00

Table 1. Number of Data Points for Each Incidence Angle and Polarization in WISE 2001

θ_i	25°	30°	35°	40°	45°	50°	55°	60°	65°
H-pol	143	36	232	35	478	33	348	36	125
V-pol	305	34	532	56	656	57	511	49	190

performance of SMOS, since the two-dimensional imaging capability of MIRAS will allow the observation of pixels in a wide range of incidence angles. This is a unique characteristic of this data set to study SSS retrievals and to test several theoretical electromagnetic L-band emissivity models. Table 1 shows the amount of data acquired during the campaign for each elevation angle. The radiometric sensitivity is 0.2 K for 1 s integration time and the absolute calibration accuracy is lower than 0.5 K.

[7] EuroSTARRS was an airborne campaign also organized by ESA in November 2001 as part of the SMOS preparatory studies [*Berger et al.*, 2002]. An L-band V-polarized multi-angular radiometer [*Miller and Goodberlet*, 2003] of different technology was flown over the same oil platform area in coincidence with WISE 2001.

3. Models

[8] The brightness temperature of the sea surface can be modeled by equation 1, composed of a term due to the emissivity of a flat surface plus the term that accounts for the effect of the sea roughness,

$$T_{B,p}(\theta, SST, SSS, U_{10}) = e_p(\theta, SST, SSS) \cdot SST + \Delta T_{B\ rough,p}(\theta, U_{10}) \quad (1)$$

where $e_p = 1 - \Gamma_p$ is the emissivity of the flat sea surface for each polarization (horizontal and vertical), Γ_p is the Fresnel power reflection coefficient and θ is the elevation angle. In this formulation, the information on sea surface roughness is parameterized through the wind speed measured at 10 m above sea level (U_{10}).

[9] *Camps et al.* [2004] have proposed an empirical model of $T_{B\ rough}$ derived from WISE data, by fitting the sensitivity of T_B to wind speed at different incidence angles, and the two polarizations.

[10] *Gabarró et al.* [2003] retrieved surface salinity from WISE measurements using in the computation different theoretical sea surface emissivity models and the above-mentioned empirical model, all depending on wind speed. Two models for electromagnetic surface scattering (Two-scale, and Small Slope Approximation) and two theoretical wave spectrum models [*Durden and Vesecky*, 1985; *Elfouhaily et al.*, 1997] were tested. The retrieval of SSS appeared to be more efficient when using the empirical model derived from WISE measurements than any other combination of theoretical models.

[11] All these models consider the surface wave spectrum only dependent on the local wind speed, and consequently fully developed sea conditions. So, they do not include either the possible situation of growing and decaying winds or the swell effect. *Miranda et al.* [2003] demonstrated that the measured spectra frequently are not well approximated using fully developed models.

[12] New formulations for the modelisation of the sea surface are being developed now based on the Local Curvature Approximation concept [*Elfouhaily et al.*, 2003]. The effects of sea roughness on L-band emissivity occur in the range of decimetric wavelengths, but the present situation indicates that we will probably have to rely only on the regularly available diagnosed parameters at global scale: wind speed and direction, if necessary, and SWH.

[13] From these considerations, a new empirical model of $\Delta T_{B\ rough,p}$ derived from WISE 2001 measurements is presented here (Equation 2). It explains the variability of T_B depending on local wind speed (U_{10}), and also on SWH, by fitting simultaneously the T_B data to both variables recorded in situ.

$$\begin{aligned} \Delta T_h &\approx 0.12 \cdot \left(1 + \frac{\theta}{24^\circ}\right) \cdot U_{10} + 0.59 \cdot \left(1 - \frac{\theta}{50^\circ}\right) \cdot SWH \\ \Delta T_v &\approx 0.12 \cdot \left(1 - \frac{\theta}{40^\circ}\right) \cdot U_{10} + 0.59 \cdot \left(1 - \frac{\theta}{50^\circ}\right) \cdot SWH \end{aligned} \quad (2)$$

Then, this model considers the effects on surface roughness of both the local wind and other processes that can contribute to SWH formation.

4. Sea Surface Salinity Retrieval

4.1. WISE Field Experiment

[14] Inverting this new forward model, SSS has been retrieved again from WISE T_B data. The algorithm used is a recurrent Levenberg-Marquardt least-square fit [*Press et al.*, 1992], applied to ensembles of data recorded in a series of multi-angular radiometric observations performed under constant sea and wind conditions. T_B is computed setting an initial guess for SSS into the direct emissivity model (Equations 1 and 2). The Klein and Swift model (*Klein and Swift* [1977]) has been applied in order to calculate the dielectric constant from SSS and SST, and then e_p. This T_B value is compared with the T_B measured by the radiometer, and then an increment δSSS is added to the previous SSS to initiate a new computation. This recursive system stops when the difference between the measured and the computed T_B is smaller than a threshold. The retrieved salinity is mostly insensitive to the initial guess for SSS.

[15] An assessment of the retrieval error is obtained by the difference between the retrieved SSS and the one measured in situ by a SeaBird 37 instrument (effective accuracy 0.02 psu) during the series of T_B observations. The average error when using the new model dependent on wind speed and wave height ($\Delta SSS = 0.33$ psu and $\sigma_{\Delta SSS} = 0.05$) is considerably smaller than using the empirical model that considers only local wind speed ($\Delta SSS = 0.52$ psu and $\sigma_{\Delta SSS} = 0.12$) [*Gabarró et al.*, 2003]. The standard deviation has also been reduced. A reduction in error budget is expected in any regression when the degree of freedom is increased. But in this case it has a physical meaning since SWH data contain information from processes that modify the sea surface spectrum other than contemporaneous local wind. The substantial reduction on the SSS error (about 35%) confirms that swell and varying winds have an important role in the final balance of emissivity of the sea.

4.2. EuroSTARRS Field Experiment

[16] This model has also been tested to retrieve salinity from the EuroSTARRS data set. Although the data resulted

Table 2. Comparison of Different Sources for Wind Speed and Significant Wave Height

SOURCE	Spatial resolution	Temporal resolution
HIRLAM	0.12°	3 hours
ARPÈGE	0.25°	6 hours
QuikSCAT	25 Km	3 days
WAM	0.12°	3 hours
RA-ERS	15 Km	35 days

to be very noisy and some beams were affected by calibration problems, a series of 800 data points along a straight line over relatively homogeneous fields were averaged to retrieve salinity. The results confirm that this new model retrieves salinity much better (ΔSSS = 0.13 psu) than the model only dependent on U_{10} (ΔSSS = 0.24 psu). These EuroSTARRS errors are highly improved with respect to WISE results due to the much larger number of radiometer snapshot measurements averaged before retrieval, and hence reducing the experimental noise. Nevertheless, the model should be tested with other data sets measured in different locations and sea conditions to validate this conclusion.

5. Sea Surface Salinity Using Auxiliary Data

[17] To retrieve salinity from SMOS, auxiliary variables (wind speed, wave height and SST) are needed with good quality, and as simultaneous in time and space as possible to the spaceborne radiometer measurements. One possibility is to use observations made by other sensors (scatterometers, altimeters, SAR) embarked on satellites with similar orbit, but these measurements will hardly be simultaneous. On the other hand meteorological and oceanographic marine models could also be used, with the advantage of having much higher temporal resolution, and having assimilated satellite and other sources of information. Both cases will present inaccuracies on the measurements due to instrumental errors and sampling limitations.

[18] The determination of sea roughness non-coincidental to SMOS overpasses is a major problem due to its high variability and accuracy limitations in satellite measurements and models. Sea surface temperature, nevertheless, is not as critical as roughness, since its variability is much lower, the sensitivity of T_B to SST is also lower, and satellite measurements are very accurate (0.3 K) and frequent. We have analyzed here the effect on SSS retrieval of using different sources for roughness information.

[19] The following numerical model outputs and satellite measurements of wind speed and SWH were obtained for the area and time of the WISE 2001 campaign,

[20] 1. Wind speed information:

[21] (i) HIRLAM: numerical model with assimilation of satellite data (Spanish Instituto Nacional de Meteorología)

[22] (ii) ARPÈGE: numerical model with assimilation (Météo-France)

[23] (iii) QuikSCAT: radar scatterometer on board SEAWINDS NASA polar orbit satellite

[24] 2. Significant wave height information:

[25] (i) WAM: numerical model with assimilation of satellite data, only for atmospheric parameters

[26] (ii) RA-ERS: radar altimeter on board ESA ERS-2 satellite

[27] Table 2 summarizes the spatial and temporal resolutions of each data source. Figures 1 and 2 show the temporal sequence of wind speed and wave height obtained from these sources. For wind speed, the models and satellite outputs are quite similar to in situ measurements except for some punctual occasions. The mean difference between wind speed in situ measurements and HIRLAM model output is 1.98 m/s, with respect to ARPÈGE model output is 1.93 m/s, while to satellite data is 1.59 m/s (although in this last case there are much less data points available). These differences are above the 1.5 m/s accuracy in wind speed initially required for SMOS SSS retrieval from preliminary simulations.

[28] The SWH given by the model is similar to the buoy measurement, except for high wave height events, where the model overestimates it. The satellite measurements are not very realistic, which is not surprising since their temporal resolution is very low and a lot of spatial averaging has to be done to cover the WISE area. The mean difference between in situ measurements and WAM model is 0.22 m,

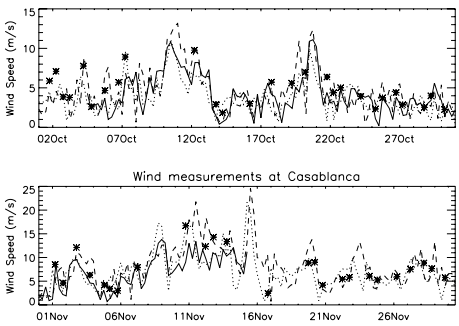

Figure 1. Comparison of different sources of wind speed information during WISE campaign. In situ buoy (plain line), HIRLAM model (dashed line), ARPÈGE model (dotted line) and QuikSCAT satellite (*).

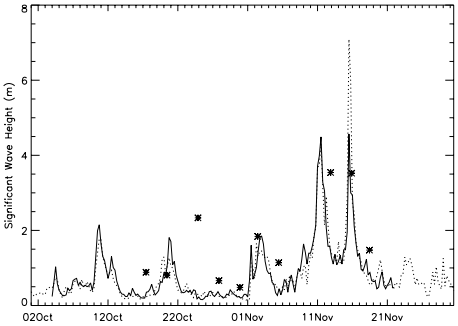

Figure 2. Comparison of different sources of significant wave height information during WISE campaign. In situ buoy (plain line), WAM model (dotted line) and Radar Altimeter-ERS (*).

while the mean difference grows to 1.16 m with respect to satellite measurements.

[29] The retrieval of SSS in the WISE case has been tested using different combinations of these sources of wind speed and wave height information. For SST in situ measurements have always been used.

[30] An alternative way to retrieve salinity, in case of missing or bad quality auxiliary data, is to consider the two variables as unknown parameters in the forward model, and then allow the inversion algorithm to converge simultaneously to a value for salinity, and also for U_{10} and SWH. In this case the cost function to minimize would have three parameters instead of only one. This option has also been tested for WISE and the selected first guess values for U_{10} and SWH have been the HIRLAM and WAM model outputs.

[31] Table 3 summarizes the error on the SSS retrieved for different sources of auxiliary data with the model presented in equation 2. It shows that better results are obtained when leaving the auxiliary data free as variables to optimize, than fixing them with excessively erroneous values. Furthermore, the error on the wind speed and wave height retrieved with the optimization process ($\Delta U_{10} = |U_{10\ in\ situ} - U_{10\ retrieved}|$) is smaller than the error of the model outputs and satellite measurements. Figure 3 plots the results of retrieved U_{10} respect to in situ measurements and HIRLAM output model for several data sets. It shows that the retrieved U_{10} is nearer to in situ measurements than HIRLAM output, even though the first guess parameter was that model. So it seems that by leaving U_{10} as free parameter for retrieval, the algorithm can improve its initial values.

[32] Table 3 shows also that the use of meteorological model data (with assimilation of space-borne observations) is better than to use satellite data directly, since the latter have much worse temporal resolution.

6. Conclusion

[33] This paper describes a new empirical model of L-band sea surface emissivity dependent on wind speed and significant wave height derived from radiometric and in situ data gathered in the NW Mediterranean. Salinity is retrieved with smaller errors when using this model than other models dependent on wind speed and then considering only the presence of fully-developed wind waves.

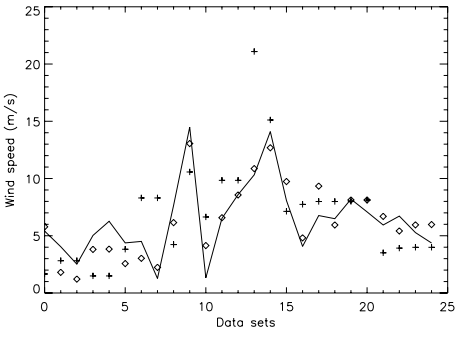

Figure 3. Comparison of wind speed measurement U_{10} determinations: measured in situ (diamonds), output from HIRLAM analysis (crosses), and retrieved by the algorithm when it is set to be free (line). It can be seen that retrieved wind speed is nearer to in situ measurements than model output.

Table 3. Errors on the Retrieved Salinity $\Delta SSS = |SSS_{in\ situ} - SSS_{retrieved}|$, Error on Wind Speed ΔU_{10} and on Wave Height ΔSWH for Different Ancillary Data

Source U_{10}	Source SWH	ΔSSS	ΔU_{10}	ΔSWH
In situ	in situ	0.33	–	–
HIRLAM	WAM	0.59	1.98	0.22
ARPÈGE	WAM	0.49	1.94	0.22
QuikSCAT	ERS	0.61	1.59	0.46
Free	free	0.40	1.22	0.22

[34] Since T_B is sensitive to surface roughness, it is necessary to have accurate auxiliary data to obtain accurate estimates of SSS. In this paper different sources for acquiring auxiliary data during the SMOS mission have been presented. The error with respect to in situ measurements and the influence of this error on the accuracy of the SSS retrieval have been analyzed.

[35] An important conclusion is that using data from meteorological models to retrieve salinity is better than using direct satellite data, since the former have smaller temporal resolution. From the analysis of WISE dataset, it appears that in absence of accurate in situ observations, the best method to retrieve salinity is to leave U_{10} and SWH as free parameters, and let the retrieval algorithm to take advantage of the multi-angular view capability of SMOS imaging configuration.

[36] These conclusions are only applicable to the WISE field site, in the north Mediterranean, and can not be automatically extrapolated to other ocean areas. This empirical model may need to be adapted to different oceanographic characteristics. The accuracy and resolution of meteorological models can also vary in other regions, as well as the accuracy of satellite data. This work is a regional study, but could be a first step for a global scheme applicable to SMOS observations.

[37] **Acknowledgments.** This study was funded by ESA-ESTEC under WISE (14188/00/NL/DC) and EuroSTARRS (15950/02/NL/SF) contracts, and by the Spanish National Program on Space Research under grant ESP2001-4523-PE.

References

Berger, M., A. Camps, J. Font, Y. Kerr, J. Miller, J. Johannessen, J. Boutin, M. Drinkwater, N. Skou, N. Floury, M. Rast, and H. Rebhan (2002), Measuring Ocean Salinity with ESA's SMOS mission — Advancing the Science, *ESA Bulletin — European Space Agency*, *111*, 113–121.

Camps, A., J. Font, M. Vall-llossera, C. Gabarró, R. Villarino, L. Enrique, J. Miranda, I. Corbella, N. Duffo, F. Torres, S. Blanch, J. Arenas, A. Julià, J. Etcheto, V. Caselles, A. Weill, J. Boutin, S. Contardo, R. Niclòs, R. Rivas, S. Reising, P. Wursteisen, M. Berger, and M. Martín-Neira (2004), The WISE 2000 and 2001 Campaigns in Support of the SMOS Mission: Sea Surface L-band Brightness Temperature Observations and their Application to Multi-Angular Salinity Retrieval, *IEEE Trans. Geosci. Remote Sens*, in press.

Durden, S., and J. Vesecky (1985), A Physical Radar Cross-Section Model for a Wind-Driven Sea with Swell, *IEEE J. Oceanic Eng.*, OE-*10*, 445–451.

Elfouhaily, T., B. Chapron, K. Katsaros, and D. Vandermark (1997), A Unified Directional Spectrum for Long and Short Wind-driven Waves, *J. Geophys. Res.*, *102*(C7), 15,781–15,796.

Elfouhaily, T., S. Guignard, R. Awadallah, and D. Thompson (2003), Local and Non-local Curvature Approximation: A New Asymptotic Theory for Wave Scattering, *Waves Random Media*, *13*(4), October.

Gabarró, C., M. Vall-llossera, J. Font, and A. Camps (2003), Determination of Sea Surface Salinity and Wind Speed by L-band Microwave Radiometry from a fixed Platform, *Internat. J. Remote Sens.*, *25*(1), 111–128.

Hollinger, J. (1971), Passive Microwave Measurements of Sea Surface Roughness, *IEEE Trans. Geosci. Electron.*, GE-*9*(3), 165–169.

Kerr, Y., J. Font, P. Waldteufel, and M. Berger (2000), The Second of ESA's Opportunity Missions: The Soil Moisture and Ocean Salinity Mission-SMOS, *Earth Observation Quarterly*, *66*, 18–26.

Klein, L., and C. Swift (1977), An Improved Model for the Dielectric Constant of Sea Water at Microwave Frequencies, *IEEE Trans. Antennas Propag.*, *AP-25*(1), 104–111.

Lagerloef, G., C. Swift, and D. M. Levine (1995), Sea Surface Salinity: The Next Remote Sensing Challenge, *Oceanogr.*, *8*(2), 44–50.

Lerner, R., and J. Hollinger (1977), Analysis of 1.4 GHz Radiometric Measurements from Skylab, *Remote Sensing Environment*, *6*, 251–269.

Miller, J., and M. Goodberlet (2003), Development and Application of STARRS — a Next Generation Airborne Salinity Imager, *Internat. J. Remote Sens.*

Miranda, J., M. Vall-llossera, R. Villarino, and A. Camps (2003), Sea State and Rain Effects in the Sea Surface Emissivity at L-Band, *Proceedings of the WISE/LOSAC/EuroSTARRS campaigns Workshop. ESA*, SP-*525*, 155–162.

Press, W., S. Teukolsky, W. Vetterling, and B. Flannery (1992), *Numerical Recipes in C. The Art of Scientific computing*, 2nd edition, Cambridge Univ. Press.

Webster, W., and T. Wilheit (1976), Spectral Characteristics of the Microwave Emission from wind Derived foam Coverage Sea, *J. Geophys. Res.*, *81*, 3095–3099.

C. Gabarró, J. Font, and A. Julià, Institut de Ciències del Mar, CMIMA-CSIC, Passeig Marítim de la Barceloneta 39–47, Barcelona 08003, Spain. (cgabarro@icm.csic.es)

A. Camps and M. Vall-llossera, Departament de Teoria del Senyal i Comunicacions, UPC, Campus Nord, D4 08034 Barcelona, Spain.

Appendix B

Instrumentation technical documentation

This appendix summarise the performance characteristics for several instruments used during WISE 2000 and WISE 2001 campaigns. A diagram of data acquisition and transmission in buoy 1 has also been included. Finally, the specifications of the microprocessor that was used and programed are attached.

SeaBird MicroCAT system (model SBE37-SM)

The SeaBird SBE37-SM is a conductivity and temperature recorder, with internal power supply and memory for data recording. It has a RS232C serial interface and it can be programmed to give sampling rates between 10 seconds and 9.1 hours. The system uses a 24-bit A/D converter to digitise the temperature sensor voltage.

The RMS deviation on the salinity calculation from conductivity and temperature is 0.002 psu. The memory capacity, expressed as number of samples, of the SBE 37-SM MicroCAT, is 410.000 samples (C and T only). For C, T and time, the capacity is 225.000 samples. The battery power pack is made of six 9 V lithium batteries, having a total of 6 Ah charge.

Salinometer Guildline Autosal

	Temperature	Conductivity
Measurement range	-5 to 35°C	0 to 7 S/m
Initial accuracy	0.002°C	0.0003 S/m
Typical stability (per month)	0.0002 °C	0.0003 S/m
Resolution	0.0001 °C	0.0001 S/m

Table B.1: Temperature and conductivity characteristics of SeaBird Microcat instrument

The salinometer that was used is the Model 8400B. This instrument measures the conductivity and the temperature of a sample comparing from a reference water. This reference water, called "Copenhagen water", has a salinity of 35.0000 psu. The technical characteristics of the instrument are the following:

	salinity
Accuracy	0.002 psu
Resolution	0.0002 psu
Stability on temperature	0.001 °C/day

Table B.2: Salinity characteristics of Salinometer Guildline Autosal

USONIC anemometer

The Usonic is a competent ultrasonic anemometer for universal usage. It is constructed for high precision, inertia free measurements of wind speed, directions and temperature.

It has the big advantage of no wear of mechanical parts. The whole system with all electronic parts is completely integrated in a robust stainless steel housing.

The data output is pre configurable by remote PC. It can transmit digital (RS-232/RS485) or analogue data from the interface.

Coastal Monitoring Buoy (CMB3280) from Aanderaa Instruments

	Wind speed	Wind direction	Temperature
Meas. range	0 to 60 m/s	0°-360°	-30° C .. 60°
Meas. accuracy	0.1 m/s (below 5 m/s) or $< 1.5\%$ (above 5 m/s)	$< \pm 3°$	$< \pm 1°$ C
Resolution	0.05 m/s	1°	0.1° C

Table B.3: Performance characteristics of the Doppler ultrasonic anemometer model 5010-0005 from USONIC.

Parameter	Accuracy	Resolution
Wind speed	2%	0.075 m/s
Wind direction	5º mag.	0.4 º
Air temperature	0.1 ºC	0.05 ºC
Solar radiation	20 W/m2	0.4 W/m2
Relative humidity	2%	0.1 %
Wave height	0.2 m, 10%	0.01 m
Wave period	10%	0.03 s

Table B.4: Performance characteristics of the standard Coastal Monitoring Buoy (CMB3280) from Aanderaa Instruments.

The method of measurement for this instrument is the average over the past measured interval. The wind speed measurements have been done with a three-cup rotor. Significant wave height is measured as the mean of the highest third of all the waves during the sampling interval.

AANDERAA RCM9 current meter

The instrument is a Doppler sensor, and the acoustic frequency is 2MHz .

	Current speed	Current direction	Water temp.
Meas. range	0 to 500 cm/s	0°-360°	-8 to 41° C
Meas. accuracy	0.2 cm/s or ±2% of actual speed	±5° to 0-15° tilt of the buoy and ±7.5° for 15 - 35° tilt of the buoy	±0.1°C

Table B.5: Performance characteristics of the AANDERAA RCM9 current meter

Meteorological Station on the platform

This meteorological station was manufactured by MCV,S.A. This station was located in a tower, 69 m above sea level. Just before starting the WISE experiments the wind instruments were calibrated.

	Wind speed	Wind direction
Meas. range	0 to 56 m/s	0°-360°
Meas. accuracy	$< \pm 1$ m/s (<10 m/s) or $< \pm 10\%$ elsewhere	$< \pm 10°$
Resolution	0.2 m/s	1°

Table B.6: Performance characteristics of the meteorological station manufactured by MCV.

Microprocessor FM-200 Embedded controller

This microprocessor if manufactured at the Cambridge MICROPROCESSOR system limited company.

Features of the microprocessor are:

- 68000 Compatible CPU
- 512 k-bytes of on board programmable Flash EEPROM
- 512 k-bytes of battery backed Static RAM

- Three independent serial ports
- I2C high speed serial
- Real Time Calendar Clock
- Two timer/counters
- Software Watchdog
- 5 Volt only operation
- Ten TTL/CMOS digital I/O channels
- Small Size 90 x 100 mm

The code of the micro was programed in 'C' language. More information on this microprocessor can be found in http://www.cms.uk.com/.

Figure B.1 shows a diagram of the data acquisitions, the storage and the transmission all controlled by the microprocessor located in buoy 1.

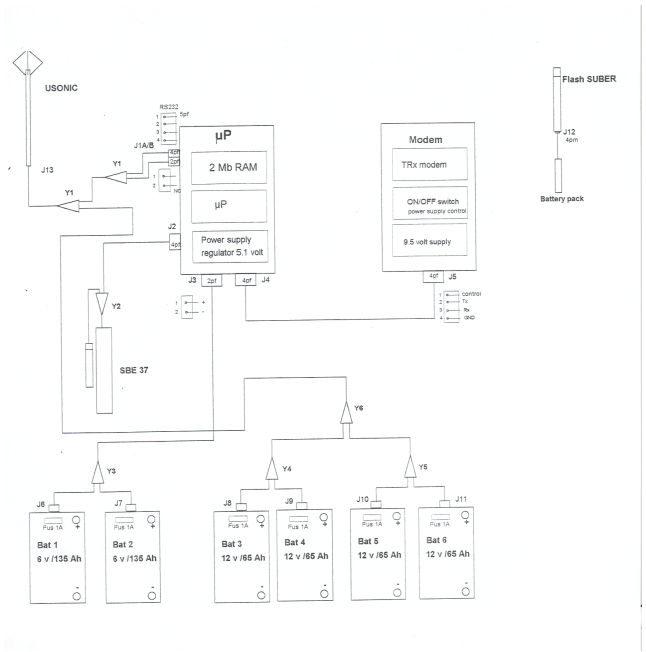

Figure B.1: Diagram of data acquisition and transmission.

Bibliography

Blanch, S. and Aguasca, A. (2004). Seawater dielectric permittivity model from measurements at l-band. *Proceedings of IGARSS 2004, Alaska*.

Blume, H., Kendall, B., and Fedors, J. (1978). Measurements of Ocean Temperature and Salinity vis Microwave Radiometry. *Boundary-Layer Meteorology*, 13:295–308.

Blume, H., Love, A., Van Melle, M., and Ho, W. (1977). Radiometric observations of sea temperature at 2.65 GHz over the Chesapeake Bay. *IEEE Transactions on Antennas and Propagation*, AP-25:121–128.

Camps, A. (1996). *Application of Interferometric Radiometry to Earth Observation. Ph.D.* PhD thesis, Universitat Politècnia de Catalunya.

Camps, A., Corbella, I., Vall-llossera, M.and Duffo, N., Marcos, F., Martínez-Fadrique, and Greiner, M. (2003a). The SMOS End-to-end Performance Simulator: Description and Scientific Applications. *Proceedings International Geoscience and Remote Sensing Symposium, Toulouse, France*.

Camps, A., Corbella, I., Vall-llossera, M.and Duffo, N., Torres, F., Villarino, R., Enrique, L., Miranda, J., Julbe, J., Font, J., Julià, A., Gabarró, C., Etcheto, J., Boutin, J., Weill, A., Caselles, V., Rubio, E., Wursteisen, P., Berger, M., and Martín-Neira, M. (2003b). L-band Sea Surface emissivity: Premilinary results of the WISE-2000 campaign and its application to salinity restrieval in the SMOS mission. *Radio Science*, 93(4):8071,doi:10.1029/2002RS002629.

Camps, A., Duffo, N.and Vall-llossera, M., and Vallespin, B. (2002a). Sea Surface Salinity Retrieval using multi-angular L-band Radiometry: Numerical Study Using the SMOS End-to-end Performance Simulator. *Proceedings IGARSS, Toronto, Canada*.

Camps, A. et al. (2001). Wind and Salinity Experiment 2000 (WISE 2000): Scientific Analysis Report. Technical report, ESTEC, ESA. Contract No. 14188/00/NL/DC.

Camps, A., Font, J., Vall-llossera, M., Gabarró, C., Villarino, R., Enrique, L., Miranda, J., Corbella, I., Duffo, N., Torres, F., Blanch, S., Arenas, J., Julià, A., Etcheto, J., Caselles, V., Weill, A., Boutin, J., Contardo, S., Niclòs, R., Rivas, R., Reising, S., Wursteisen, P., Berger, M., and Martín-Neira, M. (2004a). The WISE 2000 and 2001 Campaigns in Support of the SMOS Mission: Sea Surface L-band Brightness Temperature Observations and their Application to Multi-Angular Salinity Retrieval. *IEEE Transactions on Geoscience and Remote Sensing*, 42(4):804–823.

Camps, A., Font, J.and Etcheto, J., Caselles, V., Weill, A., Corbella, I., Vall-llossera, M., Duffo, N., Torres, F., Villarino, R., Enrique, L., Julià, A., Gabarró, C., Boutin, J., Rubio, E., Reising, S., Wursteisen, P., Berger, M., and Martín-Neira, M. (2002b). Sea Surface Emissivity Observations at L-band: First Results of the Wind and Salinity Experiment WISE-2000. *IEEE Transactions on Geoscience and Remote Sensing*, 40(10):2117–2130.

Camps, A., Vall-llossera, M., Bartes, F., Torres, F., Duffo, N., and Corbella, I. (2004b). External Calibration In L-Band 2D Synthetic Aperture Radiometers: Application To Sea Surface Salinity Retrieval. *Proceedings International Geoscience and Remote Sensing Symposium (IGARSS) , Anchorage, Alaska (EEUU)*, pages 0–7803–8743–0/04.

Camps, A., Vall-llossera, M., Bartes, F., Torres, F., Duffo, N., and Corbella, I. (2004c). Retrieving Sea Surface Salinity with Multi-Angular L-band Brightness Temperature Improvements by Spatio-Temporal Averaging. *IEEE Transactions on Geoscience and Remote Sensing, in press.*

Corbella, I., Camps, A., Zapata, M., Marcos, F., Martínez, F., and Vall-llossera (2003). End-to-end simulator of 2D interferometric radiometry. *Radio Science*, 38(8058):doi:10.1029/2002RS002665.

Debye, P. (1929). *Polar Molecules.* New York: Reinhold.

Dinnat, E. (2003). *De la Détermination de la Salinité de la Surface des Océans à Partir de Mesures Radiométriques Hyperfréquences en bande L.* PhD thesis, Laboratoire d'Océanographie DYnamique et de Climatologie. France.

Drange, H., Johannessen, J., NERSC, CLS, LODYC, IFREMER, LEGI, SOC, UCL, UPC, DLR, and CSIC (2001). Scientific requirements and impact of

space observations of ocean salinity for modelling and climate studies. Technical report, NOAA, USA. Agencia Espacial Europea (ESTEC Contract No. 14273/00/NL/DC).

Durden, S. and Vesecky, J. (1985). A Physical Radar Cross-Section Model for a Wind-Driven Sea with Swell. *IEEE Journal of Oceanic Engineering*, OE-10:445–451.

Elfouhaily, T., Chapron, B., Katsaros, K., and Vandermark, D. (1997). A Unified Directional Spectrum for Long and Short Wind-driven Waves. *Journal of Geophysical Research*, 102:15781–15796.

Ellison, W., Balana, A., Delbos, G., Lamkaouchi, K., Eymard, L., Guillou, C., and Prigent, C. (1998). New Permittivity Measurements of Sea Water. *Radio Science*, 33(3):639–648.

Emelianov, M., Font, J., J., A., Gabarró, C., LLoret, M., and Solé, J. (2003). Sea Surface Fiels at Casablanca Site (NW Mediterranean) during the EuroSTARRS Campaign. *Proceedings of the WISE/LOSAC/EuroSTARRS Campaigns Workshop. ESA PUBLICATIONS*, SP-525:73–80.

Emery, W. J. and Thomson, R. E. (1997). *Data analysis methods in physical oceanography*. Great Britain: Pergamon.

Etcheto, J., Dinnat, E., Boutin, J., Camps, A., Miller, J., Contardo, S., Wesson, J., Font, J., and Long, D. (2004). Wind speed effect on L-band brightness temperature inferred from EuroSTARRS and WISE 2001 field experiments. *IEEE Transactions on Geoscience and Remote Sensing (in press).*

Flattau, T., Becker, S., and Leber, A. (1976). Passive l-band radiometer for remote sensing of earth resources. *Microwave Symposium Digest, MTT-S International*, 76(1):328–330.

Font, J., Gabarró, C., Julià, A., Emelianov, M., Lloret, M., Etcheto, J., Contardo, S., Lourenço, A., Boutin, J., and Moll, M. (2003a). Oceanographic Conditions during WISE 2000 and 2001. *Proceedings of the WISE/LOSAC/EuroSTARRS Campaigns Workshop. ESA PUBLICATIONS*, SP-525:51–60.

Font, J., Kerr, Y., and Berger, M. (2000). Measuring Ocean Salinity from Space: the European Space Agency's SMOS Mission. *Backscatter*, 11(3):17–19.

Font, J., Lagerloef, G., Kerr, Y., Skou, N., and Berger, M. (2003b). Sea surface salinity mapping with SMOS space mission. *Building the European capacity in operational oceanography. Proceedings of the 3rd EuroGOOS Conference: H.*

Dahlin, N.C. Flemming, K. Nittis, S.E. Petterson Eds., Elsevier Oceanography Series, 69:186–189.

Font, J., Lagerloef, G., LeVine, D., Camps, A., and Zanife, O. (2004). The Determination of Surface Salinity with the European SMOS Space Mission . *IEEE Transactions on Geoscience and Remote Sensing (in press).*

Gabarró, C., Camps, A., Font, J., and Vall-llossera, M. (2003). Retrieved Sea Surface Salinity and Wind Speed from L-band Measurements for WISE and EuroSTARRS Campaigns. *Proceedings of the WISE/LOSAC/EuroSTARRS Campaigns Workshop. ESA PUBLICATIONS*, SP-525:163–172.

Gabarró, C., Font, J., Camps, A., Vall-llossera, M., and Julià, A. (2004a). A New Emprical Model of Sea Surface Microwave Emissivity for Salinity Remote Sensing. *Geophysical Research Letters*, 31(L01309):1–5.

Gabarró, C., Vall-llossera, M., Font, J., and Camps, A. (2004b). Determination of Sea Surface Salinity and Wind Speed by L-band Microwave Radiometry from a fixed Platform. *Internation Journal of Remote Sensing*, 25(1):111–128.

Goodberlet, M. and Miller, J. (1997). NPOESS Sea surface Salinity. Technical report, NOAA, USA. contract 43AANE704017.FINAL REPORT.

Guerrero, R. and Piola, A. (1977). Masas de agua en la plataforma continental. *El mar Argentino y sus recursos pesqueros*, 1:107–118.

Hertz, J. A., Krogh, A., and Palmer, R. G. (1991). *Introduction to the theory of neural computation.* Addison-Wesley, Wokingham, U.K.

Ho, W. and Hall, W. (1973). Measurements of the Dielectric Properties of Seawater and NaCl Solutions at 2.65 GHz. *Journal of Geophysical Research*, 78(27):6301–6315.

Ho, W., Love, A., and MELLE, M. (1974). Measurements of the Dielectric Properties of Seawater at 1.43 GHz. Technical report, NASA. Technical Report CR-2458.

Hollinger, J. (1971). Passive Microwave Measurements of Sea Surface Roughness. *IEEE Transactions on Geoscience Electronics*, GE-9(3):165–169.

Klein, L. and Swift, C. (1977). An Improved Model for the Dielectric Constant of Sea Water at Microwave Frequencies. *IEEE Transactions on Antennas and Propagation*, AP-25(1):104–111.

Kudryatsev, N., Makin, V., and Chapron, B. (1999). Coupled Sea Surface - Atmosphere Model. Spectrum of Short Wind Waves. *Journal of Geophysical Research*, 104(C4):7625–7639.

Lagerloef, G. (1998). Report of the First Workshop, Salinity Sea Ice Working Group. Technical report, NASA, USA. La Jolla, USA, 7-8 Feb.

Lagerloef, G., Swift, C., and D. M., L. (1995). Sea Surface Salinity: the Next Remote Sensing Challenge. *Oceanography*, 8(2):44–50.

Le Vine, D. and Abraham, S. (2004). Galactic Noise and Passive Microwave Remote Sensing from Space at L-Band. *IEEE Transactions of Geoscience and Remote Sensing*, 42:119–129.

Le Vine, D., Griffis, a., Swift, C., and Jackson, T. (1994). ESTAR: A Synthetic Aperture Microwave Radiometer for Remote Sensing Applications. *Proceedings of the IEEE*, 82(12):1787–1801.

Levitus, S., Burgett, R., and Boyer, T. (1994). World Ocean Atlas 1994 Volume 3: Salinity. *NOAA NESDIS 3*.

Marquardt, D. (1963). An algorithm for least-squares estimation of non-linear parameters. *Journal on Applied mathematics*, 11(2):431–441.

Martín-Neira, M. and Goutoule, J. (1997). A Two-Dimensional Aperture-Synthesis Radiometer for Soil Moisture and Ocean Salinity Observations. *ESA Bulletin*, 92:95–104.

Miller, J., Goodberlet, M., and Zaitzeff, J. (1998). Airborne Salinity Mapper makes Debut in Coastal Zone. *EOS Trans. American Geophysical Union*, 79(14):175–177.

Miranda, J., Vall-llossera, M., Camps, A., Duffo, N., Corbella, I., and Etcheto, J. (2003). Sea State on the Sea Surface Emissivity at L-Band. *IEEE Transactions of Geoscience and Remote Sensing*, 41(10):2307–2315.

Nelder and Mead (1965). Sea State on the Sea Surface Emissivity at L-Band. *Computer Journal*, 7:308–313.

Piola, A., Campos, E., Möller, O., Charo, M., and Martinez, C. (2000). Subtropical shelf front off eastern South America. *Journal of Geophysical Research*, 105:6566–6578.

Ribó, S. (2003). Research on Image Validation and Signal Processing of Aperture Synthesis Radiometry. Technical report, ESTEC. Internal ESTEC Working Paper No. 2182, pp. 81-92.

Ruf, C. (1988). Synthetic Aperture Interferometric Radiometer (SAIR). *Proceedings of the Earth Science Geostationary Platform Technology Workshop, NASA Langley Research Center, Hampton, VA, NASA*, 3040:179–190.

Sivestrin, P., Berger, M., Kerr, Y., and Font, J. (2001). ESA's Second Earth Explorer Opportunity Mission: The Soil Moisture and Ocean Salinity Observations. *IEEE Transactions of Geoscience and Remote Sensing Newsletter*, 118:11–14.

Skou, N. (1989). *Microwave Radiometer System: Design and Analysis.* Artech House.

Skou, N. (1995). An Overview of Requirements and Passive Microwave Radiometer options. Consultative Meeting on Soil Moisture and Ocean Salinity Measurement Requirements an Radiometer Techniques (SMOS). Technical report, Noordwijk ESA. pp. 41–48.

Skou, N. (2003). Faraday Rotation and L-band Oceanographic Measurements. *Radio Science*, 38(4):MAR24–1–8.

Smith, N. and Lefebvre, M. (1997). The Global Ocean Data Assimilation Experiment (GODAE), Monitoring the Oceans in the 2000s: An integrated Approach. *International Symposiun, Biarritz, October 15-17, 1997.*

Stoffelen, A. and Anderson, D. (1993). Wind retrieval and ERS-1 Scatterometer Backscatter Measurements. *Advance Space Research*, 13:553–560.

Swift, C. (1974). Microwave Radiometer Measurements of the Cape Cod Canal. *Radio Science*, 9(7):641–653.

Swift, C. (1980). Passive Microwave Remote Sensing. *Boundary-layer Meteorology*, 18:25–54.

Ulaby, F., Moore, R., and Fung, A. (1981). *Microwave Remote Sensing.Active and Passive.* Addison-Wesley Publishing Company.

UNESCO (1978). Background papers and supporting data on the Practical Salinity Scale. Technical Report 37, UNESCO Technical Papers in Marine Science.

Vall-llossera, M., Miranda, J., Camps, A., and Villarino, R. (2003). Sea Surface Emissivity Modeling At L-Band: An InterComparison Study. *Proceedings of the WISE/LOSAC/EuroSTARRS campaigns Workshop. ESA*, SP-525:143–154.

Villarino, R., Camps, A., Vall-llossera, M., Miranda, J., and Arenas, J. (2003). Sea Foam Effects on the Brightness temperature at L-Band. *IGARSS 2003, Toulouse, France*.

Villarino, R., Enrique, L., Camps, A., Corbella, I., and Blanch, S. (2002). Design, implementation and test of the UPC L-band Automatic Radiometer. *URSI Commission-F 2002 Open Symposium,Garmisch-Partenkirchen, Germany*.

Voronovich, A. and Zavorotny, V. (2001). Modelling of Backscattering of Radar Signals from Sea Surface at Ka- and C-bands. *Proceedings of the URSI General Assembly Maastricht.CD-ROM*.

Wilson, W., Yueh, S., Dinardo, S., Chazanoff, S., Li, F., and Rahmat-Samii, Y. (2001). Passive Active L- and S-band (PALS) Microwave Sensor for Ocean Salinity and Soil Moisture Measurements. *IEEE Transactions on Geoscience and Remote Sensing*, 39(5):1039–1047.

Wilson, W., Yueh, S., Dinardo, S., and Li, F. (2004). High stability l-band radiometer measurements of saltwater. *IEEE Transactions on Geoscience and Remote Sensing*, 42(9):1829–1835.

Wursteisen, P. and Fletcher, P. (2003). EuroSTARRS, WISE, LOSAC. First Results Workshop. *Proceedings of the WISE/LOSAC/EuroSTARRS Campaigns Workshop. ESA PUBLICATIONS*, SP-525:1–249.

Yueh, S., West, R., Wilson, W., Li, F., Nghiem, S., and Rahmat-Samii, Y. (2001). Error Sources and Feasibility for Microwave Remote Sensing of Ocean Surface Salinity. *IEEE Transactions on Geoscience and Remote Sensing*, 39(5):1049–1059.

Yueh, S., Wilson, W., Li, F., Nghiem, S., and Ricketts, W. (1997). Polarimetric Brightness Temperatures of the Sea Surface Measured with Aircraft K- and Ka-Band Radiometers. *IEEE Transactions of Geoscience and Remote Sensing*, 35(5):1177–1187.